

# **Review and Study of Aerodynamic Simulations of Lifting Bodies with Ice Accretion**

---

A Thesis

Presented to

the faculty of the School of Engineering and Applied Science

University of Virginia

---

in partial fulfillment

of the requirements for the degree

Master of Science

by

**Spencer J. Stebbins**

December 2018

APPROVAL SHEET

The Thesis  
is submitted in partial fulfillment of the requirements for the degree of  
Master of Science

Spencer J. Stebbins

Author

The thesis has been read and approved by the examining committee:

Dr. Eric Loth

Advisor

Dr. Daniel Quinn

Dr. Haibo Dong

Dr. Chao Qin

Accepted for the School of Engineering and Applied Science:



Craig H. Benson, Dean, School of Engineering and Applied Science

December 2018

---

## Acknowledgements

---

I would like to thank Dr. Eric Loth, Dr. Andy Broeren, Dr. Mark Potapczuk, and Chris Porter for their leadership, guidance, and patience while working with me through my graduate studies. They have all taught me a great number of things regarding the aerospace engineering field, whether it pertained to technical or non-technical skills. I would also like to thank Dr. Chris Qin, for his continual insight and assistance with my research. I would also like to thank my family, friends, and cat who have supported throughout my time here at University of Virginia. Finally, I would like to acknowledge support by the National Aeronautics and Space Administration under Grant Number NNX16AT17H issued through the NASA Education Minority University Research Education Project (MUREP) through the NASA Harriett G. Jenkins Graduate Fellowship activity. Any opinions, findings, and conclusions or recommendations expressed in this article are those of the author and do not necessarily reflect the views of the National Aeronautics and Space Administration.

---

# Table of Contents

---

<b>Acknowledgements</b> .....	<b>3</b>
<b>Table of Contents</b> .....	<b>4</b>
<b>Abstract</b> .....	<b>6</b>
<b>1. Introduction</b> .....	<b>7</b>
<b>2. Review of Computational Aerodynamics of Lifting Surfaces with Ice Accretion</b> .....	<b>10</b>
1 - Introduction.....	10
1.1 - Previous Surveys of Aerodynamic Icing .....	10
1.2 - Present State of Computational Fluid Dynamics.....	12
1.3 - Objectives for Present Study .....	13
2 - Classification of Iced-Airfoil Aerodynamics and Computational Approaches .....	14
2.1 - Characteristics of Ice Shapes and Aerodynamics .....	15
2.2 - Characteristics of Computational Approaches .....	19
3 - Numerical Methodologies.....	20
3.1 - Review of Turbulence Models .....	21
3.2 - Review of Meshing Techniques .....	25
3.3 - Classification of Previous Computational Studies .....	27
4 - Computational Iced Airfoil Aerodynamics Results and Predictive Fidelity.....	28
4.1 - Ice Roughness .....	28
4.2 - Streamwise Ice.....	29
4.3 - Horn and Scallop Ice .....	29
4.3 - Spanwise-ridge Ice .....	34

5 - Conclusions and Recommendations .....	37
5.1 - Techniques Used, Rationale for Choices, and Overall Effectiveness .....	37
5.2 - Recommendations for Future Work .....	41
Tables .....	43
Figures .....	48
References .....	100
<b>3. Computations of Swept Wing Icing Aerodynamics .....</b>	<b>106</b>
1 - Introduction .....	106
2 - Computational Domain and Methodology .....	107
2.1 - Problem Description .....	107
2.2 - Numerical Methodologies .....	109
2.3 - Meshing Technique .....	112
3 - Results .....	113
3.1 - Flow Field Analysis .....	114
3.2 - Time Averaged Data .....	116
4 - Conclusion .....	119
Figures .....	121
References .....	139
<b>4. Conclusions .....</b>	<b>141</b>

---

# Abstract

---

To ensure substantial progress in airframe safety with icing, it is important to understand icing effects in realistic aerodynamic geometries. The first objective of this research is to review and classify previous three-dimensional computational studies that have analyzed the impact of ice accretion of lifting surface geometries over the past three decades. The classification has considered and discussed aspects of: airfoil/wing geometry, ice shape, prediction accuracy (via experimental validation), flow conditions, meshing type/technique, numerical schemes, and turbulence model (RANS, DES, ZDES, IDDES, etc.). The review of previous studies allows for an informed commentary on the current gaps of knowledge present with regards to computational iced aerodynamics, and recommended strategies for the research community to address these issues.

The second objective of this research is to develop a fundamental understanding of how three-dimensional ice accretions can affect the aerodynamics of a modern, realistic swept wing near stall. Recent experimental data at NASA Glenn Research Center's Icing Research Tunnel has developed realistic ice shapes for the leading edge of a 65% scaled Common Research Model (CRM65). These ice shapes were then converted into sub-scaled 3D-printed models that were used in aerodynamic testing at the Wichita State University's Walter H. Beech Wind Tunnel. This research leverages those experimental data sets to assess the ability of Reynolds-Averaged Navier-Stokes (RANS) to predict the flow physics and aerodynamic performance parameters for an 8.9% scaled CRM65 wing. RANS proved to be capable of simulating the flow at angles of attack up to stall. This numerical methodology show that iced swept wing flow is highly-complex and three-dimensional and requires more in-depth analysis to fully understand the governing factors for the resulting aerodynamics.

# Chapter 1

---

## Introduction

---

The study of ice accretion and its impact on aircraft aerodynamics has a long and rich history. Researchers first began looking into icing phenomena on aircraft in the 1920's, while in the 1940's, aircraft icing research became increasingly important due to a significant number of icing incidents/crashes in World War II for military aircraft. In order to fully address the concerns that icing can cause detrimental effects to lifting surfaces, NASA developed the Lewis Icing Research Tunnel (IRT). Researchers began focusing on both measuring ice accretion's impact on aerodynamic performance parameters and developing technologies to prevent the accumulation of ice on lifting surfaces. However, after icing research stalled due to the Space Race, the field was rejuvenated with the help of an International Workshop in Aircraft Icing that was held at NASA in 1978. This workshop aimed at gathering the key research groups and industries who have focused on understanding the impact of ice accretion on lifting surfaces.

After the workshop, the push to understand icing experimentally via wind tunnels and flight tests, was complemented by a push to predict the effects through numerical simulations. A sizeable portion of experimental data collected after the workshop, was done in order to provide validation to the computationally predicted aerodynamic flow fields produced by CFD. Even with the increase in data being collected by groups around the world, the crash of the Roselawn ATR-72 in 1994 made it readily apparent that there were still gaps in the knowledge on how dangerous icing actually was to aircraft. This crash also caused the icing community to realize that studying simple airfoil geometries was not enough. Modern lifting surfaces are dramatically affected by both the presence of the ice shape and the angle of attack. Icing was finally seen as being more complex than what was suggested by two-dimensional experimental and computational studies.

While extensive reviews on the impact of ice accretion on aircraft aerodynamics have been conducted previously, the reviews focused only on experimental findings. To the author's knowledge, there has been no review that have considered an in-depth study of the development, implementation and fidelity of computational fluid dynamics (CFD) as a tool to understand the impact of icing on airfoil and wing aerodynamics. Nevertheless, there has been considerable development in the areas of CFD. While, current industrial standards in aerospace rely heavily upon CFD software based on Reynolds-Averaged Navier-Stokes (RANS) turbulence models due to its balance of accuracy and computational resources for rapid and robust analysis, RANS is unable to fully capture the flow physics (i.e. turbulent structures) associated with many complex flows. Thus, it can only provide limited amounts of information for flows that require fine details in order to understand the system as a whole. Direct Numerical Simulation (DNS), on the other

hand, captures the full range of turbulent length scales in a flow down to the micro-scales, using the time-accurate Navier-Stokes equations without modeling. However, with the full resolution in time and space of these scales for DNS requires a dramatic increase of computational resources.

In order to avoid the expensive computational cost of DNS while providing more fidelity than RANS, Large Eddy Simulation (LES) was developed. The LES approach is a time-accurate technique that resolves only the large turbulent structures and model the smaller length scales. However, LES is still often too large of a computational resource cost at the full-scale conditions of interest to the aerospace industry, and thus and has not been widely used for aerodynamic predictions. An alternative method that researchers have developed to bridge the gap between RANS and LES, belongs to the general category of Hybrid RANS-LES (HRL) models. HRL approaches capture more information of various flows including icing. With continued advancement in these models, there is increasing probability that HRL will replace RANS for aerospace industrial use, and allow increased accuracy and robustness for more complex geometries of aerodynamic surface and icing shape.

The first objective of this research is to provide a comprehensive review and commentary on experimentally-validated CFD studies of the aerodynamic impact of icing on lifting surfaces. Such a survey can offer guidance for researchers looking to further the development of computational methods to understand the complexity of three-dimensional icing on airfoil/wing geometries. This study will only focus on computational studies published in the last three decades, and only on those which include aspects of experimental validation. To the authors' knowledge, this is the first comprehensive survey that focuses on computational predictions of the effects of icing on wing aerodynamics. It is also the first study to review aerodynamic icing research in the last decade. This area is of substantial interest to the aerospace industry as predictive ability for aerodynamic icing is becoming ever more critical to the design and certification process of new aircraft and of new icing protection systems.

From the information provided by the review, it became clear that icing is not well understood in terms of the three-dimensional aerodynamics for commercial aircraft wing geometries. This is due to both the lack of experimental data for iced wing geometries, and the continual pursuit of simulating flow around two-dimensional airfoil and airfoils that have been extruded in the spanwise direction without sweep. Thus, the second objective of this research is to leverage the experimental data collected on an iced 8.9% scaled Common Research Model (CRM65) at the Wichita State University's Walter H. Beech Wind Tunnel. The research will investigate and assess the ability of Reynolds-Averaged Navier-Stokes (RANS) to predict high Reynolds number aerodynamic flows of iced wings with complex flow physics. This research is part of an initiative to understand iced wing aerodynamics by a consortium of organizations including NASA, the Federal Aviation Administration (FAA), the Office National d'Etudes et Recherches Aérospatiales (ONERA), Boeing, the University of Illinois, the University of Virginia, and the University of Washington.

---

## Review of Computational Aerodynamics of Lifting

### Surfaces with Ice Accretion

---

#### 1 – Introduction

##### 1.1 – Previous Surveys of Iced Aerodynamics

The study of ice accretion and its impact on aircraft aerodynamics has a long and rich history. Researchers first began looking into icing phenomena on aircraft in the 1920's, while in the 1940's, aircraft icing research became increasingly important due to a significant number of icing incidents/crashes in World War II for military aircraft. As noted by Carroll & McAvoy [1], research identified that the primary problem is not the weight of the ice accumulated on the wing, but it is instead the negative impact on the wing's aerodynamics that have yielded the catastrophic events. In response, the NASA Lewis Icing Research Tunnel (IRT) was developed in order to fully understand how ice occurs on airfoils and how it subsequently effects the aerodynamics [2]. Researchers focused on both measuring ice accretion's impact on aerodynamic performance parameters and developing technologies to prevent the accumulation of ice on lifting surfaces. The latter focus was pertinent due to the increase desire to utilize general aircraft in all weather conditions.

With the rejuvenation of work in the IRT at NASA in Cleveland (now named the Glenn Research Center), an International Workshop in Aircraft Icing was held in 1978 with the aim of gathering key research groups and industries who have focused on understanding the impact of ice accretion on lifting surfaces [2]. After the workshop, the push to understand icing experimentally via wind tunnels and flight tests, was complemented by a push to predict the effects though numerical simulations. By this time, computational methods were being developed at a faster pace and with increasing efficiency. After the workshop, much of the experimental data was collected in order to provide validation to the computationally predicted aerodynamic flow fields produced by CFD. Even with the increase in data being collected by groups around the world, the 1994 ATR-72 accident in Roselawn, Indiana made it readily apparent that there were still gaps in the knowledge on how dangerous icing actually was to aircraft, especially in super-cooled large droplet (SLD) icing conditions. This accident also caused the icing community to realize that studying simple airfoil geometries (i.e. NACA0012) was not enough. Different airfoils and different ice shapes can dramatically affect the degree and mode of aerodynamic performance

degradation, and icing is much more complex than what was originally suggested by two-dimensional experimental and computational studies.

There have been two canonical reviews on the impact of ice accretion on aircraft aerodynamics, both focusing on experimental findings. These extensive reviews by Lynch & Khodadoust [3] and Bragg *et al.* [4] focused on synthesizing icing research conducted over the past century up until 2000 and 2004, respectively. The review by Lynch and Khodadoust provided an in-depth survey on majority of the experimental work completed by that time for a wide variety of lifting surfaces. This survey highlighted the dependency of the baseline lifting surface for the accumulation of ice and the possible disastrous consequences of different types of ice accretions. For the former, they found that thicker lifting surfaces yielded much more sensitive stall characteristics to the presence of ice accretion, owing to their increased susceptibility for flow separation. However, thinner surfaces had a larger collection efficiency than their thicker counterparts, and thus still needed to be taken seriously, especially in context of tail-plane stall.

In terms of the possible disastrous consequences associated with ice accretion, Lynch & Khodadoust found that the four largest factors are: 1) underestimation and misunderstanding of the problem, 2) the potential for catastrophic changes in aerodynamic coefficients, 3) undefined upper limits of potential aerodynamic consequences, and 4) the direct impact on portions of the flight operation envelope. At the time of the review, the understanding of the exact impact for various sized initial leading-edge ice accretion was not well understood. In fact, in-depth high Reynolds number wind tunnel tests that have been conducted proved that even the smallest ice shapes could cause noticeable reductions in aerodynamic capabilities. Furthermore, the aforementioned tests were not able to fully discern the full extent and impact on the aerodynamics by the presence of an ice shape at flight-like Reynolds numbers. Thus, the authors recommended more work to be done in order to grasp the true dangers of ice, especially in the takeoff portion of the flight operation envelope where the margins to stall are, typically, at their minimum.

As a compliment to the review by Lynch & Khodadoust [3], Bragg *et al.* [4] took a different approach to analyzing a variety of experimental studies. Whereas, Lynch & Khodadoust focused on outlining the effect on the aerodynamic performance parameters due to various ice shapes, Bragg *et al.* focused on understanding the impact of ice accretion on airfoil flow physics. By better understanding the flow physics, it was possible to determine the main causes of the integrated aerodynamic effects due to icing, like reduced lift and increased drag. To accomplish this, Bragg *et al.* related the experimentally observed flow characteristics (i.e. separation and reattachment locations) for iced airfoils to four major characterizations of ice shape: ice roughness, streamwise ice, horn ice, and spanwise ridge ice.

The combination of these two well-known reviews provided a comprehensive understanding of icing effects on aerodynamics, as provided by experimental investigations at the time. In addition, recommendations were made for future experimental work to further fill in the knowledge gaps. However, neither of these two reviews nor any articles since has considered an in-depth study of the development, implementation and fidelity of computational fluid dynamics (CFD) as a tool to understand the impact of icing on airfoil and wing aerodynamics. Nevertheless, there has been considerable development in the areas of CFD and surveys reviewing this progress, as discussed in the next section.

## **1.2 – Present State of Computational Fluid Dynamics**

The precursor to modern-day CFD began with Richardson's work in the 1920's for meteorology [5]. Since then, computers have become more powerful (in terms of memory and speed) and the computational software has progressed significantly in terms of efficiency and accuracy of predictions. Current industrial standards in aerospace rely heavily upon CFD software based on Reynolds-Averaged Navier-Stokes (RANS) turbulence models, as this approach is often the most effective balance of accuracy and computational resources for rapid and robust analysis [6]. However, while RANS is the least time-consuming method associated with modern-day turbulence models and requires the least amount of computational resources, it is not able to fully capture the flow physics (i.e. turbulent structures) associated with many complex flows. Thus, it can only provide limited amounts of information for flows that require fine details in order to understand the system as a whole.

Direct Numerical Simulation (DNS), on the other hand, captures the full range of turbulent length scales in a flow down to the micro-scales, using the time-accurate Navier-Stokes equations without modeling. However, with the full resolution in time and space of these scales, DNS requires a dramatic increase of computational resources. In order to avoid the expensive computational cost of DNS while providing more fidelity than RANS, Large Eddy Simulation (LES) was developed. The LES approach is a time-accurate technique that resolves only the large turbulent structures and models the smaller length scales. However, LES is still often too large of a computational resource cost at the full-scale conditions of interest to the aerospace industry. Thus, it has not been widely used for aerodynamic predictions. An alternative method that researchers have begun to develop to bridge the gap between RANS and LES, belongs to the general category of Hybrid RANS-LES (HRL) models. HRL approaches capture more information of various flows including icing. With continued advancement in these models, there is an increasing probability that HRL will replace RANS for aerospace industrial use, and allow increased accuracy and robustness for more complex geometries such as aerodynamic surfaces and icing shapes.

However, as noted by Fujii [7], even with the recent progress of advanced RANS and HRL models, these approaches require more development to be reliable and consistently predict flows. This will help mitigate the necessity for validation against experimental data to ensure confidence in the predictions of various results. In particular, application to iced aerodynamics, which includes an intricate connection between the icing geometry and the airfoil/wing geometry, requires careful consideration of the most appropriate turbulence model, grid methodology, and boundary conditions for each case. While this can be time-intensive, the potential rewards for robust and accurate CFD of iced aerodynamics are great, since the alternative approach of experimental testing at full-scale (or even near full-scale) Reynolds numbers is extremely expensive and generally only available for a modest set of conditions (constrained by facility limitations) and only after the design process has been complete. Furthermore, CFD can provide vital information regarding the various aspects of a fluid flow (especially three-dimensional unsteady flow details) that are not easily obtainable via experimental diagnostics.

## **1.3 – Objectives of the Present Study**

The objective of this study is to provide a comprehensive review and commentary on experimentally-validated CFD studies of the aerodynamic impact of icing on lifting surfaces. Such

a survey can offer guidance for researchers looking to further the development of computational methods to understand the complexity of three-dimensional icing on airfoil/wing geometries. This simulation-focused review acts as a complement to the previously mentioned surveys by Lynch & Khodadoust [3] and Bragg *et al* [4]. However, this study will only focus on computational studies published in the last three decades, and only those which includes aspects of experimental validation. To the authors' knowledge, this is the first comprehensive survey that focuses on computational predictions of the effects of icing on lifting surfaces aerodynamics. It is also the first study to review aerodynamic icing research in the last decade. This area is of substantial interest to the aerospace industry as predictive ability for iced aerodynamics is becoming ever more critical to the design and certification process of new aircraft and of new ice protection systems.

The rest of this survey is organized in terms of classification, numerical methodologies, results and summary/recommendations. The classification portion given in Section 2, first characterizes the various lifting surface geometries and basic ice shapes in relationship to their aerodynamics, and then characterizes the key computational approaches in terms of their method (turbulence and meshing aspects). The numerical methodologies discussed in Section 3 are driven by the commentary of Spalart with regards to modern-day turbulence modeling as well as meshing technique and numerical schemes [8], [9]. The results discussed in Section 4 will focus on three-dimensional CFD studies that investigated the impact of ice accretion on airfoil/wing aerodynamics. The computational studies will be considered in terms of airfoil/wing geometry and ice shape in terms of aerodynamic performance (pressure coefficient, angle of attack influence on lift, drag, pitching moment curves, stall behavior, etc.) as well as flow physics following the approach of Bragg *et al.* [4] and Diebold *et al.* [10]. Finally, this study will summarize, with an informed commentary, the current capability of computational methods, on the gaps in knowledge with regard to computational iced airfoil and wing aerodynamics, and on the recommended strategies for the research community to address these issues.

## **2 - Classification of Iced-Airfoil Aerodynamics and Computational Approaches**

Since this survey involves a large number of widely varying studies, it is helpful to define a set of pertinent classifications for different ice shapes as is relevant to aerodynamics (Section 2.1), and computational studies as is relevant to their approaches (Section 2.2). The former category will largely focus on the geometry of the ice shape and airfoil/wing examined by each study. The latter categorization will focus on the turbulence models and meshing techniques implemented by the researchers. The classifications are based on key characteristics designed to provide appropriate groups and sub-groups of the previous studies and to elicit conversations regarding the connection of geometries and flow conditions to computational approaches.

### **2.1 – Key Characteristics of Ice Shapes and Aerodynamics**

Prior to picking the meshing technique and turbulence model to be implemented in a computational study, it is imperative to understand the geometries and domain of the problem being investigated. This is because two of the largest factors that impacts the process of CFD (including the approach and predictive ability) are the aerodynamic and ice-shape geometries. As

such, this review will classify the following aspects of geometry for each study: airfoil/wing shape, ice shape, and stall behavior.

The first aspect of the study to consider is the base airfoil/wing geometry used. To develop this classification, it is important to define differences between a wing, wing-section and an extruded airfoil as shown in Fig. . Figure 1a presents a generic wing planform that that exhibits spanwise variation in the form of sweep, taper, twist and finite aspect ratio. However, this paper will take a more simplified definition for a “wing” and refer to it as any lifting surface that has a wing-tip and some spanwise variation. If a lifting surface does not have a wing tip, but has taper or sweep, it will be referred to as a wing section, as seen in Fig. b. Lastly, if a geometry was created by taking an airfoil and then extruding it in the spanwise direction without sweep as in Fig. 1c, it will be referred to as an extruded airfoil regardless of the presence of spanwise flow associated with end-wall conditions (as are common in a wind tunnel test).

The next aspect to consider is the ice shape analyzed by each study. As noted by Bragg *et al.* [4], the ice shape has a significant impact on the flow field around an airfoil/wing geometry and thus should be considered carefully when it comes to the impact on aerodynamics. As shown in Fig. 2, there are four major types of ice geometries that are created during various icing conditions and range in aerodynamic impact on the flow field. The four major ice shapes are: 1) ice roughness, 2) streamwise ice, 3) horn ice, and 4) spanwise ridge ice. These are arranged in the figure in terms of whether they are more likely to be associated with rime or glaze ice and to the extent that they can be aerodynamically detrimental. In general, rime ice occurs at the coldest conditions (often for temperatures below  $-15^{\circ}\text{C}$ ) whereupon the water droplets freeze almost immediately upon impingement on the wing surface and produce a white opaque appearance. In contrast, glaze ice occurs at warmer conditions (often for  $-10^{\circ}$  to  $0^{\circ}\text{C}$ ) for which the water droplets tend to spread and may run downstream before freezing on the wing surface and will generally produce a clear or translucent appearance. The specific outcome of rime vs. glaze ice also depends on flight speed, and liquid water content. Intermediate conditions can yield mixed ice. Each of these four ice shapes can have profoundly different impact with regards to aerodynamics and flow physics, and thus have to be considered separately when examined computationally.

The first of the ice shapes to consider is ice roughness. This ice shape tends to occur when the icing exposure is short-lived or during the initial stages of ice accretion, prior to the ice shape forming into either streamwise ice or horn ice. This fact is reflected in Fig. 2, where ice roughness is formed under the whole range of icing conditions. This ice shape also can have the largest range of aerodynamic impact on a wing due to the complex three-dimensionality it adds to the leading edge of a lifting surface and due to the wide range of various sized protuberances that can occur. As shown in Fig. 3, the roughness ice shape can generally be broken down into three main zones: smooth zone, rough zone, and feather region. For geometries with sweep, spanwise variation in the smooth zone can appear in the form of ripples [10] but generally the smooth zone has little aerodynamic effect. In the rough zone, even small three-dimensional protuberances can cause premature transition of the boundary layer from laminar to turbulent conditions, as compared to a smooth airfoil and thus significantly impacting the potential for upper-surface flow separation and drag increases [11][12]. However, the element heights in the rough zone and especially the feather region are often much larger than the local boundary-layer thickness and thus act as localized bluff bodies with their own three-dimensional separated flow field. Due to their impact on the overall flow field, and more specifically the boundary layer, these elements can cause boundary layer

transition and increase the likelihood of trailing edge separation. This in turn leads to reduced lift coefficients, decreased maximum lift, reduced stall angle of attack, and increased drag.

It is notable that very few CFD studies have focused on roughness. This is because the geometries (protuberance height, spacing, etc.) can vary widely and can result in complex three-dimensional surfaces with intricate shape details that are a great challenge to mesh. Their resolution would also dramatically increase the total number of nodes within the overall mesh. With the increase in mesh nodes, the necessity for more computational resources would also increase, and meshing all the small-scale features of roughness is generally prohibitive for practical computational studies. Thus, engineers and researchers have found that while ice roughness is interesting to understand in terms of aerodynamics, its impact by itself is not a priority for CFD studies when deciding which ice shapes should be allocated computational resources.

As mentioned earlier, one of the ice shapes that develops from ice roughness is streamwise ice. This type of ice tends to form under cold temperature icing conditions that results in rime icing. As seen in Fig. 2, this streamwise ice shape has the smallest aerodynamic effect of the three ice shapes that doesn't include ice roughness. This is because the accreted ice usually follows the contour of the airfoil surface, as shown in Fig. 4, which causes the flow to remain locally attached and the impact on the pressure distributions and the aerodynamic coefficients are weak. When exposure time is increased, streamwise ice has the possibility to transition into shapes that are significantly non-conformal to the airfoil surface. When the streamwise ice follows the contour of the airfoil surface, separation tends to occur near the junction of the ice shape with the airfoil, but may fluctuate depending on the angle of attack and the state of the boundary layer. For the streamwise ice with a shape that is non-conformal to the airfoil, if the formation of the ice shape results in a horn-like feature, the wing may exhibit the same separation mechanisms as the horn ice, to be discussed further below, albeit with a smaller separation bubble comparatively. At large enough angles of attack, both of these separations can grow in size and eventually cause degradation of the aerodynamic performance parameters.

Another ice shape that can arise from ice roughness is horn ice. This ice shape generally develops when a wing is exposed to icing conditions consistent with glaze and mixed ice. As shown by the example shape in Fig 5a, horn ice can be characterized by its height, the angle ( $\theta$ ) it makes with the chord line, and its location indicated by its wrap surface distance ( $s$ ) normalized by the airfoil chord length ( $c$ ) [4]. Researchers have found that for horn ice, the flow separation location remains fixed at the horn tip for most angles of attack. This separation produces a large separation bubble downstream of the horn that causes a large redistribution of pressure, which in turn, results in pitching moment changes, decreased lift, and increased drag. Due to the turbulent nature of the separation bubble, the flow is characterized as being unsteady and three-dimensional overall. Notably, the height, angle, and location of the horn is the primary determinant of the flow physics, whereas, the horn shape itself has little influence [4]. As such, experimental studies have found that the aerodynamic performance characteristics of an ice horn on an airfoil can sometimes be represented by instead placing simple geometries (i.e. leading-edge spoiler) on the airfoil [13][14]. The simple geometry has to be able to maintain the height, angle, and location of the ice horn in order to accurately reproduce the separation bubble.

The last ice shape to consider is the spanwise ridge ice, which forms downstream of the leading edge. Though generally associated with supercooled large droplet (SLD) conditions, this ice shape can occur for all droplet sizes. Ice protection systems can also contribute to the formation of spanwise ridge ice downstream of its extent. For example, an anti-icing system that does not run

in full-evaporative mode may prevent freezing in areas where heat is added, but water can run back past the heated zone and form into ridge ice accretion downstream. By a different process, a similar result can occur for a pneumatic de-icer as shown in Fig. 6. The resulting ridge ice accretions which occur downstream of the pneumatic boot are often non-uniform spanwise and thus can exhibit more three-dimensionality than the horn ice. In terms of flow field impact, spanwise ridge ice tends to accrete in regions downstream of the leading edge after the boundary layer has developed or transitioned. The ice accretion then acts as a flow obstacle and produces not only a separation bubble aft of the geometry, but also upstream of the geometry. As compared to ice shapes at the leading edge, spanwise ridge ice can be particularly dangerous since it tends to occur just downstream of the airfoil suction peak where there can be a strong adverse pressure gradient for the given airfoil design. As such, the boundary layer in this region is more susceptible to flow separation so that a protuberance of a given height in this location is much more likely to cause premature stall.

While not readily apparent from Fig. 2, streamwise ice, horn ice, and spanwise ridge ice can often have a super-imposed ice roughness and/or spanwise variation. Roughness that appears in conjunction with other ice shapes is generally considered a secondary or tertiary geometric effect when the roughness height variations are smaller than the heights that define the streamwise shape or horn ice shape. In contrast, the influence of spanwise variation is more complex, but is also often neglected. Even when three-dimensional wings or wing sections are considered, most researchers simply extrude two-dimensional representational cuts of ice shapes, as seen in Fig. 5b, in order to minimize the resources required computationally. This smooths out not only a large portion of the ice roughness of the geometry, but also any spanwise variation. However, this process also brings up an important question on whether or not spanwise variation is important or whether it is negligible like ice roughness. Due to this question, three-dimensional CFD studies reviewed herein will be classified in terms of whether their ice shape geometries are two-dimensionally extruded or whether the ice shapes have spanwise surface variations.

The last geometric aspect to consider is angle of attack ( $\alpha$ ). The impact of ice on aerodynamics has been found to generally become more profound at higher angles of attack. More specifically, since ice accretion can especially influence the stall behavior resulting in a reduced stall angle, two effects can be seen: the angle of attack at which the lift reaches a local maximum value decreases, and drag dramatically increases at angles of attack starting right before stall. This review will make special note of the studies that looked at the stall behavior of the airfoil/wing geometry via simulation and the correlation of numerical approach to the fidelity in predicting stall behavior.

## **2.2 – Key Characteristics of Computational Approaches**

Once the desired geometry, domain, and flow conditions of a system are defined, one may select the appropriate computational approach. The main choices of the computational approach are turbulence model, computational mesh, and numerical scheme. Each of these selections are important in determining the speed and accuracy of the solution. As such, the papers reviewed herein will be classified in terms of: turbulence model, flow solver, and meshing type/technique. In addition, the review will be limited to CFD studies which included experimental validation so that the summary (Section 5) can effectively classify the studies with respect to their typical prediction accuracy. The rest of this subsection will only focus on briefly introducing each aspect, while Section 3 will provide a more in-depth discussion of the various computational approaches.

The first aspect to consider for a computational approach is the turbulence model. Generally, CFD flow solvers (i.e. ANSYS Fluent, ONERA elsA, and etc.) have several built-in turbulence models available for selection, while some solvers allow the user to create and define their own turbulence model. Amongst the CFD studies highlighted by this review, there are a specific set of turbulence models that have been employed, e.g. RANS vs. DES.

The second aspect to consider is the meshing type/technique employed. There are a wide variety of mesh techniques that can be implemented in order to develop a well resolved mesh. Overall there exist two major types for meshes: structured and unstructured. Both of these types have their own positives and negatives and can even be combined into hybrid grids. The development of an appropriate mesh (type and resolution) is important because it can play a serious factor in the ability of a turbulence model to correctly simulate a given flow. The classification of each study will provide the meshing software used by the study and if the mesh created was structured, unstructured, or a hybrid of the two.

While turbulence model, numerical approach and mesh type are all key aspects that must be selected (and are used herein for classification), the key outcomes from these choices are the CPU resource requirements and expected prediction accuracy. The computational requirements can be often estimated before a simulation is conducted since it is largely determined by the size of the mesh and the numerical approach. Similarly, the predicted accuracy can be assessed in advance if the method has already been validated with well-studied and relevant fluid flow fields. Since there has never been a previous review of accuracy for CFD of iced aerodynamics, Section 4 will aim to examine such fidelity directly. Thus, this review will only focus on computational studies that have been validated against experimental data.

### **3 - Numerical Methodologies**

As noted previously, a numerical methodology can be broken down into three main aspects of selection: turbulence model, numerical scheme/flow solver and meshing technique. The two key aspects of the outcome are cost (computational time and memory to complete a simulation) and quality (the resulting prediction accuracy of key results of interests). The understanding and implementation of each one of these aspects is crucial in order to efficiently and successfully predict the characteristics of a given flow field for a desired geometry. For this review, the focus on each aspect and the rationale for method selection will be considered in the context of aerodynamics of iced airfoils/wings. In the following, all turbulence models used in this context will be defined in Section 3.1, followed by defining meshing techniques in Section 3.2. These aspects will then be used to classify all the previous CFD studies on icing aerodynamics in Section 3.3.

#### **3.1 – Review of Previously Employed Turbulence Models**

Turbulence is unsteady, three-dimensional, non-linear, diffusive, dissipative, and is characterized by a wide range of length and time scales. The length scales range from the macroscopic length scale of the physical domain ( $D$ ), to the integral length scale ( $\Lambda$ ), and finally to the Kolmogorov length scale ( $\lambda$ ). As seen in Fig. 7a., these scales can be related to turbulent energy, which in turn helps understand the development and application of turbulence models. The first section, up to  $1/D$ , of the spectrum encompasses turbulent structures (i.e. eddies) with length

scales on the order of the domain. Between  $1/\Lambda$  and  $1/\lambda$  is the inertial subrange. In this section, the turbulent kinetic energy is created from fluid instabilities at either the domain or integral scales. From here, the flow experiences a cascade of turbulent energy from the domain level to the microscale as the turbulent structures undergo an eddy breakdown until the energy is finally dissipated or destroyed by the viscous effects in the last major section of the energy spectrum [15]. This last section termed the dissipative range, contains length scales smaller than  $1/\lambda$  and is highly influenced by viscous dissipation effects which effectively filters out any remaining turbulence in the flow.

The complete spatial and temporal resolution of turbulence structures for all regions of a flow is categorized as Direct Numerical Simulation (DNS). Since DNS captures the full range of turbulent length scales in a flow, it does not require a turbulence model to solve the Navier-Stokes equations. As noted by Lawson *et al.* [16], by computing complex flows and resolving all of the turbulent length scales, a significantly more amount of computational resources is required to be successful, but DNS has enormous potential if those computational resources can be met since it includes no empiricism for the turbulence, i.e. is a direct solution of the unsteady flow equations. Even so, due to the increase in resources needed, researchers have pursued developing methods that can simulate flows at a “good-enough” level. One of the first methods utilized by researchers to solve the Navier-Stokes Equations was Reynolds-Average Navier-Stokes (RANS). RANS is a time-averaged approach in which none of the scales are resolved, as seen in Fig. 7b, and so the effect of all the turbulent length scales must be empirically modeled. Researchers found that this method has the ability to calculate boundary layers and their separation accurately, but does not always accurately reproduce large regions of separation and certain turbulent flows accurately [9]. In order to provide more accurate results than RANS but at a lower computational cost when compared to DNS, researchers developed the Large Eddy Simulation (LES) method [17]. LES aims to only resolve the large-scale eddies while modelling the small turbulent length scales. By restricting the resolution, LES is less computationally demanding (as compared to DNS) and therefore more amenable to solve complex flows. However, the implementation of LES has a downside: by modeling small turbulent length scales, the method requires a highly refined domain discretization and a large number of computational resources to accurately capture the flow. Therefore, as a method to bridge the gap between RANS and LES, researchers developed and implemented a variety of hybrid RANS-LES (HRL) models to capture flows that encompass both the boundary layer and the free shear region [18]. With enough advancement in these models, the possibility of replacing RANS in industrial use with more accurate HRL models can come to fruition.

Returning to RANS, a large amount of the studies presented in this review use this method since it the most efficient (requires the least amount of computational resources) and has the longest period of use. This is true not just for icing aerodynamics, but for CFD in general [17]. RANS is formulated from the time-averaging of the Navier-Stokes equations as seen below:

$$\frac{\partial \bar{u}_i}{\partial t} + \frac{\partial}{\partial x_j} (\bar{u}_i \bar{u}_j) = \beta \delta_{1i} - \frac{1}{\rho} \frac{\partial p}{\partial x_i} + \frac{\partial}{\partial x_j} \left[ (\nu + \nu_T) \frac{\partial \bar{u}_i}{\partial x_j} \right]$$

$$\frac{\partial \bar{u}_i}{\partial x_i} = 0$$

This averaging introduces a Reynolds Stresses term which requires empirical closure. Three popular methods for closure and in order of increasing complexity are: Linear Eddy Viscosity Models (LEV), Nonlinear Eddy Viscosity Models (NEV), and the Reynolds Stress Models (RSM).

Within each of these methods, there are specific models that can be implemented and have been used by the studies examined in this review.

For LEVs, the studies in this review utilized the Baldwin-Lomax algebraic model, the Spalart-Allmaras (SA) one-equation model, and the  $k$ -epsilon ( $k$ - $\epsilon$ ) and  $k$ -omega ( $k$ - $\omega$ ) two-equation models. The Baldwin-Lomax algebraic model does not depend on the utilization of any additional partial differential equations beyond the time-averaged Navier-Stokes equation in order to solve for the turbulent stresses and fluxes. [19] These models are formulated to depend purely on the flow variables calculated during each iteration. Wilcox [20] found that the algebraic models performed satisfactorily in cases with thin attached boundary layers, but began to deteriorate in accuracy for flows with large separations.

One-equation and two-equation models can improve the robustness and accuracy of the turbulence model. As can be seen in Table 1 and Fig. 8, SA is one of the more popular RANS models to implement for various flows [21]. This model relies on closing the Navier-Stokes equation by solving a transport equation for a turbulent-viscosity-like term that is related to the mean strain rate. As for the latter set of models,  $k$ - $\epsilon$  is good for simple free-shear flows while  $k$ - $\omega$  is good for simple boundary layer flows. Even though SA was specifically developed for aerodynamic applications,  $k$ - $\epsilon$  has become increasingly more widely accepted and used in industry. However, due to its formulation,  $k$ - $\epsilon$  is not directly applicable near walls and must rely upon the usage of wall functions. The  $k$ - $\omega$  model on the other hand, can be used for near wall flows without the need for wall functions and works well for calculating boundary layer flows. In fact, a variant of the  $k$ - $\omega$  model that has gained high popularity is Menter's  $k$ - $\omega$  SST model. [22] This model utilizes the  $k$ - $\omega$  equations near the wall and then transitions into a modified version of the  $k$ - $\epsilon$  equations away from the wall.

Even though RANS is the least time-consuming numerical method and does not require a large amount of computational resources comparatively, it is not able to resolve any turbulent structures. As noted by Spalart, Unsteady RANS (URANS), or Very Large Eddy Simulation (VLES), was originally developed in order to provide an alternative to overcoming RANS' lack of ability to model complex flows and provide information for turbulent flows. [8] This method still uses the same overall formulation of RANS, but simply considers the time dependent variables in the Navier-Stokes equations and solves them in a transient state instead of a steady state. Nishino *et al.* [23] describe URANS as a decomposition of the instantaneous variables in the Navier Stokes equations into long-time-averaged, periodic, and turbulent components instead of ensemble-averaged components represented in RANS. However, Spalart has shown that the resulting flow field characteristics produced by pure URANS cannot accurately capture the complexity in turbulence structures as well as other transient based methods like HRL [9].

As noted previously, HRL models have been developed in order to bridge the gap between RANS and LES by allowing for the computation of the Navier-Stokes equations via RANS near walls and via LES in the rest of the domain. The intent of these models is to be able to sufficiently and accurately capture thin high Reynolds number attached boundary layer flow near the wall where LES resources would otherwise be extremely expensive in comparison, while also capturing turbulent structures in the detached region where RANS is not suited. In order to accomplish this combined task, HRL models have to provide a coupling method between RANS and LES. Two of the main ways this has been accomplished is via the blending method and the interfacing method [18]. For the former, a blending equation is added in a given region in order to allow for the user to determine the rate of progression the simulation transitions from RANS to LES in that region.

As the blending region reaches a minimum, the transition between RANS and LES becomes similar to a step function and is equivalent to the interfacing method.

As noted by Fröhlich & Terzi [18], and is the case for the studies surveyed herein on computational aerodynamics of iced lifting surfaces, the interfacing method is generally given implicitly. In this soft interfacing style, the location of the switch between RANS and LES tends to be determined largely by the size of the mesh near a discretized wall and by the flow solution. The first highly successful model to use this approach is DES, which was created for high-Reynolds number flows with massive flow separation [9]. The formulation of this model originated from the modification of the SA model by changing the distance function. This new function takes into consideration the size of the grid near wall boundary locations and implements either RANS or LES based on the analyzed grid. Researchers have found that DES has indeed performed effectively for simple geometries and flows where separation was the largest influence. However, the model was not always accurate when the analyzed flow is not completely separated, e.g. an airfoil experiencing only trailing edge separation or for separated regions which reattachment. As summarized by Spalart [9], this deficiency can be attributed to three main causes: Modeled-Stress Depletion (MSD), Grid Induced Separation (GIS), and Logarithmic-Layer Mismatch. All three causes are derivatives of the fact that the sub-grid turbulence model relies heavily upon the size of the grid used in the simulation. As such, a grid with spacing that is not fine enough for LES to run with reasonable grid independence in the separated regions, can cause the blending model to misinterpret the flow field yielding an inaccurate separation location. However, considerable work has been done to improve DES in order to correct for these issues.

The first improvement to DES was to address the inaccurate separation location due to MSD and GIS. This new method, which was finalized by Spalart *et al.*[24], is termed Delayed-DES (DDES). DDES reformulates the model to actively detect the boundary layer of the flow and prevent the simulation from switching to LES even when the grid spacing would trigger such a switch. The second improvement attempted to further enhance both DES and DDES by resolving the issue with having a logarithmic-layer mismatch. This method, developed by Shur *et al.* [25] and termed Improved-DDES (IDDES), introduced a number of empirical variations to the original DES formulation, but focused on modifying the usable length scales to additionally take into the distance from the wall.

Another variant of DES, is Zonal DES (ZDES), which allows the user to specify where in the domain RANS or DES should run. As noted by Deck *et al.* [26], in the framework of ZDES, the methodology does a non-minor adjustment to the formulation of DES by changing the subgrid length scale of DES to depend not only on the grid ( $\Delta x, \Delta y, \Delta z$ ), but also on the velocity gradients ( $U_{i,j}$ ) and eddy viscosity fields ( $\nu_t$ ). In regards to the specification of RANS vs. DES, this functionality is made possible by the combination of both gridding practices and the introduction of a “switch” variable controlled by the user. This “switch” allows the specification of whether a given region should be calculated using RANS or DES. However, due to this switch, this method requires a good amount of work and information to be known *a priori* by the user in order for the implementation to be successful. Once the regions and grid has been established, this method also allows the user to simply fall back to calculating either RANS or DES throughout the whole domain due to the “switch” function. While this option is not generally exercised nor practical for iced lifting surfaces, ZDES has another, perhaps more important attribute, and this a sub-grid turbulence model that is no longer simply tied to grid size.

The last HRL model to consider is the dynamic Hybrid RANS-LES (HRL) model developed by Bhushan & Walters [27] and intended to address two key HRL issues noted by Alam *et al.* [28]. The first issue is the transition/blending between RANS and LES where the eddy viscosity is used to define the Reynolds stress in the former and to define the sub-grid stress in the latter. Due to their difference mathematically and physically, the bridging between the two regions can cause inconsistencies in the flow field. The second issue is the dependence of HRL sub-grid models and switching functions to the grid resolution. Thus, the new formulation by Bhushan & Walters sought to resolve these issues and has since been applied to a number of studies, including ice-accreted lifting surfaces.

### 3.2 – Review of Employed Meshing Techniques

The next aspect of numerical methodology to examine is the implementation of meshing techniques. Meshing is always important to consider since it is directly linked to the total number of grid points in a domain, which in turn is proportional to the computational memory and time required for solution. Thus, it is pertinent to ensure that the domain of a solution is resolved well enough to provide a grid-independent solution (especially when a structure resolving turbulence model is used) but not over-resolved as to waste computational resources. The decision on how many nodes to use in a domain can be driven by two factors: the approximate minimum grid length scales and the approximate number of continuous-phase fluid nodes. For the former, the smallest length scale is based on the minimum numerical spatial resolution in each direction (streamwise, spanwise, and wall normal). To best determine the appropriate grid size, grid independence studies are recommended, but work can be done prior to allow for a good starting point. For streamwise flow, this length scale and resulting node spacing tends to be based proportionally to the minimum size of a geometric feature in that specific direction. Lastly, for flows that are expected to have turbulence and a boundary layer present, a reasonable approach is to use a wall-normal resolution based on  $\Delta y^+ \approx 1$ .

In LES-like regions where the turbulent flow structures are resolved, the grid should be roughly isotropic, e.g. the resolution in the spanwise and streamwise direction should be similar to that in the wall-normal direction flow. As the selected numerical approach moves to greater resolution of the turbulent structures, the number of nodes in the domain as well as the number of computational resources for a given flow increases as well. As such, the choice of a turbulent flow approach (RANS, HRL, LES, DNS, and etc.) requires carefully evaluating the balance between available computational resources with the desired level of solution accuracy and robustness.

Once the determination of the size of the domain and general number of nodes to discretize the flow field has been made, it is necessary then to decide on the type of meshing that will be used to define the space. Baker [29] discussed the three main mesh types: structured, unstructured, and hybrid. As noted by Shewchuk [30], a structured mesh tends to follow a specified orderly pattern throughout the domain via a set of indices that have been defined by the space dimension, as can be seen in Fig. 9a. It is also possible to overlap two structured meshes in order to help provide enhanced resolution of a complex surface. This subset of structured meshing, which has been used by some of the studies, is called chimera or overset. Overall, researchers have found that discretization of the space via structured meshes for simple geometries is both space efficient and allows for fast convergence.

Unstructured meshes on the other hand, as seen in Fig. 9b, do not follow a given pattern in the domain. Once the surface of a geometry has been defined, the 3D discretization of the space is generally based on geometrical limits set by the end user (i.e. max element size or included angle). If the selected geometry for a study has a complex surface with either large amounts of curvature or spatial variation, an unstructured mesh allows the system to maintain these features more easily when compared to structured meshes. This is especially important for complex geometries like convoluted ice shapes.

The last mesh type to consider is hybrid meshes, with an example shown in Fig. 9c. These meshes combine both aspects of structured and unstructured grids per the example of an ice shape accreted on the leading edge of an airfoil as shown in Fig. 10. In order to properly resolve the boundary layer of the flow over the airfoil, the mesh interpolated in the wall normal-direction of the geometry can be specified as a structured mesh. Once the area in close proximity to the geometry has been well defined, the hybrid-mesh can switch from a structured discretization to an unstructured discretization in order to minimize the number of nodes in portions of the flow domain.

For meshing in general, the driving force tends to be associated with the complexity of the ice shape being modeled. If the ice shapes present very little to no spanwise variation, then a structured mesh can be appropriate for defining the surface of the geometry. However, if the ice shape presents a comparable amount of spanwise variation, it becomes extremely recommended for the user to consider how to best resolve the complexity of the ice shape. The two best methods in this instance tends to be either an unstructured/hybrid or chimera/overset mesh due to their ability to handle geometry with a lot of curvature and complexity.

### **3.3 – Summary of Numerical Approaches used for Iced Lifting Surfaces Aerodynamics**

Tables 1 and 2 provide a classification survey of the computational methodology aspects used by the studies presented in this review. The studies reviewed herein are identified and numbered according to the ice shape where “R” stands for roughness ice, “S” stands for streamwise ice, “H” stands for horn ice, and “SR” stands for spanwise ridge ice. For all the respective studies, Table 1 outlines each turbulence model that was used while Table 2 lists the flow solver, meshing software, and meshing technique used in each case (N/A notes when corresponding info was not provided). If one considers the studies chronologically, there is a trend toward use of certain turbulence models based on a combination of increased robustness and/or increased computational resources that have occurred in the last three decades. This trend is shown in Fig. 8 by indicating the number of studies that utilize a certain turbulence model within a given 5-year period from 1990 to 2018. The figure also provides a qualitative view on the right side of the total number of times a given turbulence model is used by the studies reviewed in this paper. It can be seen that certain turbulence models have become less used over time. For example, among RANS approaches, the Baldwin-Lomax model was initially popular but has not been used in the past decade.

## **4 - Discussion of Computational Iced Airfoil Aerodynamics and Predictive Fidelity**

This section is broken up into four major parts based on the four major ice shapes (ice roughness, streamwise ice, horn/scallop ice, and spanwise ridge ice) examined by the various

studies. For each type of ice shape, this review paper will first analyze the various aerodynamic characteristics and flow physics captured by the studies reflected in Tables 3 to 5, and secondly analyze the predictive accuracy of each numerical method employed by the studies. The results will be summarized in Section 5 providing insight into the capabilities of the various approaches to help engineers best determine which numerical method may be most appropriate for a given geometry and flow condition and to provide recommendations to researchers for critical development needed in this area.

#### **4.1 – Ice Roughness**

There have been very few CFD predictions of the impact of ice roughness on airfoils and wings. As shown in Tables 1-3, studies R01 and R02 used a VLES approach combined with a Lattice-Boltzmann method to examine the effects of ice roughness on an extruded airfoil geometry. These studies analyzed a high-fidelity complex ice surface shape on an extruded NACA23012 airfoil. This ice shape had been obtained experimentally in the NASA IRT. The orthogonal and cross-sectional view of the leading edge of the airfoil with the ice shape can be seen in Fig. 11. Fig. 11b shows the ice roughness heights were on the order of 0.2% or less of the chord length. This would suggest a small impact on the aerodynamic characteristics of the extruded airfoil at low to moderate angles of attack. The impact of the ice roughness at angles of attack near stall is shown in Fig. 12. In this figure, it can be seen that at a moderate angle of attack the flow is well attached but there is strong separation at an  $\alpha = 12$ -deg. The authors attribute this separation to the presence of spanwise variation in the geometry of the ice shape, which then reduces the local health of the boundary layer. Such an early onset of separation can cause an earlier onset of stall and an increase in drag.

The comparison of experimental and predicted aerodynamic coefficients (lift, pitching moment, drag and pressure) for this case are shown in Figures 13 and 14. In general, the VLES method with the Lattice Boltzmann method well predicts the general trend of the aerodynamic characteristics at angles of attack up to and including 10-deg., but tends to show differences at higher angles of attack. Fig. 14 shows that at 10-deg., the pressure distribution was well predicted with some discrepancies near the leading edge of the geometry. Beyond 10-deg., the simulation does not accurately capture the location of stall reflected in the experimental lift and moment, nor the increase in drag. The simulation over predicts the stall angle by 1-degree. In general, this shows that roughness cases can be reasonably addressed with high-resolution CFD at angles of attack up to the stall angle.

#### **4.2 – Streamwise Ice**

Streamwise ice is another case which has been the subject of very few CFD studies, since, again, the impact of ice on the aerodynamics is typically weak. As shown in Table 3, there is only one streamwise ice study that met the current review criteria (a recent study with experimental validation). For study S01, the authors used RANS k- $\epsilon$  to examine a streamwise ice shape accreted on an extruded NACA23012 airfoil, based on experiments in the IRT. The high-resolution mesh created by the authors to detail the complex surface structure of the ice shape along the leading edge of the geometry can be seen in Fig. 15. The simulated gauge pressure contour plots for the clean and iced extruded NACA23012 airfoil at 0-deg. are shown in Figures 16a and 16b. The iced

case shows an enhanced greater suction peak along the upper surface, but a reduced suction pressure along the lower surface when compared to the un-iced geometry. This indicates that the ice effectively increases the camber of the airfoil causing greater lift. In general, the pressure coefficient prediction at  $\alpha = 0$ -deg. is rather good as shown in Fig. 16c, though the lower surface suction peak is not as high as that given in the experiments, where there may be a small degree of separation.

The impact of Reynolds and Mach number on the coefficient of lift is shown in Fig. 17. From this figure, it is worth noting that the error between the experimental and computational values decreases as the Reynolds number increases. This trend is consistent with RANS approaches generally having greater success as the Reynolds number gets larger. Once again, this is the only study that analyzed streamwise ice and met the criteria for this review. Based on the data provided, streamwise ice was not reasonably addressed by the numerical method employed over the range of angles of attack examined by the study.

### 4.3 – Horn and Scallop Ice

Horn ice is one of the most analyzed ice shapes for CFD since it is a common icing condition that can have a strong impact on aerodynamics. As shown in Table 4, many of the horn ice studies are based on an extruded ice shape on an extruded GLC305 airfoil including unswept cases for H01 to H11, and swept cases for H12 and H13. For these studies, the authors used RANS – SA, RANS – SST, DHRL, DES, DDES, IDDES, and ZDES. The geometry for this ice shape on the GLC305, and an example of its extrusion, can be seen in Fig. 5. For airfoil geometries with horn ice shapes, a separation bubble generally forms aft of the horn as can be seen in Fig. 18. As the angle of attack increases, the predicted separation bubble becomes more pronounced and covers a majority of the upper surface of the extruded airfoil. However, as compared to the experimental data, the separation region extent is over-predicted by both RANS and time-averaged DES. Specifically looking at the 6-deg. case, the flow should reattach close to the mid-chord, but both the RANS and DES predict reattachment closer to the trailing edge of the extruded airfoil, though DES has a slightly better prediction.

Drilling into 6-deg. specifically, Fig. 19 combines data from studies H08 to H10 at three chord-wise locations (from  $x/c = 0.15$  to  $0.55$ ) in comparison to experimentally measured streamwise velocity profiles. In general, all of the simulations fail to predict the velocity distributions in the vicinity of the separation bubble, though RANS – SA, IDDES, and ZDES performed the best. Aft of the experimentally measured separation region at  $x/c = 0.55$ , the simulations also fail to predict the quantitative characteristics of the flow field. For capturing the general trend of the streamwise velocity profiles at both  $x/c = 0.55$  and  $0.75$ , SA is the best RANS model, while ZDES is the best HRL model.

Fig. 20 provides a comparative look of the studies in terms of their ability to capture the distribution of pressure. At  $\alpha = 4$ -deg., similar to what was seen in the streamwise velocity contour plot, DES is able to capture the extent of the separation region, as characterized by the presence of a region of constant pressure or “plateau” feature along the upper surface, but not the exact pressure distribution in the region. As for RANS – SA and ZDES, they’re able to capture the maximum magnitude of the plateau characterizing the separation region in the pressure distribution, but not the extent of the separation region. For  $\alpha = 6$ -deg., none of the simulations accurately capture the pressure distribution, e.g.  $C_p$  errors are as large as 30% for certain portion of upper surface for each

of the methods. This is important, since the upper surface is where the flow will generally first separate. DES has the best matching distribution in terms of matching the separation region, while IDDES and ZDES are able to capture the magnitude of the plateau in the pressure distribution more closely. With regards to the lower surface, all of the simulations tend to line up with one another with DHRL being the largest outlier near  $x/c = 0.5$ .

In terms of integrated performance, Fig. 21 shows that the coefficient of lift is accurately predicted by both DES and DDES, while ZDES differs by a slight percentage at  $\alpha = 6$ -deg. For RANS – SA, it's able to accurately capture low angles of attack, but begins to diverge around  $\alpha = 4$ -deg. and fails to capture the maximum coefficient of lift. The coefficient of drag plot shows that RANS – SA, DES, and ZDES underpredict the value of drag with RANS – SA being the worst of the three models. Overall, while the numerical methods employed were unable to accurately predict the flow field and pressure distribution for this iced case, DES, DDES and ZDES were able to predict the integrated performance well. However, by just having the integrated performance be correct, does not prove the simulation provide accurate results. This is an instance where the simulations produce the correct results for the wrong reason by not properly replicating the pressure distribution curves which nominally represent the flow field around the iced geometry.

Study H14 used ILES to examine a different ice horn than studies H01 to H13 on the leading edge of an extruded GLC305 airfoil. As seen in in Fig. 10, this study examines a high-fidelity version of the ice shape that includes spanwise variation. Fig. 22 takes a look at the separation of the flow aft of the via a Q-criterion iso-surface plot. As the angle of attack increases from 4-deg. to 12-deg., the size of the turbulent structures that define the separation grow in size. Comparing, the iso-surfaces at  $\alpha = 12$ -deg. and 15-deg., turbulence structure present in the flow are relatively similar and do not provide as large of a contrast as 4-deg to 12-deg. Overall, this figure provides some insight to the level of separation aft of the ice horn and shows that the inclusion of the ice shape on the leading edge of the extruded airfoil creates unsteadiness in the flow.

With regards to the unsteadiness present in the flow, Fig. 23a provides information regarding the effects of the turbulent structures on the coefficient of lift for the geometry. Combining Fig. 22 with Fig. 23, the size of the turbulent structures reflected in the iso-surfaces directly correlates to the amplitude of the fluctuation in the lift seen in Fig 23a. As the angle of attack increases and the turbulent structures increase in strength, the amplitude of the fluctuations in the coefficient of lift increases as well. The time-average of this data reflected in Fig. 23b, shows that ILES is able to predict the coefficient of lift at angles of attack up to 12-deg. However, the numerical method fails to accurately capture the coefficient of lift at 15-deg. and predicts that the lifting surface has stalled, which is not reflected in the experimental data. Overall, the study has shown that the flow physics and aerodynamic parameters can be well predicted by ILES up to moderate angles of attack, but fails to perform well at high angles of attack near stall.

Study H15 uses DES and DDES to examine an ice horn accreted on an extruded M5-6 airfoil, whose geometry can be seen in Fig. 24. Fig. 24 also shows that there are a number of turbulent structures along the upper surface of the extruded airfoil. The strongest of these fluctuations, which correspond to a separation region, are aft of the ice horn. The extent of the separation is indicated by the pressure plateau in the distribution of pressure in Fig. 25. Fig. 25a shows that the simulations at 8-deg. do not accurately capture the peak of the pressure distribution, but do capture the general extent of the separation plateau aft of the ice shape.

In terms of aerodynamic performance parameters, Fig. 26 shows that at moderate angles of attack leading up to stall, DES is able to accurately predict both the coefficient of lift and drag. Beyond 8-deg., the study only implemented DDES and Fig. 26 shows that it could not predict the coefficient of lift trend for the wing. The overprediction of the coefficient of lift is reflected in Fig. 25b. The time averaged DDES simulates a much higher-pressure distribution plateau as compared to the experimental data. For this study, the numerical methods were able to capture the resulting aerodynamic coefficients up to stall, but failed to accurately predict the flow physics and aerodynamic coefficients post-stall.

Studies H16 to H22 uses the RANS Baldwin Lomax method to examine the effect of an ice horn accreted to the leading edge of a straight-edged NACA0012 wing. As seen in Fig. 27, this ice shape was developed by simplifying an ice shape generated in the IRT. Studies H16 to H19 provide information of this simplified ice shape on an unswept extruded airfoil while H20 to H22 examines the ice shape on a swept wing with a sweep angle of 30-deg. For the former series of studies, the flow at  $\alpha = 4$ -deg. was largely attached while there was significant flow separation at  $\alpha = 8$ -deg. Insight of the aerodynamics and flow physics for this case is given by Fig. 28. Fig. 28 show that though the simulation over-predicts the pressure distribution peak in the separation region, the general trend remains similar to the experimental data. What is not reflected in Fig. 28, is that the paper also explored the difference between the 8-deg. case when the wall boundary condition was set to either a symmetry plane or a no-slip condition. Near the wall, without a symmetry plane condition set, the simulation failed to capture the pressure distribution near the root of the wing and predicts large amounts of separation. However, with the no-slip condition set, the simulation behaved more accurately in terms of pressure distribution. This difference emphasizes the necessity to properly define the fluid domain and its respective boundary conditions.

Studies H20 and H21 also used the Baldwin-Lomax model and Fig. 29 shows how the introduction of sweep can significantly change the flow physics of an iced wing. At 4-deg., a spanwise running vortex is present aft of the ice shape. Within this region, the flow is separated, but begins to reattach to the upper surface of the wing around a chord location of  $x/c = 0.20$ . This separation is also reflected in the pressure distribution shown in Fig. 30. As for  $\alpha = 8$ -deg., both the experimental and computational surface flow visualization show that the spanwise running vortex has effectively burst. This burst has caused the flow to completely separate over majority of the upper surface with some reattachment near the trailing edge of the wing. This point is reemphasized by the pressure distribution curves in Fig. 31. Progressing along the spanwise direction of the wing shows an increase in the size of the separation region and thus a decrease in the area of attached flow.

As seen in Fig. 32, the studies H16 to H19 were able to accurately capture the spanwise distribution of lift for straight-edged wing at  $\alpha = 4$ -deg. However, there were some inaccuracies for the geometry at an  $\alpha = 8$ -deg. As noted earlier, one of the major issues encountered by the studies was the setting of the wall boundary condition. For the case with the wall boundary condition set to be a symmetry plane, the simulation improperly predicted separation along the upper surface of the wing close to the root. This separation is reflected in the spanwise lift distribution. However, when the boundary condition is properly set to no-slip, the simulation still overpredicts the spanwise lift distribution at the wing tip. Overall, these studies have shown that Baldwin Lomax is able to accurately predict iced wing aerodynamics at low angles of attack, but presents some issues with flow separation.

Study H23 used DES and DDES to examine a different ice horn on an extruded NACA0012 airfoil. As shown in Fig. 33, this ice shape has a more complex profile and is not as smooth as the one in the previous studies. Fig. 34 shows both the level of detail captured by the simulations and how complex the flow aft of the ice horn can be. The instantaneous snapshot shows turbulent structures extending over majority of the chord. Figure 35 shows both qualitatively and quantitatively the separation and reattachment location of the flow. Fig. 35a shows that depending on the methodology employed, the reattachment location fluctuates between  $x/c = 0.4$  and  $0.6$ . On average, the reattachment location of  $x/c = 0.5$  agrees with the corresponding experimental data collected by Gurbacki. Fig. 35b shows that the fluctuation and variation of the reattachment location is not just present in the chordwise direction, but is also present in the spanwise direction.

In terms of aerodynamic coefficients, Fig. 36 shows that both methods were able to capture the general trend of the pressure distribution of the geometry when compared to the experimental data. However, the difference between the two methods can be seen in Fig. 37. The coefficient of lift is similar for both methods, but IDDES outperforms DDES when predicting the coefficient of drag over time. Though mesh resolution has not been discussed thus far in this review, Fig. 37 does show that with the proper discretization of the flow field, the flow field can be better simulated and thus allow for better prediction of the aerodynamic coefficients when compared to the experimental data. Both methods showed their ability to reasonably simulate the aerodynamics of an ice horn on an extruded airfoil before stall.

Studies H24 to H28 used VLES with the Lattice Boltzmann method, RANS, and DDES to analyze a horn ice on an extruded NACA23012 airfoil. As seen in Fig. 38, studies H24 and H25 examined an ice shape with no spanwise variation, while H26 to H28 examined the same ice shape with spanwise variation. Fig. 39 combines both the instantaneous and time-averaged Mach/velocity contour plots from studies H25 and H27. In the figure, both studies present similar instantaneous and time-averaged separation bubbles just aft of the ice horn and illustrates the complexity of the turbulent flow structures along the entire chord of the lifting surface. Specifically comparing Fig. 39a to Fig. 39c and Fig. 39b to Fig. 39d, the similarities in the flow physics between the different ice shapes are consistent with the conclusions made by Bragg *et al.* [4] in their review. Spanwise variation in an ice shape is not always important to capture when predicting its impact on the aerodynamics of a lifting surface. However, this should still be studied case by case in order to ensure independence of spanwise variation.

Fig. 40 compares the pressure distribution of the two ice shapes at angles of attack of 6 and 12-deg. Studies H26 to H28, which used VLES, was able to more accurately capture the overall trend of the pressure distribution at both angles of attack. DDES overpredicts the extent of the separation region and does not accurately follow the trend of the pressure distribution along the upper surface. In terms of aerodynamic coefficients, Fig. 41 compares the coefficient of lift, drag, and moment for VLES against the experimental data. For coefficient of lift and drag, VLES generally performs well, but over predicts the values around the stall angle. For the coefficient of pitching moment, VLES overpredicts the magnitude of the moment past stall. Overall, these studies show that DDES and VLES are able to accurately predict the aerodynamics of an ice horn on an extruded NACA23012 airfoil up to stall.

A lot of the studies mentioned henceforth have examined ice shape geometries that were based on ice accretions obtained in an icing research tunnel. However, studies H29 and H30 used RANS and DES to analyze the aerodynamic impact of a simplified geometry that replicates the basic geometrical description of a horn ice shape. As the height of the ice horn becomes larger, so does

the corresponding separation bubble. Thus, the airfoil/wing geometry will stall at increasingly lower angles of attack. Figure 42 shows both the geometry of the ice shape and the resulting flow field for a very large ice horn height. The result shows massive separation over majority of the upper surface at a relatively low angle of attack of 3-deg, consistent with previous experimental studies [4]. This point is demonstrated via the pressure distribution in Fig. 43, which shows a large region of nearly constant upper surface pressure, indicating massive separation. Overall, RANS and DES are unable to reasonably predict the pressure distribution over this large ice horn. However, the DES approach used here was one of the first such simulations and did not include sufficient resolution to capture three-dimensional instabilities (see Fig. 42).

#### 4.4 – Spanwise-ridge Ice

Studies SR01 to SR03 use RANS, DES, and IDDES to examine a forward-facing quarter round shape on the upper surface of an extruded NACA23012 airfoil. The shape has a height equivalent to 1.39% of the chord length and is placed at a location of  $x/c = 0.10$ . As seen in Fig. 44, this shape is a simple geometric representation of spanwise ridge ice. Similar to horn ice, a number of experimental studies have shown that this simple quarter-round shape is effective in simulating the aerodynamics of a realistic spanwise ridge ice [4]. Fig. 45 shows instantaneous vorticity contours comparing DES to IDDES. Both methods show that aft of the ice shape, the flow is complex and there are a number of turbulent structures. The two-dimensional contour plot in the figure shows a small recirculation bubble forming just ahead of the ice shape. As noted in Section 2, this recirculation region tends to be present for spanwise ridge ice shapes.

In regards to the accuracy, Fig. 46 examines the pressure distribution for these studies. Both models can capture the general shape of the pressure distribution, but fail to capture the exact value of the distribution on both the upper and lower surface of the extruded airfoil. The inability of the models to capture the pressure distribution is also reflected in the coefficient of lift plot shown in Fig. 47. For  $\alpha = -6$ -deg. to 0-deg., RANS is able to predict the coefficient of lift, but underpredicts the value between  $\alpha = 0$ -deg and 5-deg. and does not capture the stall reflected in the lift curve. For DES, the model is not able to fully capture the trend of the lift curve, and overpredicts the lift before stall and under predicts the lift after stall.

Studies SR04 to SR07 use RANS – SA, RANS –  $k-\omega$  SST, EARSM  $k-w$ , RSM SSG- $w$ , and ZDES to examine a realistic spanwise ridge ice shape on an extruded NACA23012 airfoil. As seen in Fig. 48, the ice shape is present on both the upper and lower surface of the geometry. Fig. 48 not only shows that this ice shape causes separation along both the upper and lower surfaces, but also causes a recirculation bubble to form just before the ice shape on the upper surface. The separations seen in the time-averaged velocity streamlines is reflected in the pressure distribution plot shown in Fig. 49.

In regards to the accuracy of these models to capture the pressure distribution at  $\alpha = 2$ -deg., all of the models are able to accurately calculate the pressure distribution along the lower surface of the geometry, but fail to predict the upper surface pressure distribution. All of the models except RANS – SA underpredict the pressure plateau, while RANS – SA overpredicts the pressure peak and does not exhibit the pressure plateau that indicates the presence of a separation region aft of the ice shape. Despite these short comings, RANS – SA is the closest model in generally predicting the trend of the distribution.

Fig. 50 compares the ability of the models to capture the aerodynamic coefficients against one another. RANS – SA was the only model to be employed for all of the angles of attack investigated by the studies. This model captures the coefficient of lift and drag accurately up to  $\alpha = 2$ -deg., but then begins to underpredict the values. For the coefficient of moment, RANS – SA over predicts the value up to  $\alpha = 4$ -deg, and then follows the experimental trend more accurately. Beyond  $\alpha = 0$ -deg., DRSM was generally the most accurate model for calculating the coefficient of lift. However, ZDES performed better at  $\alpha = 2$ -deg. For the coefficient of drag, DRSM, EARSM, and ZDES overpredict the values, while RANS – SA and RANS – k-w SST underpredicts the values. None of the models were able to accurately capture the coefficient of moment values well until  $\alpha = 4$ -deg. Overall, these studies show the complexity in the predicting the flow field around ice shapes and proves that more work needs to be done in order to properly model the flow field around this specific spanwise ridge ice shape.

Study SR08 was the last study to examine a spanwise ridge ice shape. This study used RANS – SA to simulate the flow field of a quarter-round artificial spanwise ridge ice shape placed on the upper surface of a reflection plane type wing based on a laminar flow airfoil. The geometrical shape had a height equivalent to 0.328% of the chord length and was placed at a location of  $x/c = 0.01$ . A two-dimensional cut of the wing and ice shape can be seen in Fig. 51. From Fig. 51, the inclusion of the ice shape creates a separation bubble along the lower surface of the wing. Upstream of the ice shape, there is a small separation bubble present as well. Due to the wing geometry, the large plateau observed in Fig. 52 does not correspond to the typical plateau used by this paper to characterizes a separation region and does not reflect the separation bubble seen in Fig. 51 and. The study notes that by zooming in on just the leading-edge portion of the wing, the sudden peak in the pressure seen in the Fig. 52 is the beginning of a pressure plateau that grows in size when the angle of attack increases beyond 11-deg.

In regards to accuracy, the study only examined the aerodynamics and flow physics of the geometry at a relatively low angle of attack of 7-deg. For this angle of attack, the simulation was accurate in calculating the pressure distribution. As seen in Fig. 52, the largest discrepancy between the simulated and experimental results comes near the trailing edge where the simulation does not exactly capture the pressure recovery. With regards to accuracy in terms of the other aerodynamic coefficients, the simulation is reported by the study to predict the coefficient of lift within 1% and the coefficient of drag within 3%. Overall, the numerical methodology employed by this study was able to reasonably resolve the flow field over a spanwise ridge ice shape on a laminar wing before stall.

## **5 – Summary, Conclusions and Recommendations**

### **5.1 – Summary of Techniques Used, Rationale for Choices, and Overall Effectiveness**

The objectives of this review were to provide a comprehensive survey on experimentally-validated CFD studies of the aerodynamic impact of ice on lifting surfaces in the last three decades. It is the first such review to the authors’ knowledge and complements previous reviews on experimental studies of icing aerodynamics done by Lynch & Khodadoust [3] and Bragg *et al.* [4]. This section offers a summary to engineers who seek to understand the capabilities and characteristics of the numerical methods and to researchers who seek to develop computational methods to support new understanding of icing on airfoil and wing geometries. The guidance below makes use of

- Definition of key aspects for the iced geometries and numerical methodologies from Section 2.
- Examination of the turbulence models and meshing techniques from Section 3.
- Capability and accuracy of the various CFD approaches from Section 4.

This information can be leveraged prior to selecting a numerical methodology (including mesh and turbulence model) for a study to best employ the user's available time and resources. In the following, key information is summarized from each of these sections.

In Section 2, the key aspects of an iced airfoil/wing computational study were broken up into two main categories: iced airfoil/wing geometry and aerodynamics, and numerical methodologies. For the former category, the first key aspect was to define the type of lifting surface being analyzed by a study: extruded airfoil, wing section, or wing. The second key aspect was to define the different ice shapes and their potential impact on a lifting surface's aerodynamics. The four main ice shapes were ice roughness, streamwise ice, horn ice, and spanwise ridge ice. Ice roughness introduces elements to the leading edge of a lifting surface that have a height much larger than the local boundary layer and creates boundary-layer transition and trailing-edge separation. Streamwise ice tends to have the smallest aerodynamic impact similar to roughness and its effect is not noticed until moderate to high angles of attack, except in drag coefficient. Horn ice is characteristically known to have features that protrude into the oncoming flow at an angle and thus creates large separated flow regions aft of the horn. Spanwise ridge ice tends to form downstream of the leading edge and act as a flow obstacle that not only cause separation aft of the features, but also recirculation regions upstream of the features. The aerodynamic impact can be significant because spanwise ridges are typically located in the adverse pressure gradient region of the clean airfoil.

Though Section 2 introduced the key aspects of the numerical methodologies, Section 3 explored these aspects in depth. Paramount of these aspects is the treatment of turbulence, which are primarily separated into three categories for the icing studies reviewed herein: Reynolds-Averaged Navier-Stokes (RANS), Large Eddy Simulation (LES) and Hybrid RANS/LES (HRL). These three approaches have much different objectives and computational resolution requirements. RANS is the most efficient of the computational methods due to modeling all of the turbulent structures in a flow. Due to its inability to capture turbulent structures, researchers have found that RANS can tend to not accurately predict complex geometries or fully separated flows. In order to provide more accurate results at a lower computational cost than DNS, researchers developed LES. This method resolves only the large eddies within the flow and models the smaller turbulent length scales. However, researchers have found that LES is inefficient for some engineering flows and requires a highly refined domain discretization in order to model small turbulent length scales. As a bridge between RANS and LES, researchers have developed hybrid RANS-LES (HRL) models to accurately and efficiently capture the boundary layer and flow separation in various flows.

In terms of meshing technique, the three key aspects are mesh dimensionality, mesh type and mesh resolutions. In terms of mesh dimensionality, a 3-D mesh is needed if any of the following aspects occur: a) the lifting surface is three-dimensional (e.g. a wing or wing section with wing-tip, taper and/or twist), b) the turbulence model resolves the turbulent structures (e.g. use of HRL or LES), and c) the ice-shape has spanwise variation such that the surface of the geometry has to be discretized appropriately. If three-dimensionality is to be employed, the number of grid points will be much larger, which will significantly impact the amount of computational resources required to accurately capture the flow. In terms of mesh type, either a structured, unstructured,

or hybrid mesh can be utilized. Generally, structured meshes are chosen when the geometry is simple and capturing the spanwise variation of the ice shape is unimportant. Some of the studies have proven that a subset of structured meshes, chimera/overset mesh, does well in discretizing the space around a complex geometry. Unstructured meshes are usually chosen when the geometry is more complex and the spanwise variation is important to capture. In order to leverage the pros and cons of both meshes, some studies in this paper used a hybrid mesh. Hybrid meshes allow the discretization of the ice shape surface in order to capture important features, switches to a structured grid in order to provide proper discretization of the boundary layer flow, and then either uses a structured or unstructured grid to define the rest of the domain. The proper selection of the mesh type and mesh resolution greatly influences the ability of the turbulence models to perform accurately throughout the flow.

In Section 4, the computational studies were grouped according to the type of ice shape examined. For each group of studies, the predicted flow physics was reviewed, as well as the accuracy of the numerical methodology to capture the aerodynamic performance parameters. For the case of roughness ice, the study reviewed in this paper found that in order to accurately predict the flow field around ice roughness, the surface of the geometry must be fully defined. The height and spanwise variation of the ice roughness plays a significant part in the boundary layer transition and separation. Thus, if a mesh does not properly discretize either the surface of the wing or the wall normal direction, the flow field could be incorrectly computed. An unstructured mesh would work well in maintaining the features of each ice element. In the wall normal direction, resolving the boundary layer plays a large part in ensuring the proper simulation of the flow field around the airfoil. A structured grid is ideal for smoother boundary layer regions as this reduces numerical dissipation and improve accuracy of wall shear stress, which is critical to determine any flow separation.

For the case of streamwise ice, experimental studies have found that there is little spanwise variation in the accumulation of streamwise ice for unswept geometries, but the roughness can play an important role. Thus, hybrid meshes can be used due to their ease of implementation in capturing both the surface geometry and the boundary layer. For geometries with sweep, spanwise ice surface variation becomes more significant as the degree of sweep increases, and thus introduces complex three-dimensionality in the surface meshing. A structured grid is ideal in resolving the wall normal direction with a similar argument to the ice roughness case. A small separation bubble can occur at the junction of the ice shape followed by an attached boundary layer that is not as full when it reaches the adverse pressure gradient after the section peak. This, along with the surface roughness, reduces health of the boundary layer and can then cause early onset of airfoil trailing edge stall or even full separation. Therefore, appropriate treatment is needed with a focus on a high-resolution structured mesh with nodes focused in the separation bubble and near the point at which downstream separation may occur. If the overall geometry is too complex for a structured grid throughout, an unstructured or chimera mesh can be used beyond the boundary layer to define the rest of the domain.

Ice roughness and streamwise ice are very similar in their effect on the aerodynamic parameters and flow field. In particular, these ice shapes accrete onto the leading edge in a conformal way that effectively extends the geometry and thus primarily impacts the aerodynamics of the leading edge of the airfoil. The two main components of the ice shape that drives the change in aerodynamics are: 1) the aft juncture between the ice shape and the airfoil, and 2) the roughness of the actual ice shape. At low angles of attack, researchers have found that RANS was sufficient

in resolving the flow field due to the lack of separation. As the angle of attack increases, HRL and LES proved to be more appropriate due to the early onset of flow separation over the lifting surfaces.

Due to the complex nature of horn ice and spanwise ridge ice, it is imperative to ensure that majority of the geometry is preserved throughout the meshing process or that a full geometry study is conducted. While some experimental data has shown that simplified geometries can produce the overall characteristic aerodynamics for these ice shapes, improper simplification of the ice shape without could lead to incorrect predictions of both the flow physics and aerodynamic coefficients. Researchers have either meshed the surface of the geometry with an unstructured grid, or have applied a chimera/overset grid to account for the complex shapes. The studies took special care to both ensure suitable mesh growth in the wall normal direction of the geometry in order to properly resolve the boundary layer, and ensure the region of shear layer emanating from the ice shape was well discretized.

Aerodynamics of horn ice and spanwise ridge ice shapes are generally more complicated to simulate than both ice roughness and streamwise ice since the flow separation regions for horn and ridge are significant even at small angles of attack. For both horn ice and spanwise ridge ice, depending on the original geometry of the lifting surface the ice was accreted on, the spanwise variation can range from having a slight impact to having a considerable impact on the flow physics of the airfoil. The primary flow feature caused by the presence of these ice shapes is a large separation bubble aft of the features at most of angles of attack. In addition to this, due to the ice shape being farther downstream of the leading edge, the ice acts as a flow obstacle and produces a recirculation region upstream. Researchers have found that though RANS is able to capture the aerodynamic characteristics of the flow at low angles of attack, the utilization of this method washes out majority of the turbulent structures present in the flow. At higher angles of attack, the separation becomes a more pronounced and requires either HRL or LES to properly capture the turbulent structures that greatly influence the flow physics.

Overall, both the rationale for turbulence model selection and meshing techniques for each ice shape is very similar. The main differences between each ice shape that drives the selection of the turbulence model is the expected flow field behavior. At low angles of attack, researchers have found RANS to be sufficient. As the angle of attack increases however, the point at which a user should implement either an HRL method or LES becomes more dependent upon the ice shape and airfoil/wing geometry. Generally, ice roughness and streamwise ice tends to not have as high of an aerodynamic effect when compared to horn and spanwise ridge ice.

## **5.2 – Recommendations for Future Work**

CFD is a powerful tool that has been leveraged by engineers and researchers around the world. Since it's conception, it has been consistently developed upon and implemented in a number of fields. Within the first two decades of its implementation to the icing field, a lot of the studies conducted were done for two-dimensional airfoil geometries. However, as seen by the studies presented in this review, icing is not a two-dimensional phenomenon and cannot be evaluated as such. After the first decade of computational research, more effort was put into understanding the three-dimensional effect of icing on lifting surfaces. These studies have further cemented the fact that the turbulent structures caused by the presence of the ice shapes, are highly three-dimensional and complex in nature. CFD is able to provide crucial information regarding the flow physics

around an iced wing that would take considerable amount of resources and effort to do the equivalent experimentally. Thus, future studies must not rely on two-dimensional information to infer the impact of ice on lifting surfaces, and must analyze the effect of ice in a three-dimensional domain. However, the three-dimensional computational studies presented in this review brought to light three main gaps in knowledge regarding the simulation of flow field around an ice accreted lifting surface come to light. These points are as follows:

- 1) Lack of information understanding the full impact of implementing various numerical methods.
- 2) Selection of lifting surfaces and ice shapes to be analyzed.
- 3) Data collected and provided to analyze a given flow field.

As characterized and shown in this review, there are a large number of parameters that define a numerical simulation. Each one of these parameters can be uniquely selected and applied to a given case. These unique combinations of parameters can then potentially produce a variety of results for said case. However, in order to completely understand the ability of numerical methodologies to explore the effect of icing on the flow field of a lifting surface, it is necessary to limit the parameters that can be changed from simulation to simulation. In order to limit the parameters, more in-depth studies must be conducted amongst the community such that a clear understanding of how each parameter effects the overall solution is known, e.g. examining the impact of discretizing the space around a given geometry using a structured, unstructured, or hybrid mesh. For the example mentioned, general recommendations have been made thus far regarding which mesh to implement based on the studies reviewed. However, there is no concrete evidence for any single iced geometry that a structured mesh or an unstructured mesh outperforms the other. This fact can also be applied to the implementation of turbulence models. Only a few of the studies have individually analyzed more than two turbulence models for a given iced geometry.

The selection of the turbulence model also impacts the selection of lifting surfaces. The studies reviewed in this paper largely favored analyzing lifting surfaces that are well known experimentally. This selection is limited by the fact that numerical methodologies still require validation of accuracy and consistency. Therefore, to push the field to examine more complex lifting surfaces, further studies must be conducted in order to highlight which numerical methodologies can accurately and consistently predict the flow field around a given ice shape. Studies that analyze extruded airfoils and wing sections must go beyond the selection of just two turbulence models, and must compare against a multitude of models to understand the impact of each one.

CFD has the ability to provide copious amounts of information regarding the flow physics of a given geometry. However, a question still remains on what information is necessary to extract from simulations in order for a researcher to understand the full impact of ice accretion aerodynamically. For example, coefficient of lift derives from integrating the coefficient of pressure along the wing. However, it is possible for the coefficient of lift to be right, while the pressure distribution to be wrong. Thus, it is then necessary to turn towards the coefficient of moment to determine if the predicted flow field is similar to the one produced by the experimental data or not. The icing community needs to set guidelines as to which aerodynamic parameters are essential to understanding how ice accretion effects lifting surfaces. By doing so, researchers can then focus on obtaining and presenting crucial information back to the community regarding how a given ice accretion can degrade aerodynamic performance for a given geometry.

## Chapter 2 Tables

**Table 1 - List of studies and turbulence models used by each study.**

Reference	Study ID	Turbulence Model		
		RANS	Hybrid RANS/LES	Other
Ribeiro <i>et al.</i> [31]	R01, H24, H28	-	-	VLES
Konig <i>et al.</i> [32]	R02, H27	-	-	VLES
Jun <i>et al.</i> [33]	S01, H26	k-e	-	-
Thompson <i>et al.</i> [34]	H01	SA	-	-
Thompson <i>et al.</i> [35]	H02	SA	DES	-
Mogili <i>et al.</i> [36]	H03	SA	DES	-
Chi <i>et al.</i> [37]	H04	SA	-	-
Chi <i>et al.</i> [38]	H05, H06, H12, H13	SA	-	-
Alam <i>et al.</i> [39]	H07	-	DDES, DHRL	-
Li <i>et al.</i> [40]	H08	-	IDDES	-
Alam <i>et al.</i> [28]	H09	SA, k-w	DDES, DHRL	-
Zhang <i>et al.</i> [41]	H10, SR06	-	ZDES	-
Xiao <i>et al.</i> [42]	H11	-	DDES	-
Brown <i>et al.</i> [43]	H14	-	-	ILES
Lorenzo <i>et al.</i> [44]	H15	-	DES, DDES	-
Kwon <i>et al.</i> [45]	H16	BL	-	-
Potapczuk <i>et al.</i> [46]	H17, H20	BL	-	-
Bragg <i>et al.</i> [47]	H18, H21	BL	-	-
Khalid <i>et al.</i> [48]	H19	BL	-	-
Kwon <i>et al.</i> [49]	H22	BL	-	-
Butler <i>et al.</i> [50]	H23	-	IDDES	-
Oztekin <i>et al.</i> [51]	H25	SA	DDES	-
Kumar <i>et al.</i> [52]	H29	SA	-	-
Pan <i>et al.</i> [53]	H30, SR02	-	DES	-
Pan <i>et al.</i> [54]	SR01	-	DES	-
Hu <i>et al.</i> [55]	SR03	-	IDDES	-
Duclercq <i>et al.</i> [56]	SR04	-	ZDES	-
Costes <i>et al.</i> [57]	SR05	SA, k-e, RSM	ZDES	-
Costes <i>et al.</i> [58]	SR07	SA, k-e, k-w, EARSM, RSM	ZDES	-
Papadakis <i>et al.</i> [59]	SR08	SA	-	-

**Table 2 - List of flow solvers and meshing techniques used by each study.**

Reference	Study ID	Flow Solver	Meshing Technique	
			Mesh Software	Mesh Type
Ribeiro <i>et al.</i> [31]	R01, H24, H28	PowerFlow	N/A	Structured
Konig <i>et al.</i> [32]	R02, H27	PowerFlow	N/A	Structured
Jun <i>et al.</i> [33]	S01, H26	National Combustion Code	Pointwise	Hybrid
Thompson <i>et al.</i> [34]	H01	Cobalt	GridTool/Vgrid	Hybrid
Thompson <i>et al.</i> [35]	H02	Cobalt	GridTool/Vgrid	Hybrid
Mogili <i>et al.</i> [36]	H03	Cobalt	GridTool/Vgrid	Hybrid
Chi <i>et al.</i> [37]	H04	Fluent-UNS	N/A	Structured
Chi <i>et al.</i> [38]	H05, H06, H12, H13	Fluent-UNS	N/A	Structured
Alam <i>et al.</i> [39]	H07	ANSYS Fluent	ANSYS Gambit	Hybrid
Li <i>et al.</i> [40]	H08	N/A	N/A	Structured
Alam <i>et al.</i> [28]	H09	ANSYS Fluent	ANSYS Gambit	Hybrid
Zhang <i>et al.</i> [41]	H10, SR06	FENSAP	N/A	Hybrid
Xiao <i>et al.</i> [42]	H11	NSAWET	N/A	Structured
Brown <i>et al.</i> [43]	H14	ANSYS Fluent	Pointwise	Unstructured
Lorenzo <i>et al.</i> [44]	H15	elsA	N/A	Structured
Kwon <i>et al.</i> [45]	H16	N/A	N/A	Structured
Potapczuk <i>et al.</i> [46]	H17, H20	N/A	N/A	Structured
Bragg <i>et al.</i> [47]	H18, H21	N/A	N/A	Structured
Khalid <i>et al.</i> [48]	H19	NPARC	HYGRID	Structured
Kwon <i>et al.</i> [49]	H22	N/A	N/A	Structured
Butler <i>et al.</i> [50]	H23	ANSYS Fluent	Pointwise	Hybrid
Oztekin <i>et al.</i> [51]	H25	OVERFLOW	NASA Chimera Grid Tool	Structured
Kumar <i>et al.</i> [52]	H29	WIND	Gridgen	Structured
Pan <i>et al.</i> [53]	H30, SR02	WIND	Gridgen	Structured
Pan <i>et al.</i> [54]	SR01	WIND	N/A	Structured
Hu <i>et al.</i> [55]	SR03	N/A	N/A	Structured
Duclercq <i>et al.</i> [56]	SR04	elsA	ICEM-CFD Hexa	Structured
Costes <i>et al.</i> [57]	SR05	elsA	ICEM-CFD Hexa	Structured
Costes <i>et al.</i> [58]	SR07	elsA	ICEM-CFD Hexa	Structured
Papadakis <i>et al.</i> [59]	SR08	ANSYS Fluent	ANSYS ICEM	Hybrid

**Table 3– CFD studies that examined ice roughness and streamwise ice on extruded airfoils.**

Reference	Study ID	Base Airfoil	Swept or Unswept?	Extruded Ice Shape?	Examine Stall?	Reynold's Number ( $10^6$ )	Mach Number
Ribeiro <i>et al.</i> [31]	R01	NACA23012	Unswept	N	Y	1.8	0.18
Konig <i>et al.</i> [32]	R02	NACA23012	Unswept	N	Y	1.8	0.18
Jun <i>et al.</i> [33]	S03	NACA23012	Unswept	N	Y	1.0, 1.8	0.1, 0.18

**Table 4 - List of studies that examine horn/scallop ice on extruded airfoils and wings.**

Reference	Study ID	Base Airfoil	Swept or Unswept?	Extruded Ice Shape?	Examine Stall?	Reynold's Number ( $10^6$ )	Mach Number
Thompson <i>et al.</i> [34]	H01	GLC305	Unswept	Y	Y	3.5	0.12
Thompson <i>et al.</i> [35]	H02	GLC305	Unswept	Y	Y	3.5	0.12
Mogili <i>et al.</i> [36]	H03	GLC305	Unswept	Y	Y	3.5	0.12
Chi <i>et al.</i> [37]	H04	GLC305	Unswept	Y	N	1.8	0.185
Chi <i>et al.</i> [38]	H05	GLC305	Unswept	Y	Y	6	0.12
Chi <i>et al.</i> [38]	H06	GLC305	Unswept	Y/N	Y	6	0.12
Alam <i>et al.</i> [39]	H07	GLC305	Unswept	Y	N	3.5	0.12
Li <i>et al.</i> [40]	H08	GLC305	Unswept	Y	N	3.5	0.12
Alam <i>et al.</i> [28]	H09	GLC305	Unswept	Y	N	3.5	0.12
Zhang <i>et al.</i> [41]	H10	GLC305	Unswept	Y	N	3.5	0.12
Xiao <i>et al.</i> [42]	H11	GLC305	Unswept	Y	N	6	0.21
Chi <i>et al.</i> [38]	H12	GLC305	Swept	Y	Y	6	0.12
Chi <i>et al.</i> [38]	H13	GLC305	Swept	Y	Y	6	0.12
Brown <i>et al.</i> [43]	H14	GLC305	Unswept	N	Y	N/A	0.12
Lorenzo <i>et al.</i> [44]	H15	M5-6	Unswept	Y	Y	3	0.2
Kwon <i>et al.</i> [45]	H16	NACA0012	Unswept	Y	Y	1.5	0.12
Potapczuk <i>et al.</i> [46]	H17	NACA0012	Unswept	Y	Y	N/A	N/A
Bragg <i>et al.</i> [47]	H18	NACA0012	Unswept	Y	Y	N/A	?
Khalid <i>et al.</i> [48]	H19	NACA0012	Unswept	Y	Y	1.5	0.12
Potapczuk <i>et al.</i> [46]	H20	NACA0012	Swept	Y	Y	?	?
Bragg <i>et al.</i> [47]	H21	NACA0012	Swept	Y	Y	?	?
Kwon <i>et al.</i> [49]	H22	NACA0012	Swept	Y	Y	1.5	0.12
Butler <i>et al.</i> [50]	H23	NACA0012	Unswept	Y	N	1.8	0.171
Ribeiro <i>et al.</i> [31]	H24	NACA23012	Unswept	Y	Y	1.8	0.18
Oztekin <i>et al.</i> [51]	H25	NACA23012	Unswept	Y	Y	1.8	0.18
Jun <i>et al.</i> [33]	H26	NACA23012	Unswept	N	N	1	0.1
Konig <i>et al.</i> [32]	H27	NACA23012	Unswept	N	Y	1.8	0.18
Ribeiro <i>et al.</i> [31]	H28	NACA23012	Unswept	N	Y	1.8	0.18
Kumar <i>et al.</i> [52]	H29	NLF0414	Unswept	Y	N	1.8	0.18
Pan <i>et al.</i> [53]	H30	NLF0414	Unswept	Y	Y	1.8	0.18

**Table 5 - List of studies that examine spanwise ridge ice on extruded airfoils and wings.**

Reference	Study ID	Base Airfoil	Swept or Unswept?	Extruded Ice Shape?	Examine Stall?	Reynold's Number ( $10^6$ )	Mach Number
Pan <i>et al.</i> [54]	SR01	NACA23012	Unswept	Y	Y	2	0.21
Pan <i>et al.</i> [53]	SR02	NACA23012	Unswept	Y	Y	2	0.21
Hu <i>et al.</i> [55]	SR03	NACA23012	Unswept	Y	N	2.1	0.21
Duclercq <i>et al.</i> [56]	SR04	NACA23012	Unswept	Y	N	15.74	0.2
Costes <i>et al.</i> [57]	SR05	NACA23012	Unswept	Y	Y	15.74	0.2
Zhang <i>et al.</i> [41]	SR06	NACA23012	Unswept	Y	N	15.9	0.2
Costes <i>et al.</i> [58]	SR07	NACA23012	Unswept	Y	N	15.74	0.2
Papadakis <i>et al.</i> [59]	SR09	Custom Wing	Swept	N	N	3.8	0.134

Chapter 2 Figures

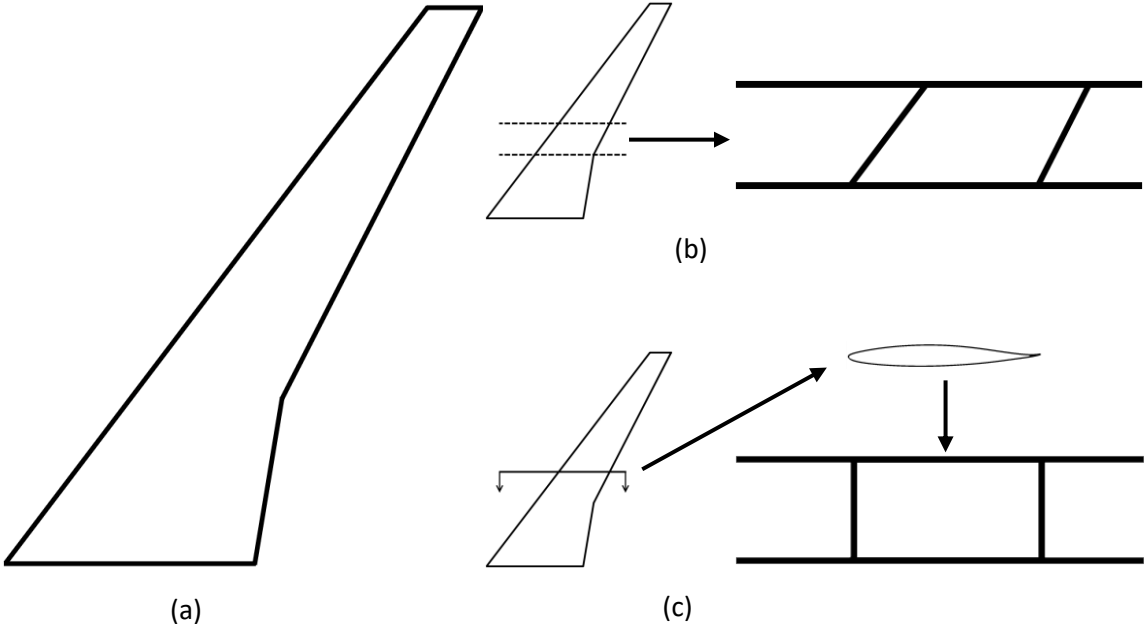


Fig. 1 a) Planform of CRM65 which is defined herein as a “wing” since it has a wing tip, alongside extractions of b) a “wing section” defined by the inclusion of taper or sweep, and c) an extruded airfoil.

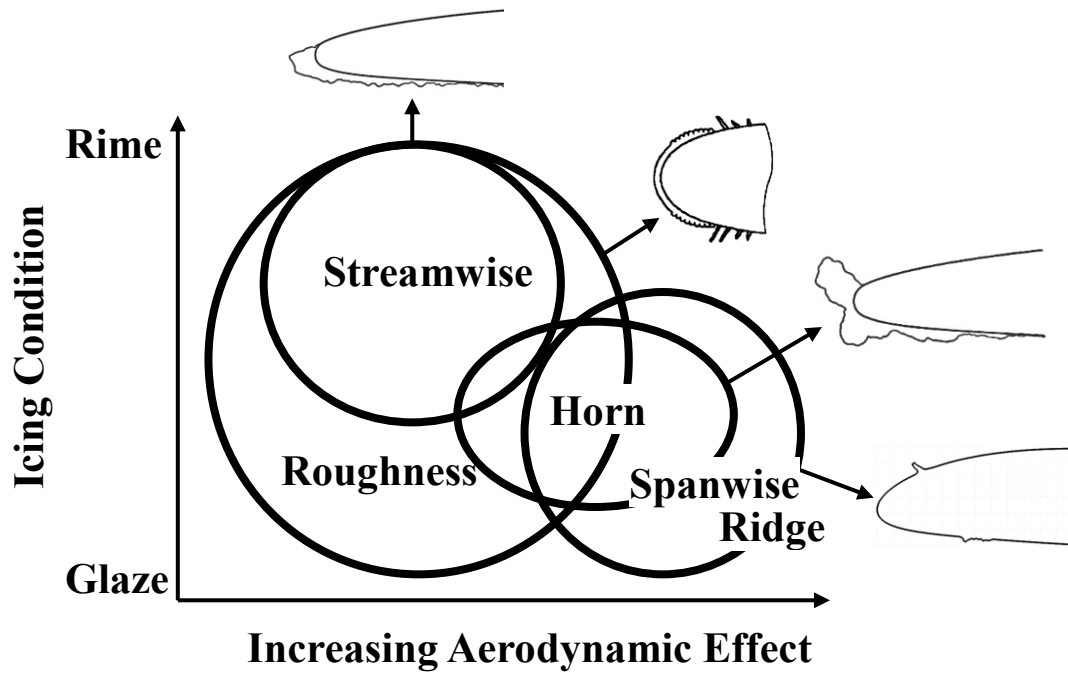


Fig. 2. Qualitative description of aerodynamic effects for various iced-airfoil flow fields in terms of conditions when they tend to occur and in terms of typical impact on aerodynamic performance, adapted from Ref. [4].

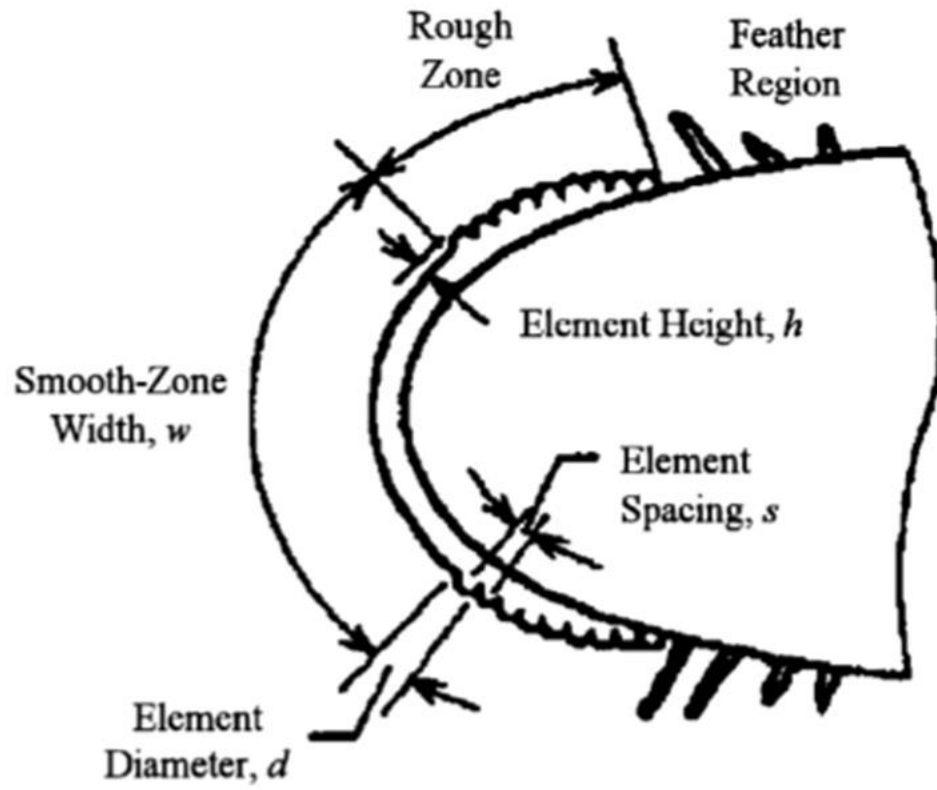


Fig. 3. Ice roughness features. [11]

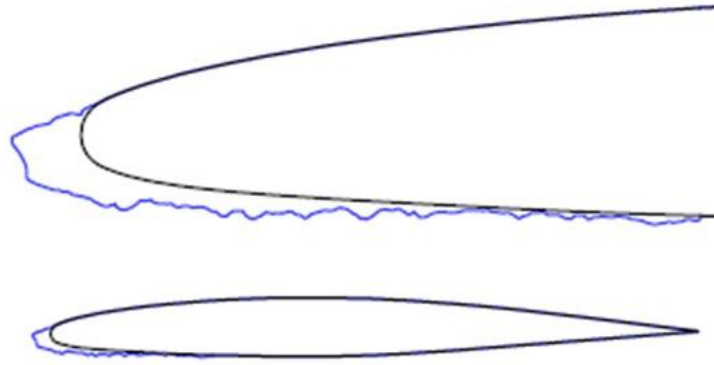


Fig. 4. Streamwise ice shape on leading edge of a GLC305 airfoil. [37]

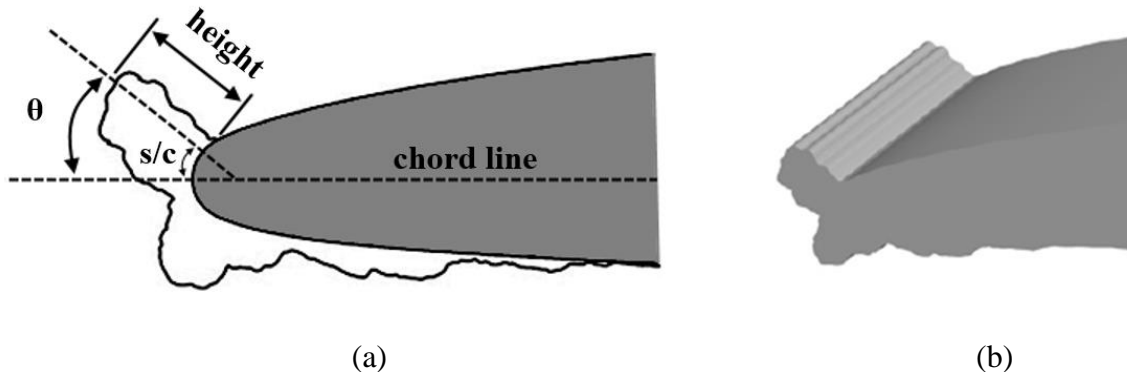


Fig. 5. a) Geometry of horn ice shape on an airfoil and b) spanwise extruded view of horn ice on an extruded airfoil based off of the GLC305 airfoil. [37]

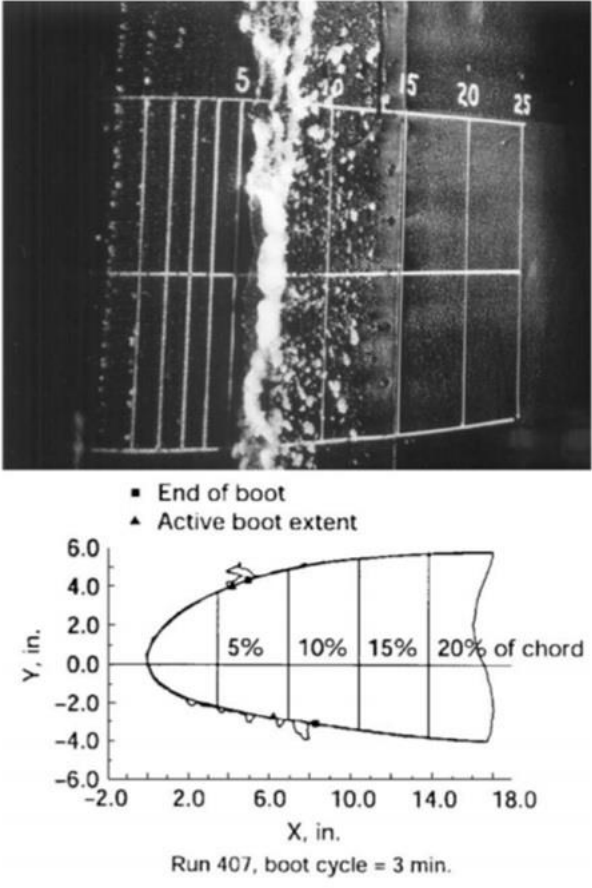


Fig. 6. Top and cross-sectional view of spanwise ridge ice shape captured via experimental studies. [4]

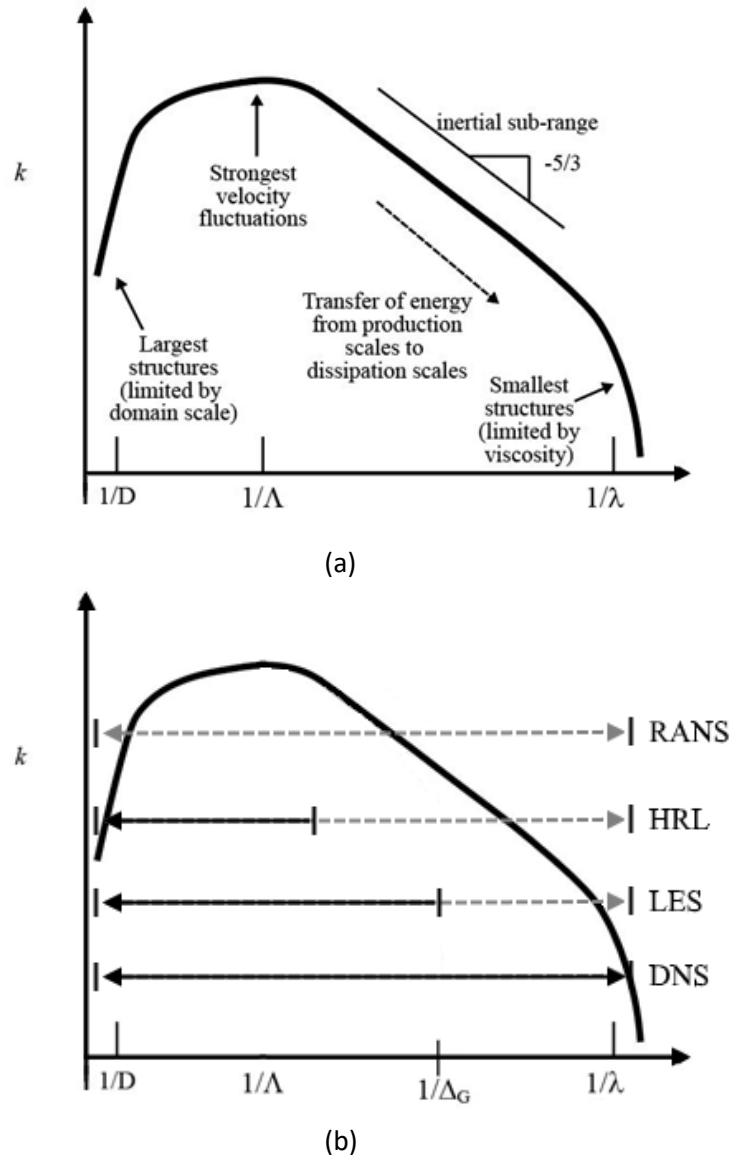


Fig. 7. a) Schematic of the specific turbulence energy spectrum plotted on a log-log scale. b) Spectrum overlaid by turbulence modeling techniques with ranges of resolved and modeled turbulence. Horizontal dashed grey lines: modeled turbulence; solid black lines: resolved turbulence.

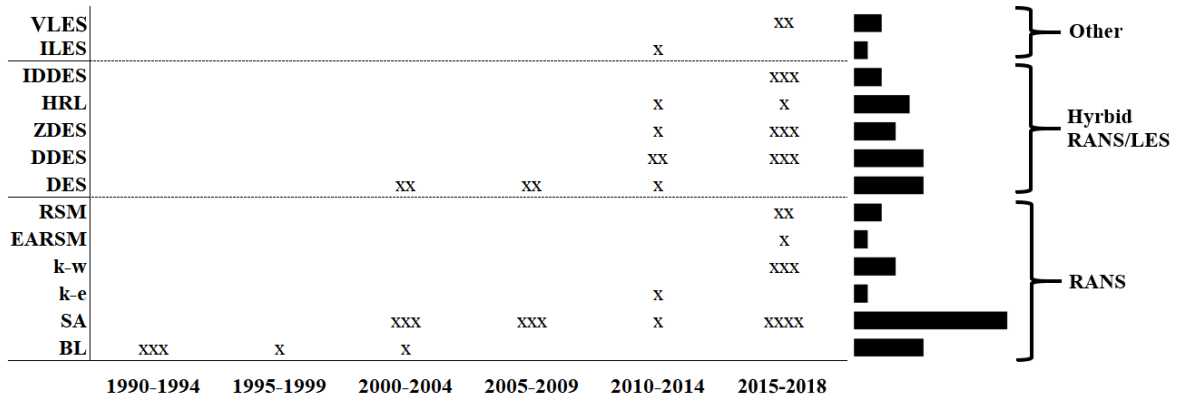
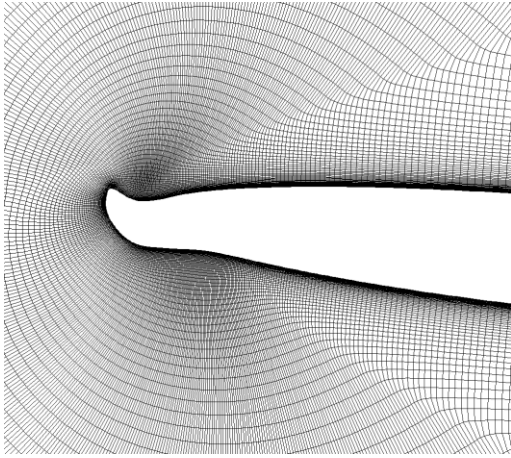
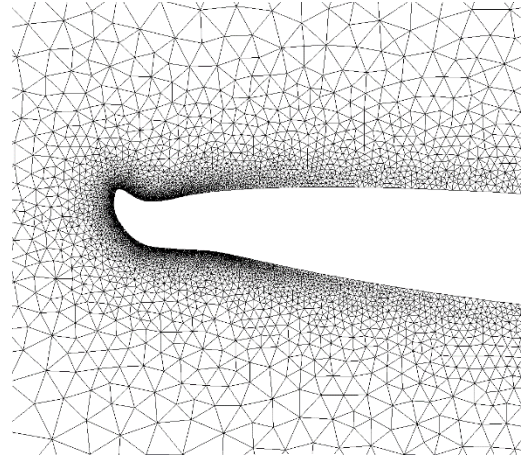


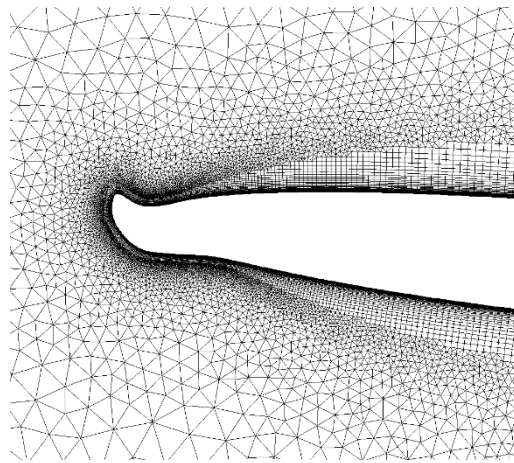
Fig. 8. Usage turbulence models from 1990 to 2018 for aerodynamics of iced airfoils and wings. The number of “x” values indicate when and how often a given turbulence model is used within a 5-year period and the right-hand bar chart summarizes total usage.



(a)



(b)



(c)

Fig. 9. View of cross-sectional cuts comparing the discretization of the domain surrounding an iced airfoil by using a) a structured, b) an unstructured, and c) a hybrid mesh.

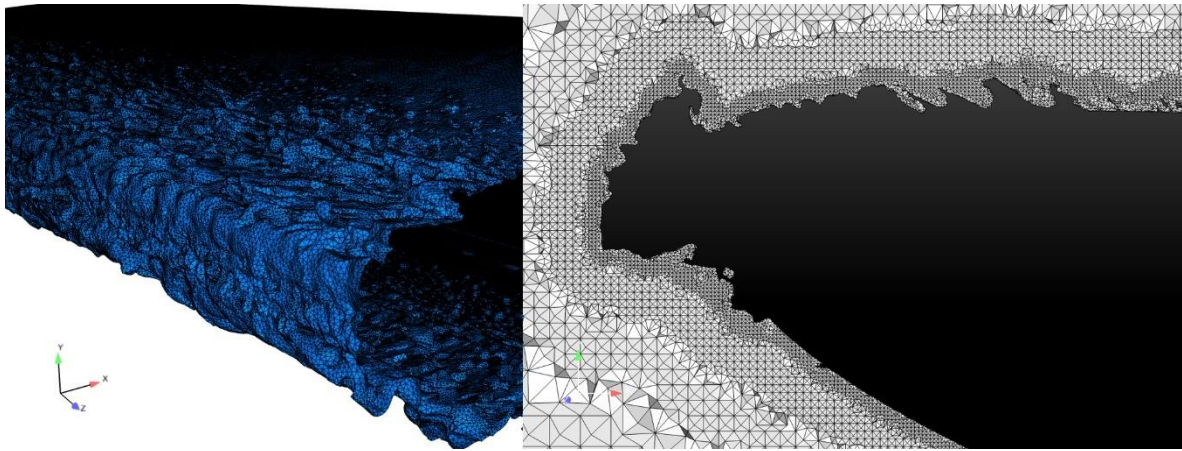


Fig. 10. High fidelity mesh view of horn ice accreted to leading edge of an extruded GLC305 airfoil. [43]

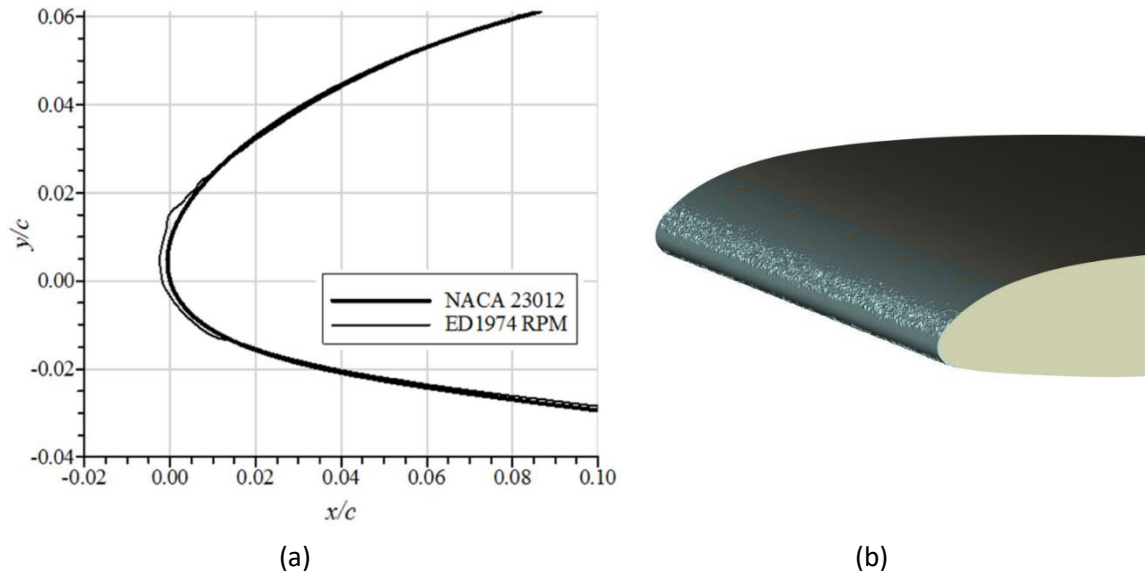


Fig. 11. a) Cross-sectional and b) orthogonal view of the ED1974 ice shape on the leading edge of an extruded NACA23012 airfoil. [31][32]

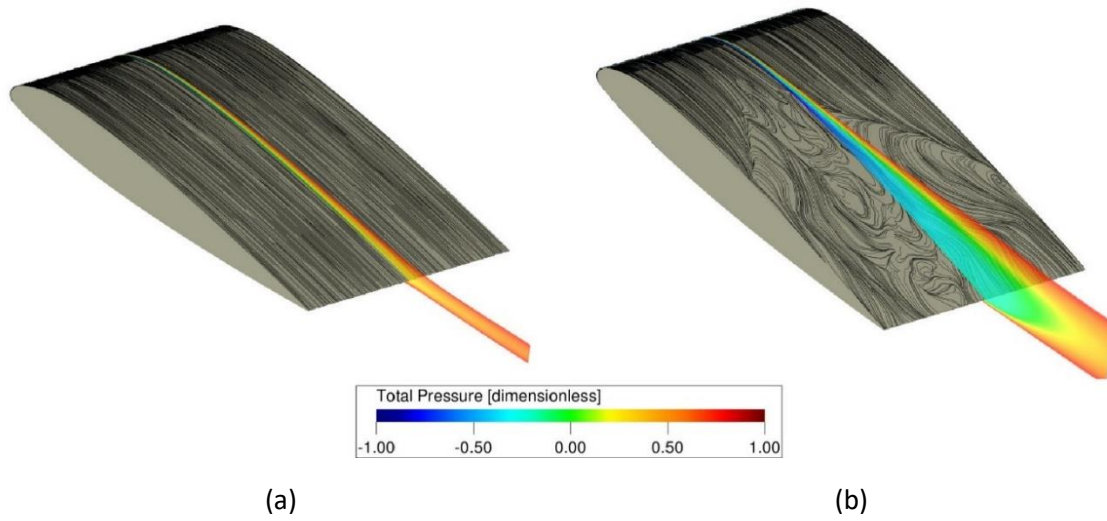


Fig. 12. Mean shear lines and total pressure midspan for ice roughness on extruded NACA23012 airfoil at a)  $\alpha = 6$  deg. and b)  $\alpha = 12$  deg. [31]

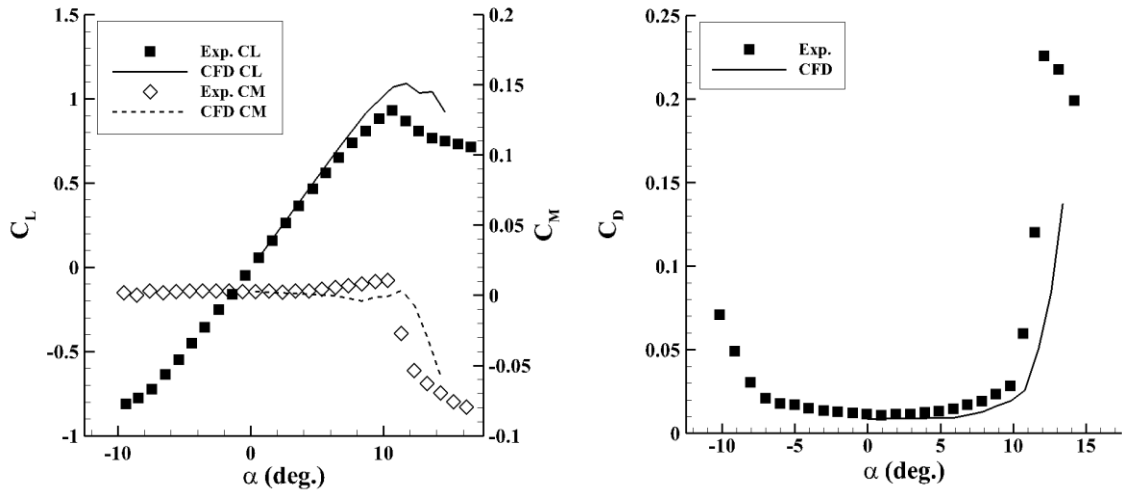


Fig. 13. Aerodynamic coefficient fidelity comparison for the iced extruded NACA23012 airfoil.  
[32]

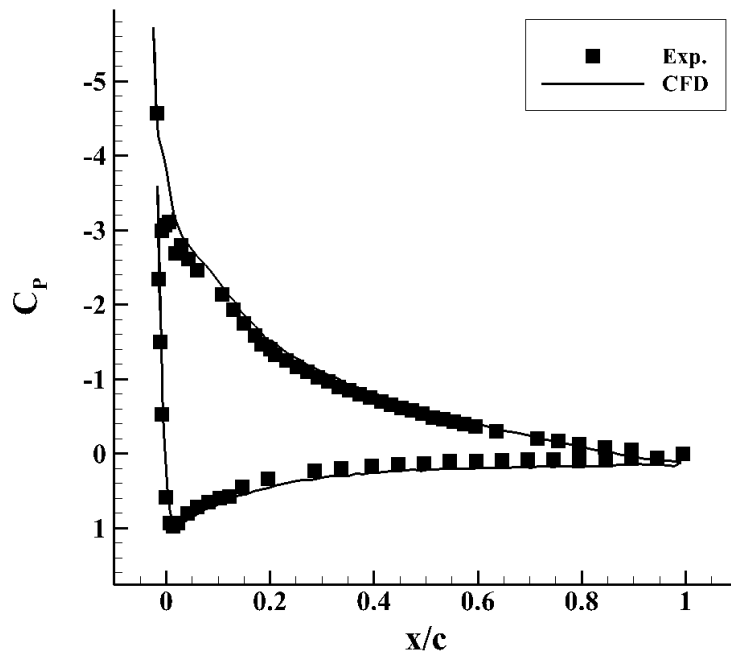


Fig. 14. Pressure distribution for ED1974 ice shape at 10 deg. [32]

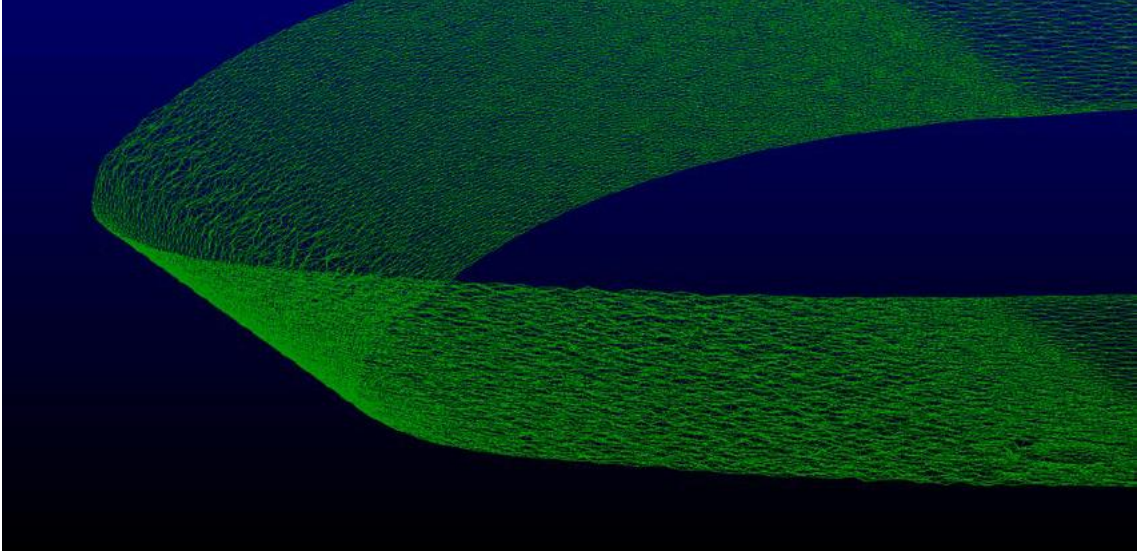
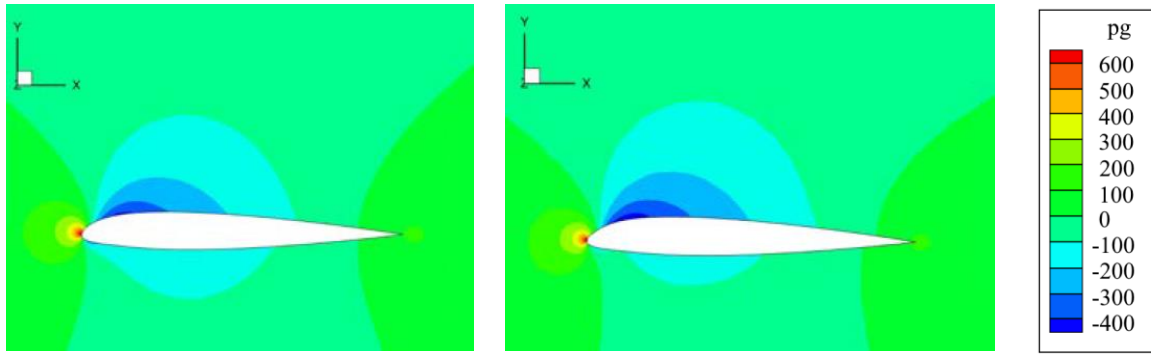
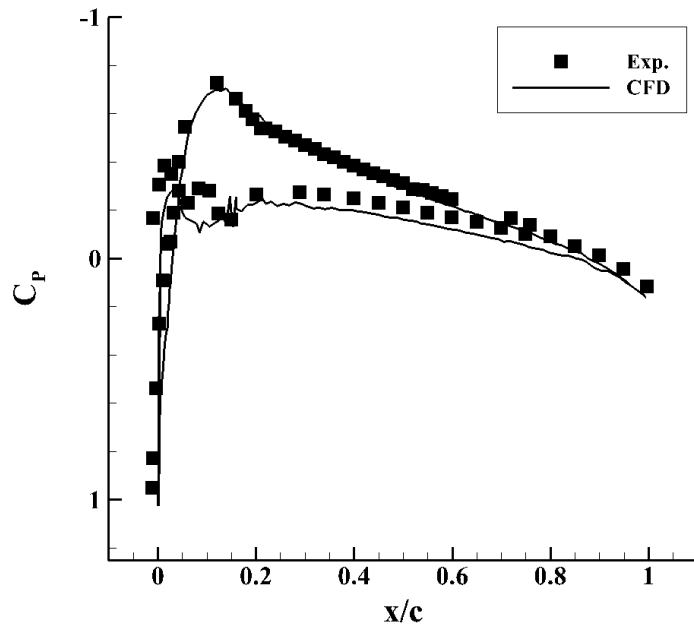


Fig. 15. High-resolution mesh geometry of streamwise ice accreted on leading edge of an extruded NACA23012 airfoil. [33]



(a)

(b)



(c)

Fig. 16. Gauge pressure contour for both the a) clean and b) iced extruded NACA23012 airfoil, and c) comparative pressure distribution for the iced NACA23012 at  $\alpha = 0$  deg. [33]

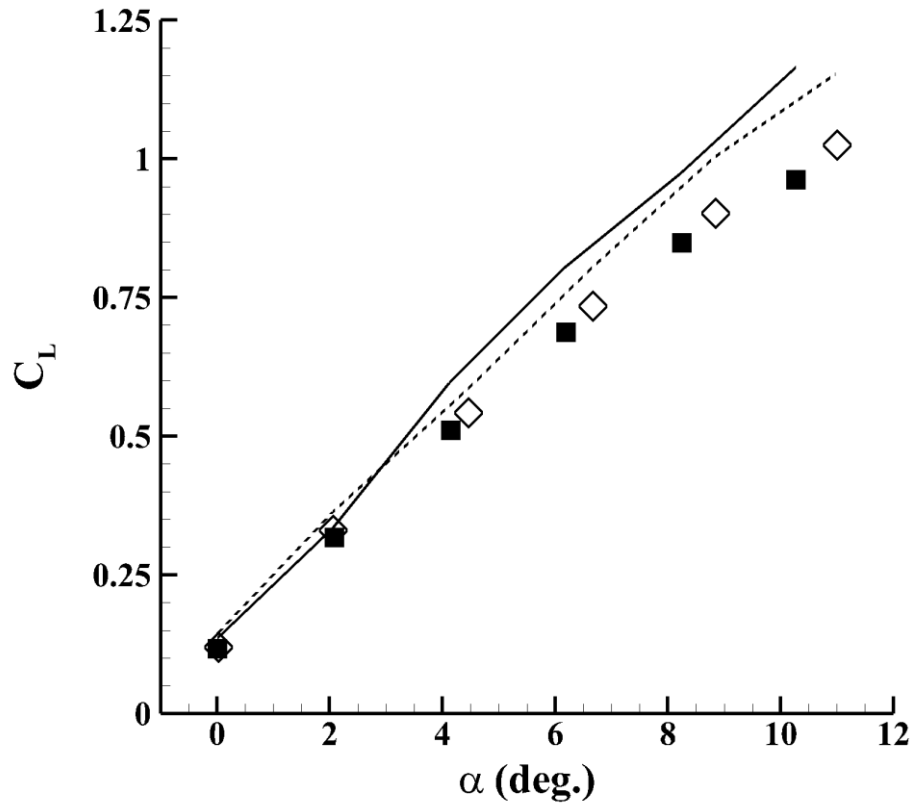


Fig. 17. Comparison of experimental (markers) and computational (lines) coefficient of lift for extruded NACA23012 airfoil with streamwise ice for  $Re = 1.0 \times 10^6$ ,  $M = 0.1$  (solid markers and line), and  $Re = 1.8 \times 10^6$ ,  $M = 0.18$  (hollow markers and dashed line). [33]

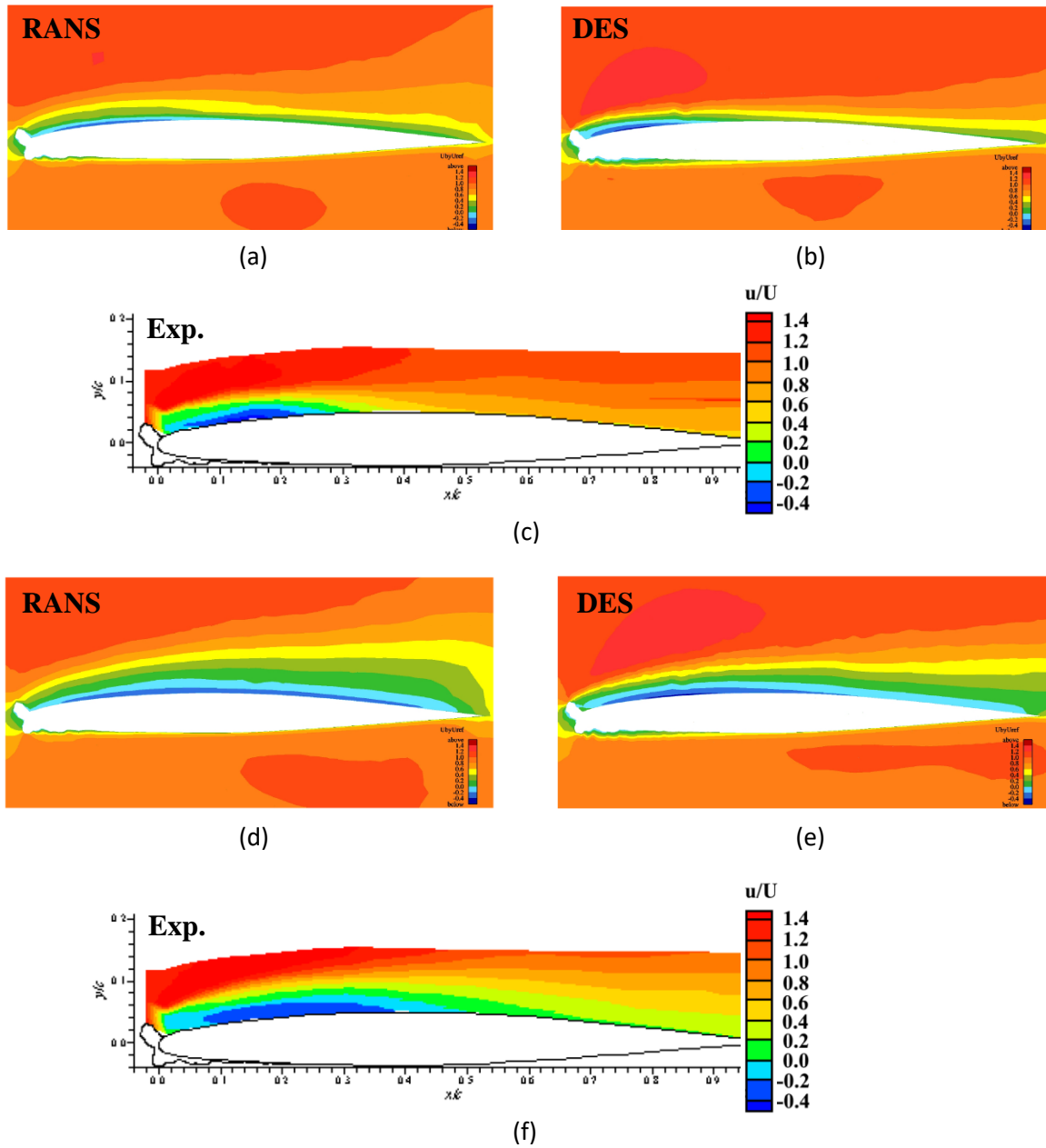


Fig. 18. Comparison of predicted midspan streamwise velocity contours against experimental data for extruded GLC305 airfoil with horn ice at angles of attack of a-c) 4 deg. and d-f) 6 deg. [36]

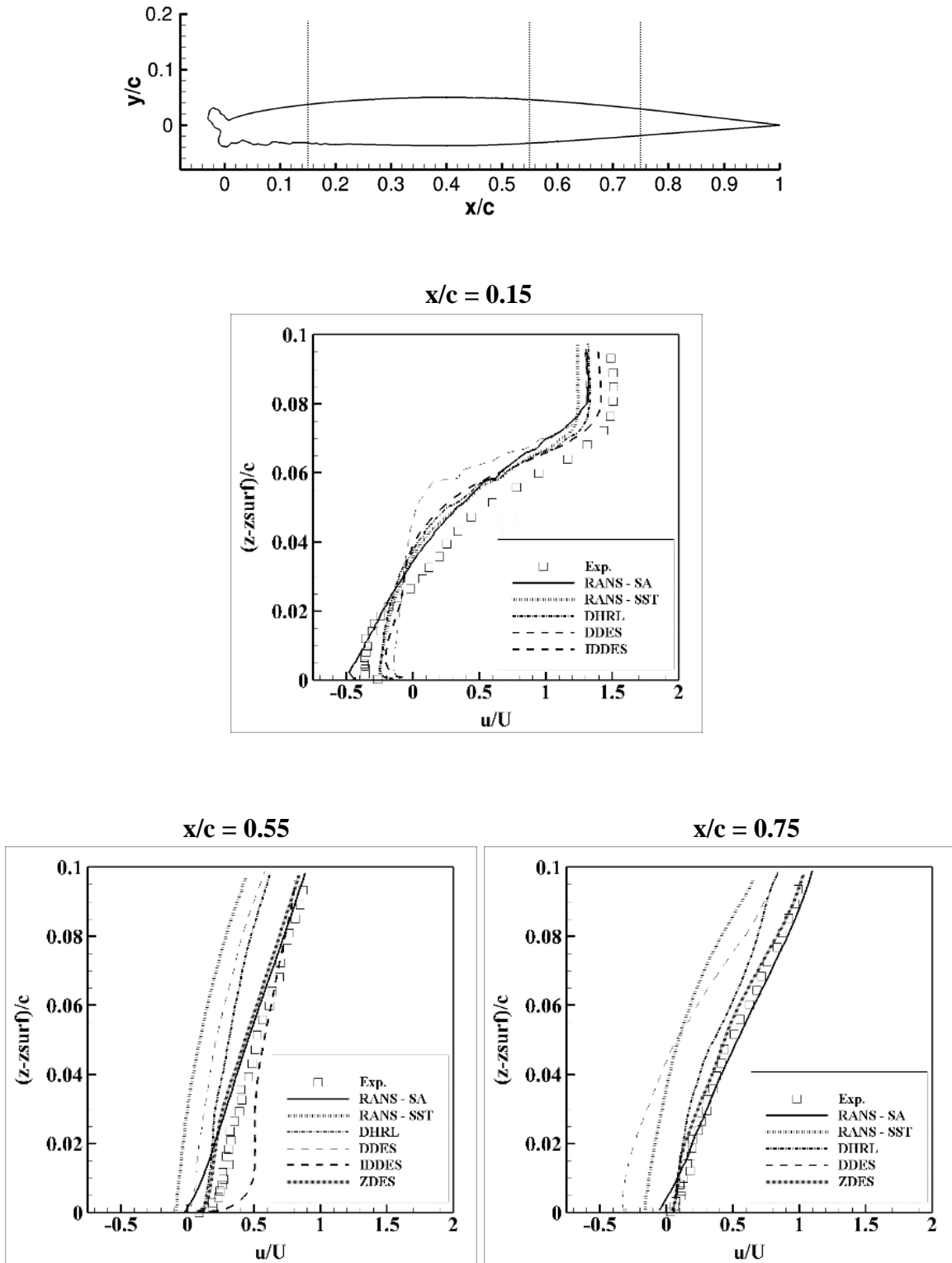
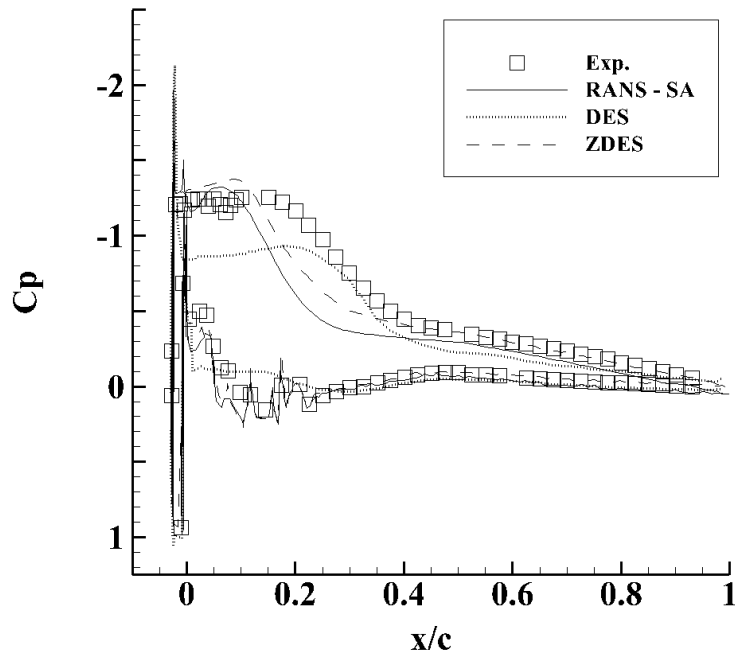
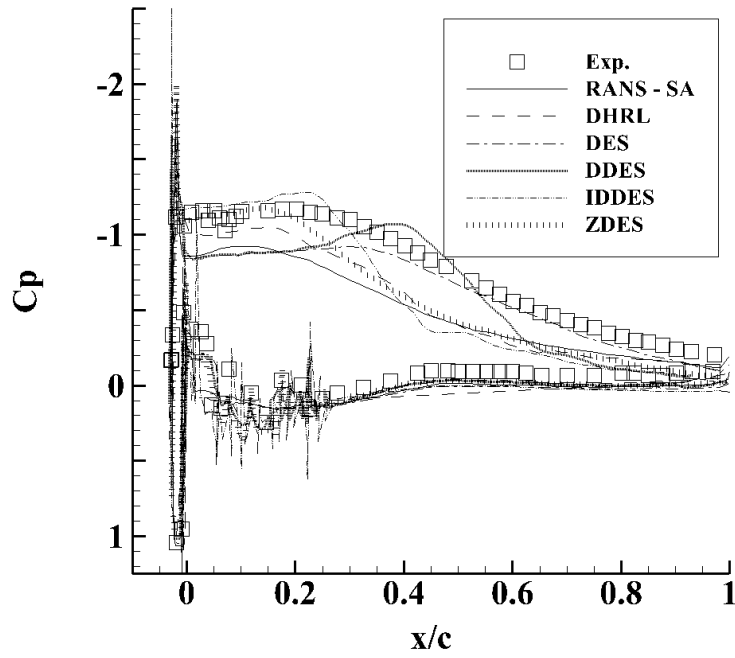


Fig. 19. Comparison of numerical methods to capture streamwise velocity over an iced extruded GLC305 airfoil at  $\alpha = 6$  deg. for various spanwise locations.

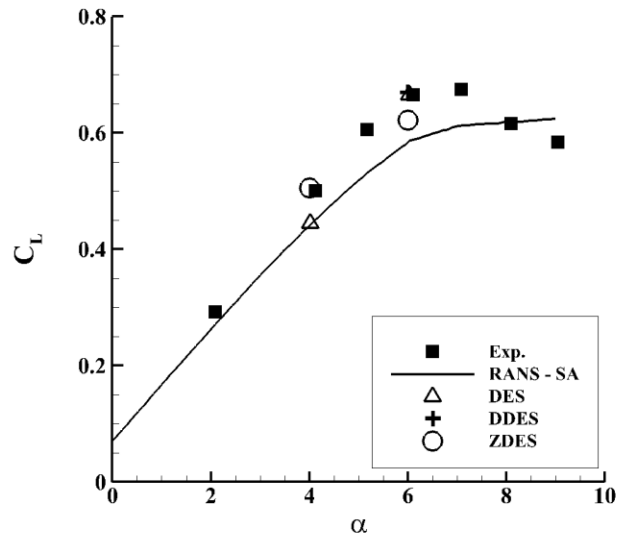


(a)

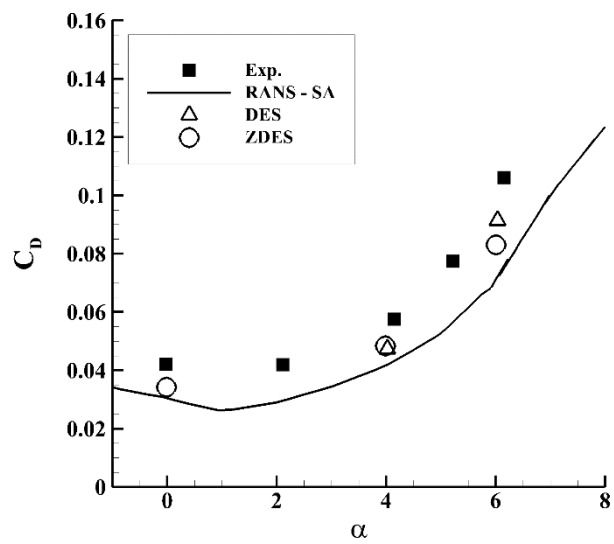


(b)

Fig. 20. Pressure distribution comparison for various numerical methods at angles of attack of a) 4 deg. and b) 6 deg.



(a)



(b)

Fig. 21. Comparison of aerodynamic coefficients for iced extruded GLC305 airfoil using various numerical methods.

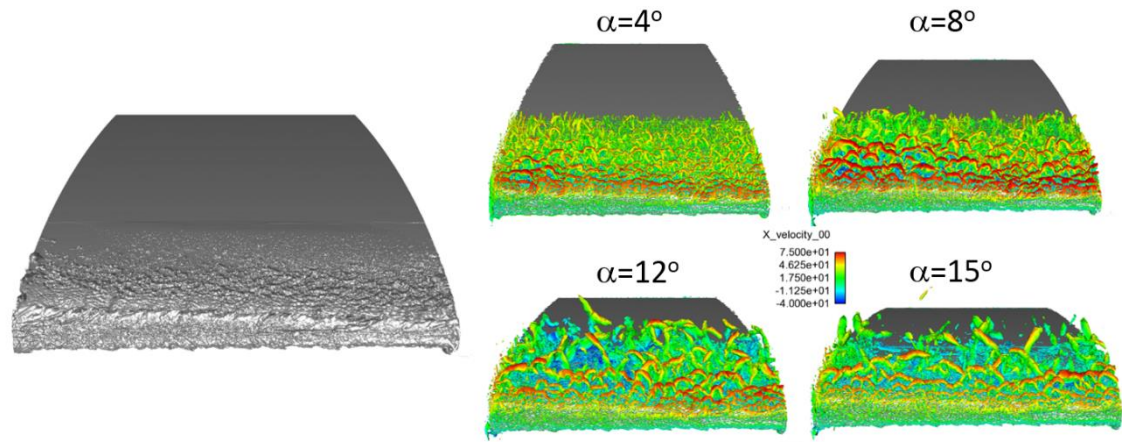


Fig. 22. Iso-surfaces of Q-criterion colored by streamwise velocity at various angles of attack. [43]

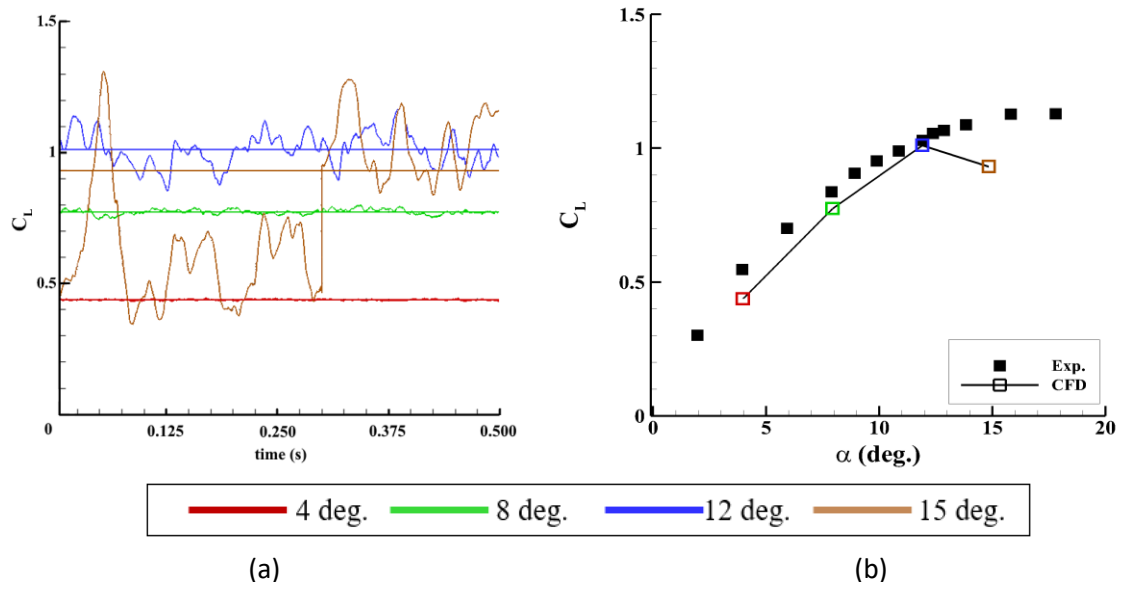
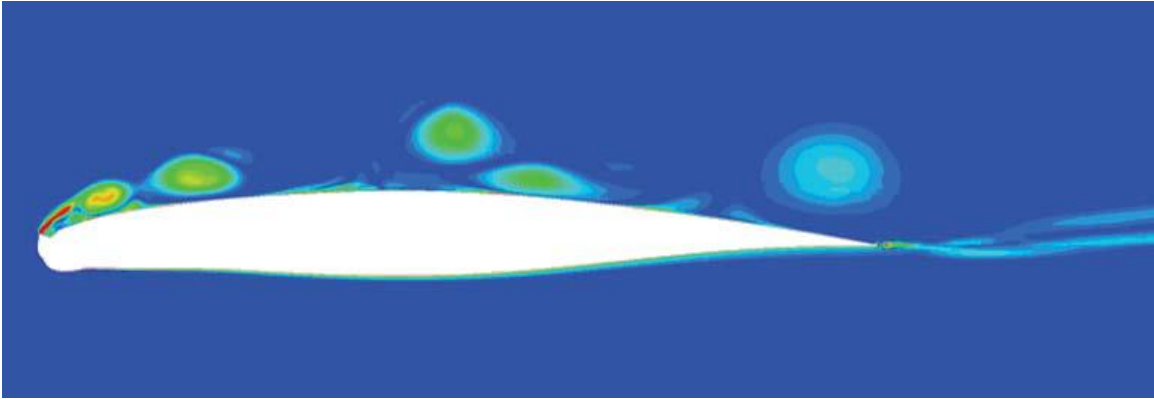
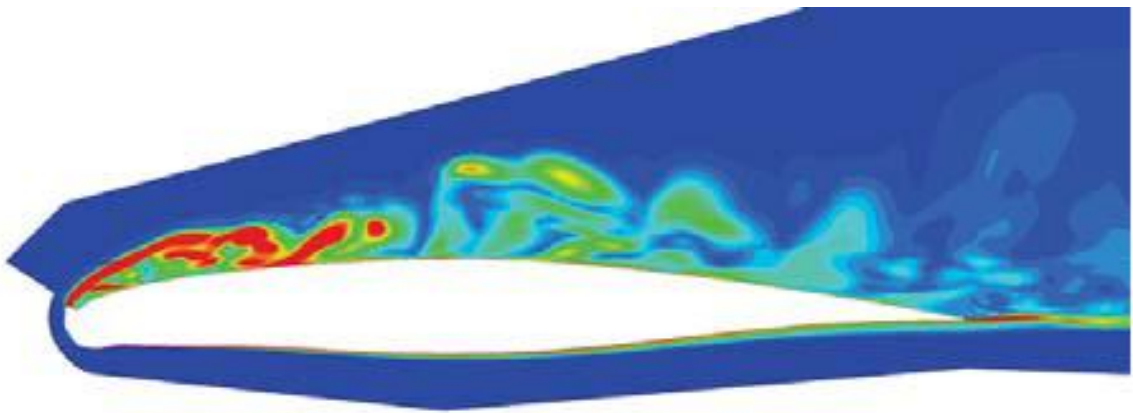


Fig. 23. a) Variation of coefficient of lift over time and b) time averaged coefficient of lift comparison for iced extruded GLC305 airfoil. [43]

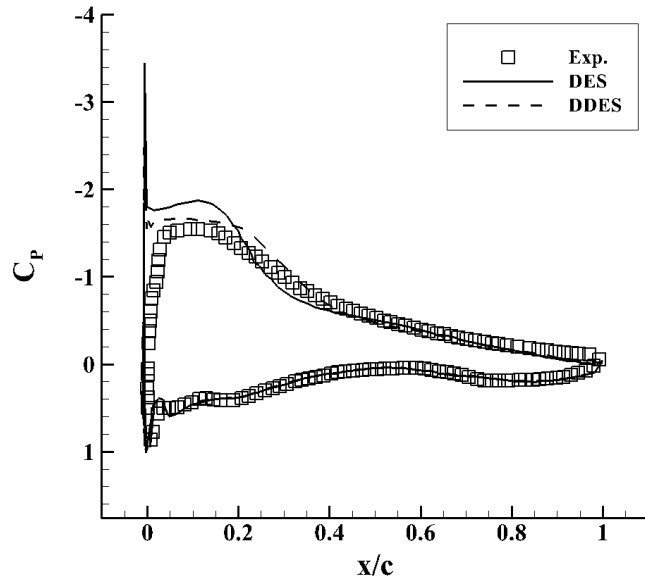


(a)

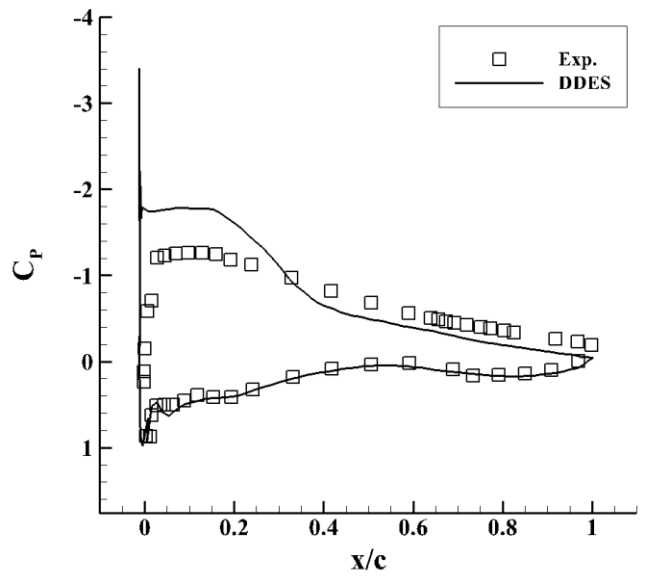


(b)

Fig. 24. Comparison of instantaneous velocity field for a a) 2D and b) 3D simulation. [44]

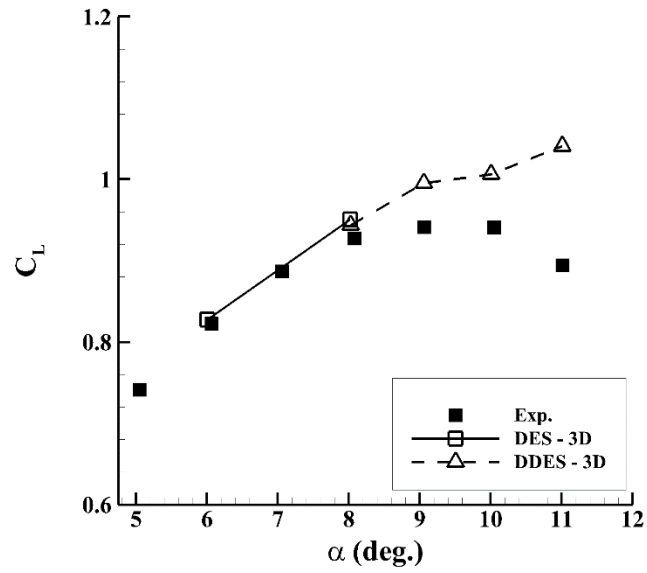


(a)

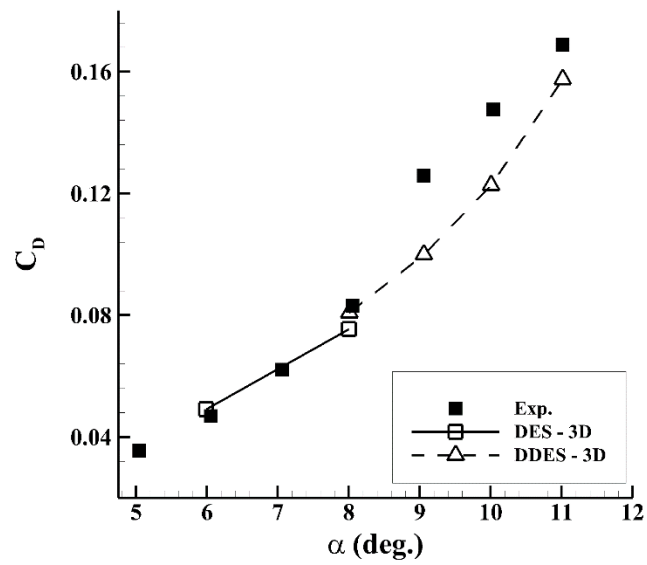


(b)

Fig. 25. Pressure distribution comparison for flow over an iced extruded M5-6 airfoil at angles of attack of a) 8 deg. and b) 9.05 deg. [44]



(a)



(b)

Fig. 26. Comparison of aerodynamic coefficients for iced extruded M5-6 airfoil. [44]

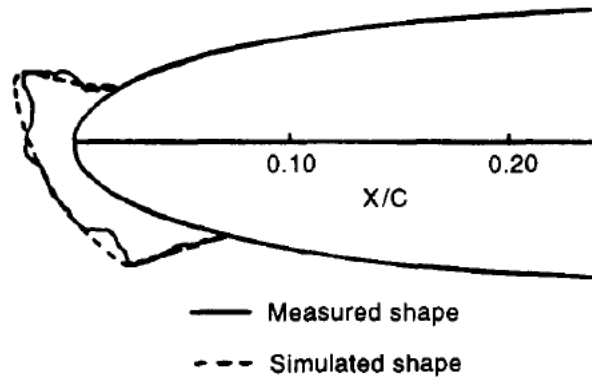


Fig. 27. Cross-sectional view of measured and simplified horn ice shape on leading edge of a NACA0012 airfoil. [47]

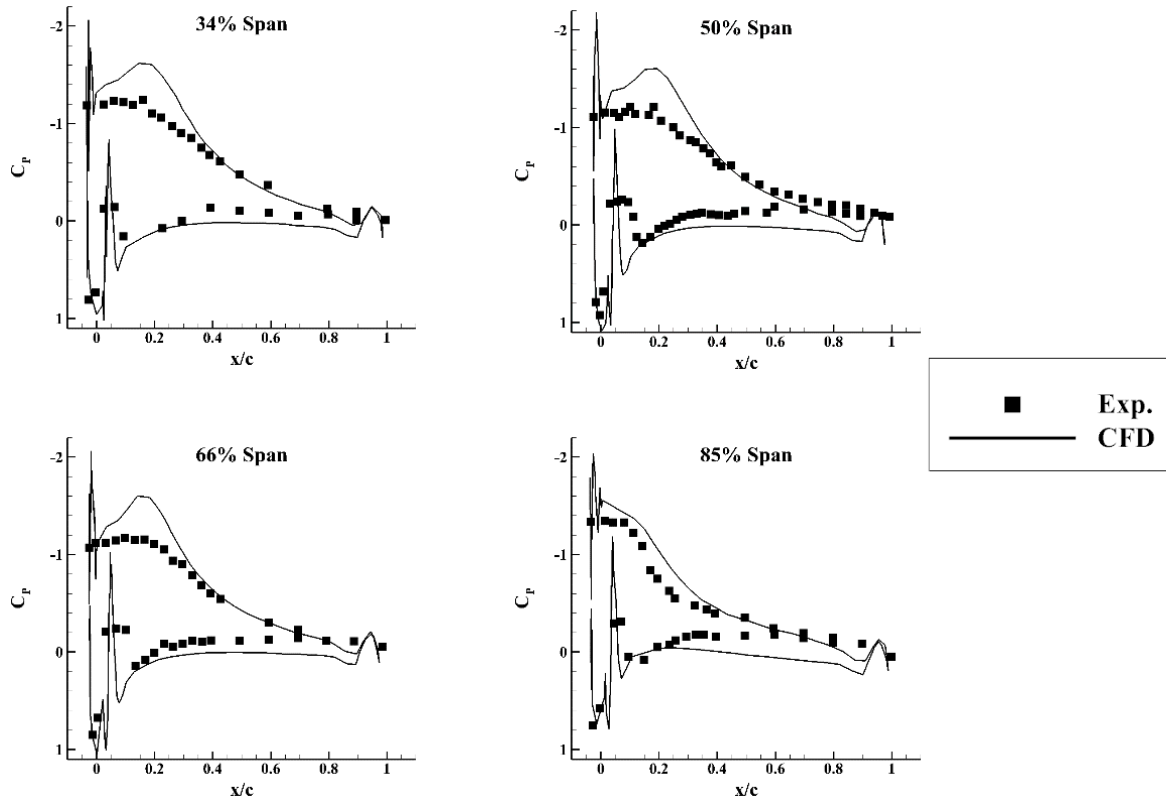
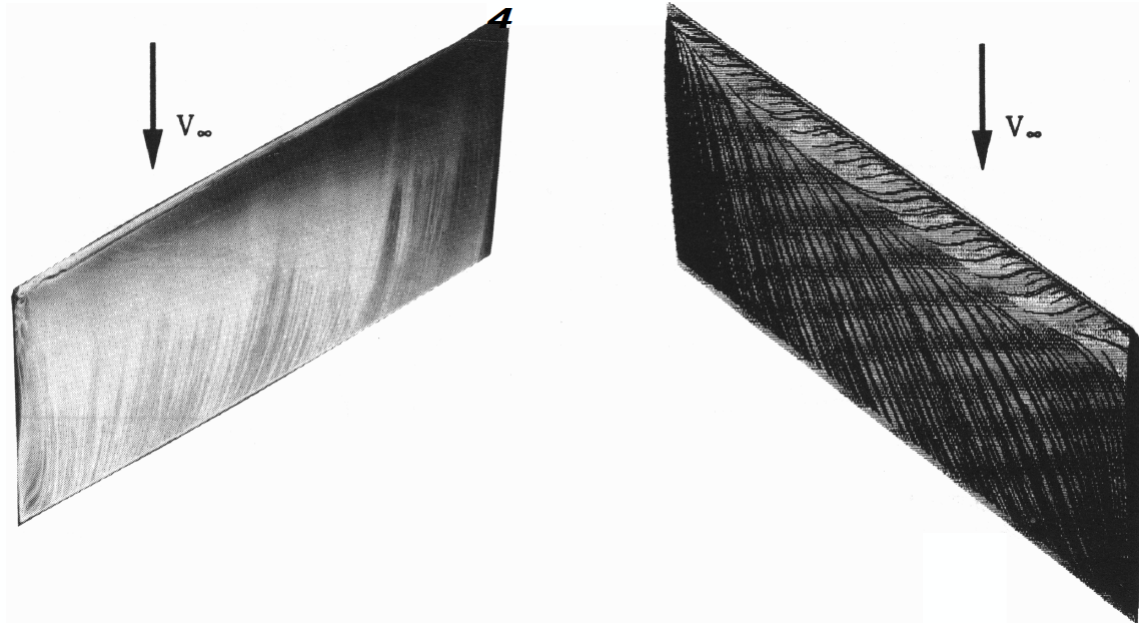
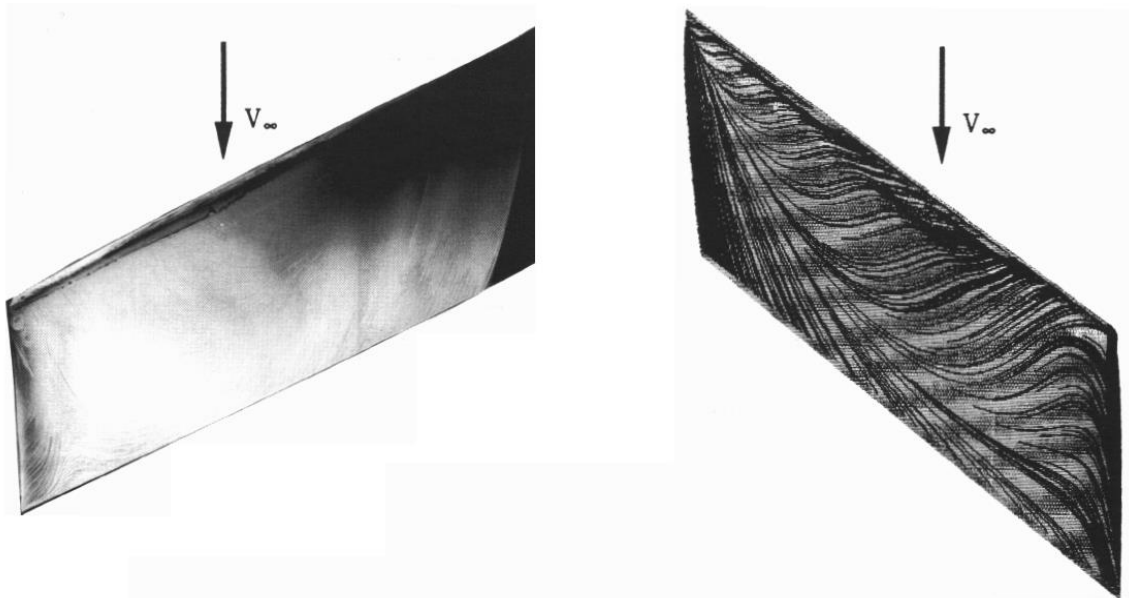


Fig. 28. Pressure distribution comparison at different spanwise location for a straight NACA0012 wing with horn ice shape at  $\alpha = 8$  deg. with wall boundary condition set to symmetry plane. [46]



(a)



(b)

Fig. 29. Experimental and computational surface flow visualization comparison for iced swept NACA0012 wing at a) 4 deg. and b) 8 deg. [47]

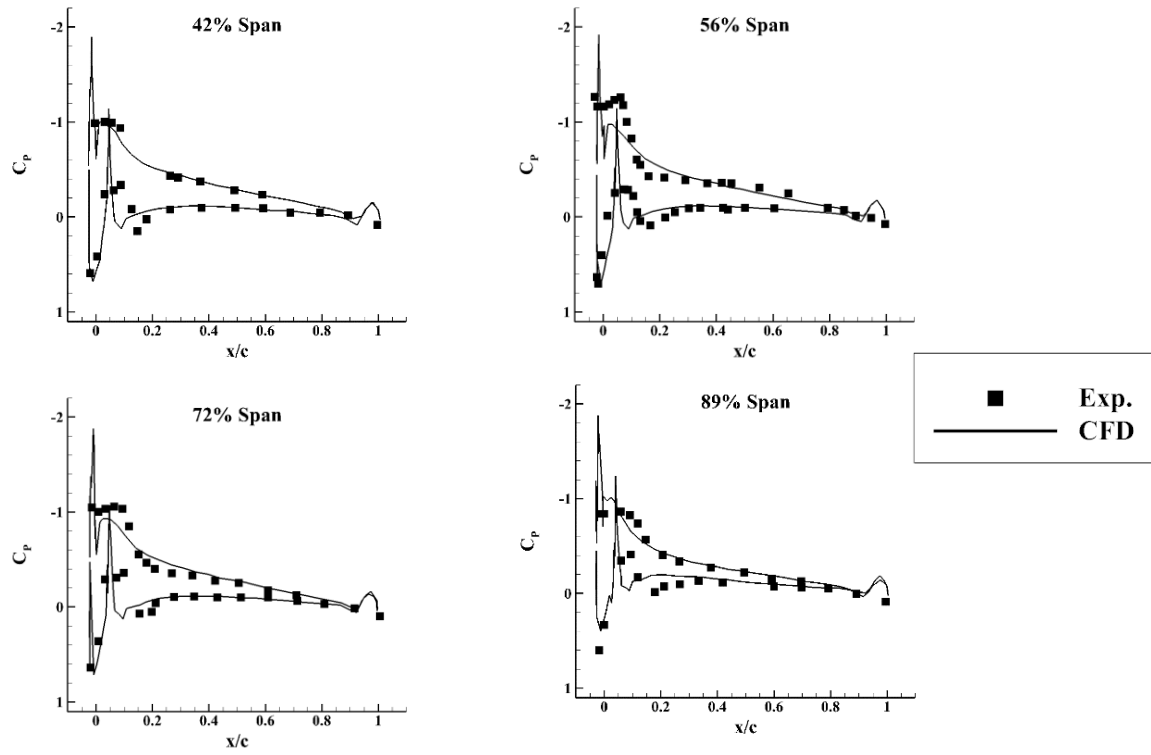


Fig. 30. Pressure distribution comparison for iced swept NACA0012 wing at 4 deg. [46]

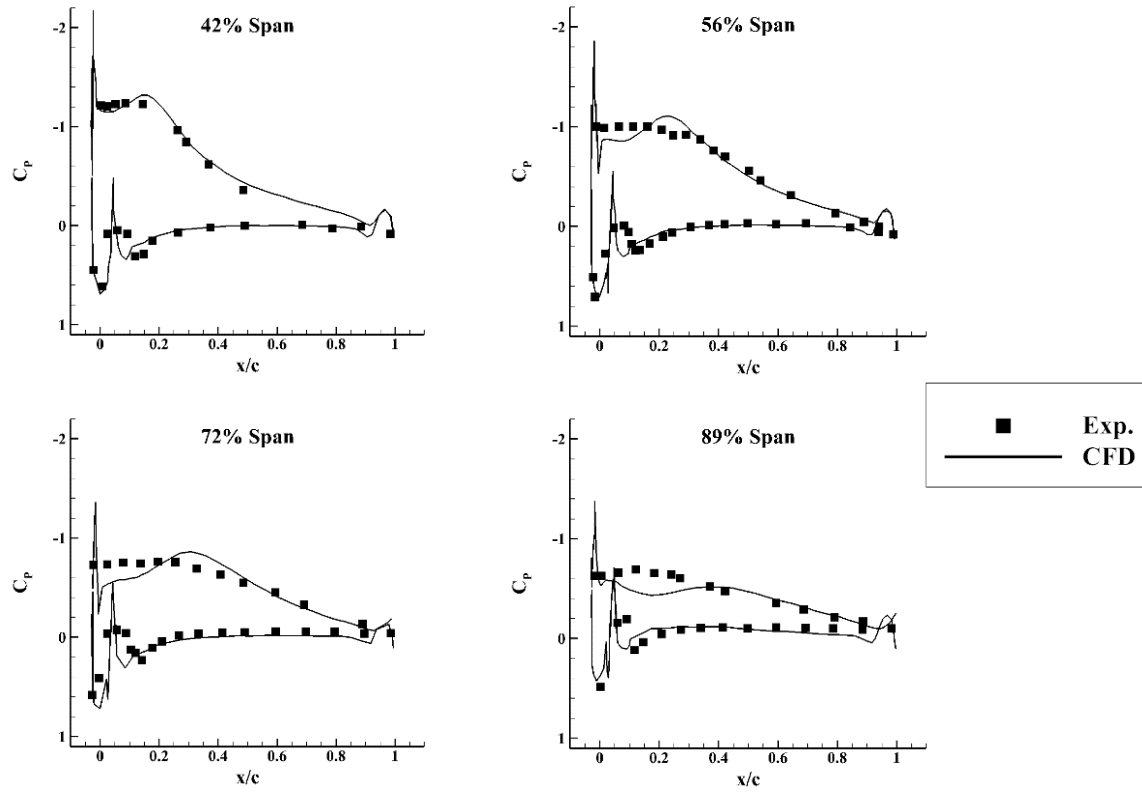


Fig. 31. Pressure distribution comparison for iced swept NACA0012 wing at 8 deg. [46]

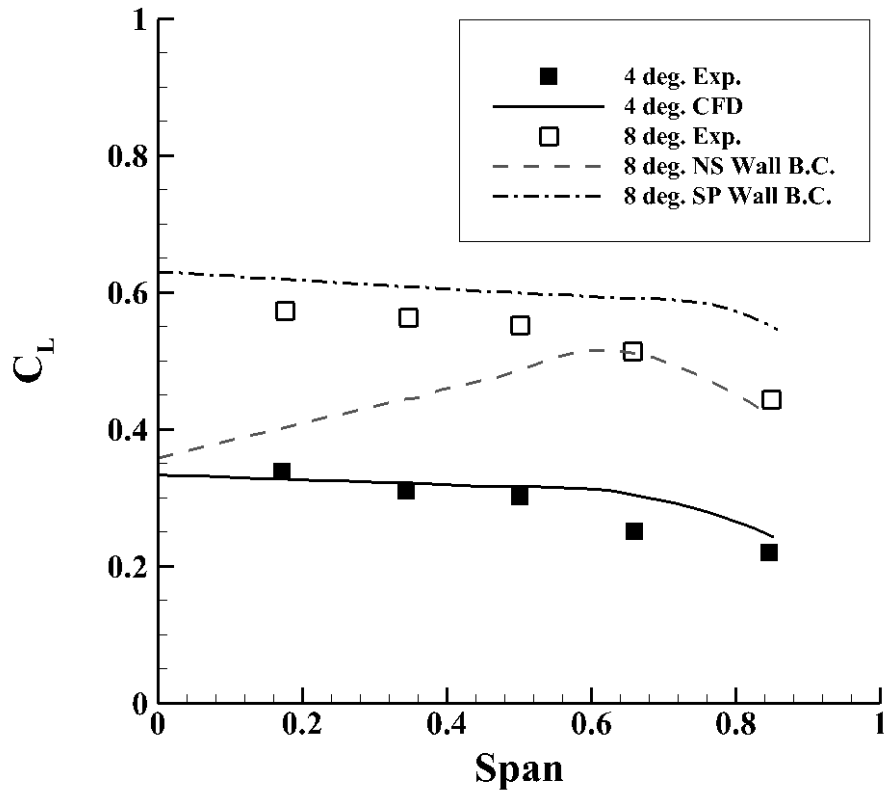


Fig. 32. Comparison of spanwise lift distribution for iced swept NACA0012 wing at 4 deg. and at 8 deg. when the wall boundary condition is applied as no-slip (NS) and applied as a symmetry plane (SP). [46]

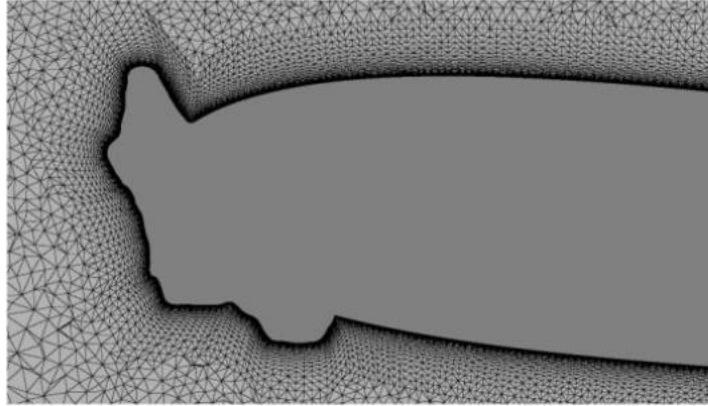


Fig. 33. Leading-edge cross-sectional view of geometry and mesh for a extruded NACA0012 airfoil with a horn ice shape. [50]

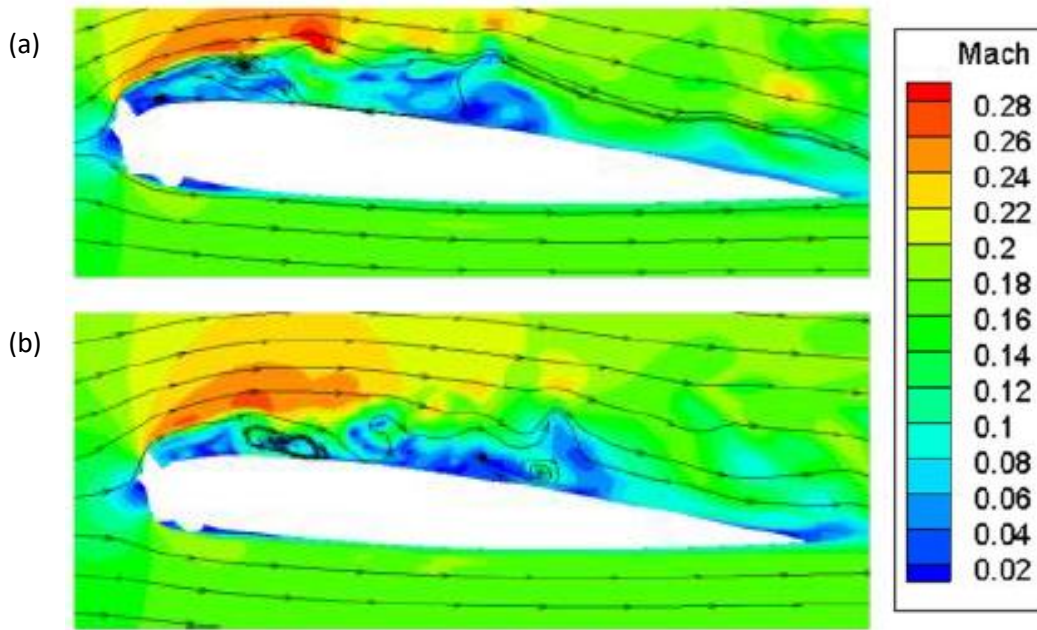


Fig. 34. Instantaneous Mach contour plots for iced extruded NACA0012 airfoil simulations at  $\alpha = 5$ -deg. using a) DDES on a baseline resolution grid and b) IDDES on a baseline resolution grid. [50]

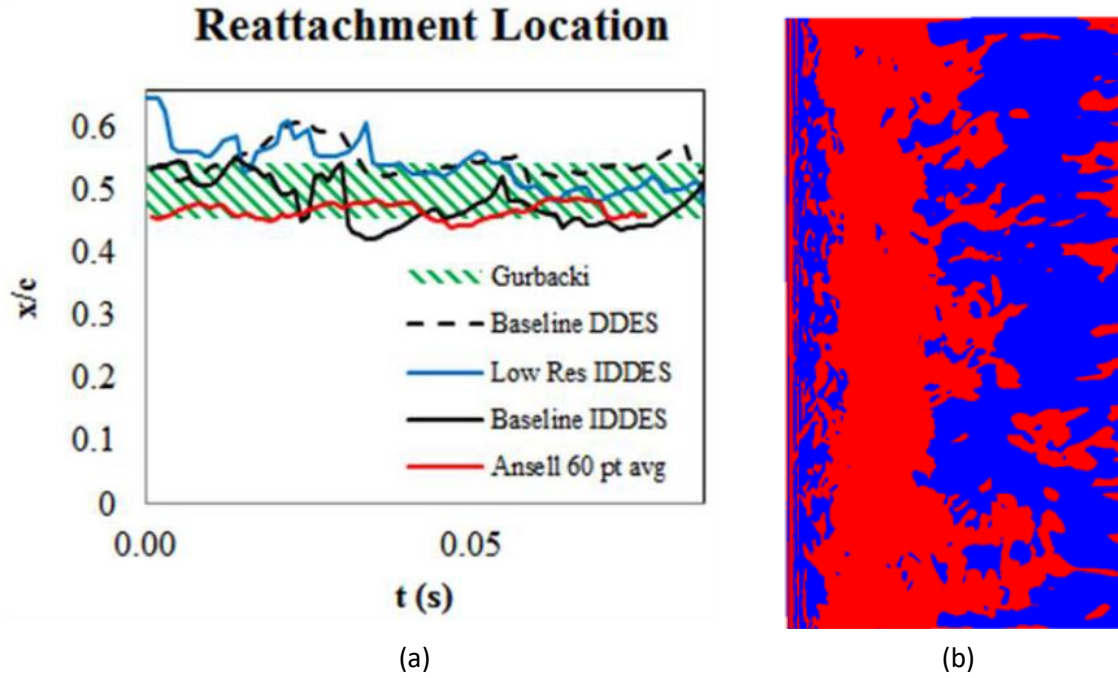


Fig. 35. a) Examination of spanwise-averaged reattachment location over time compared to experimental data and b) instantaneous contour plot of separated (red) and reattached (blue) flow at  $\alpha = 5$  deg. and using a baseline mesh for IDDES. [50]

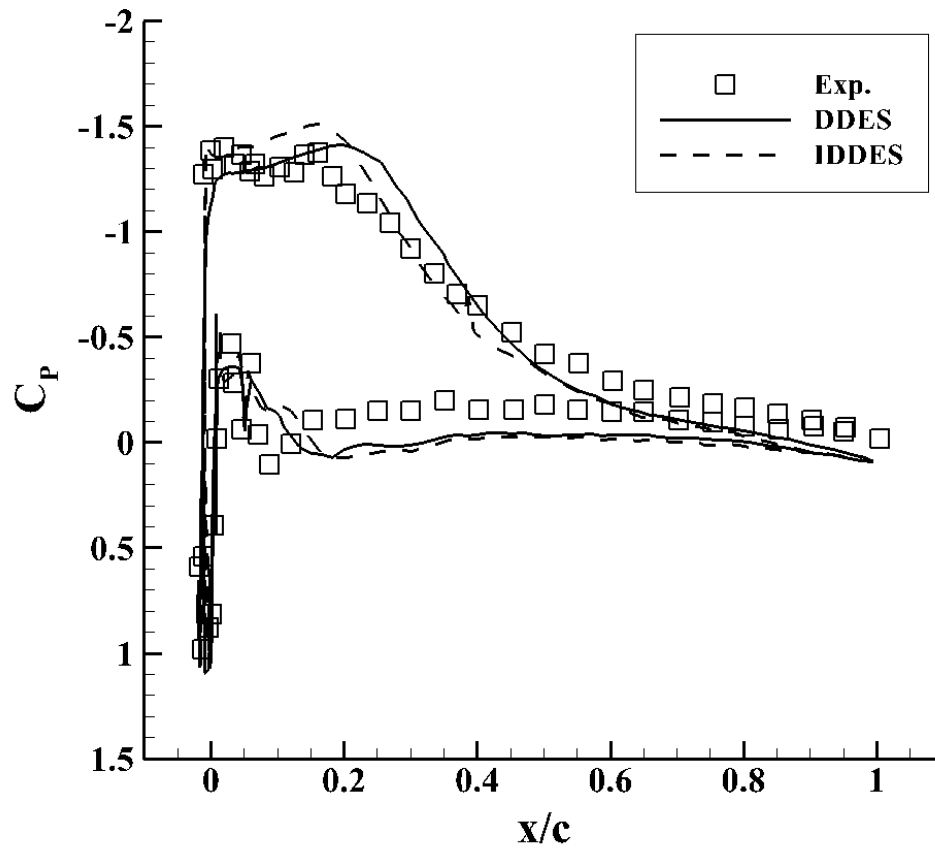


Fig. 36. Pressure distribution comparison of iced extruded NACA0012 airfoil using different numerical methods at  $\alpha = 5$ -deg. [50]

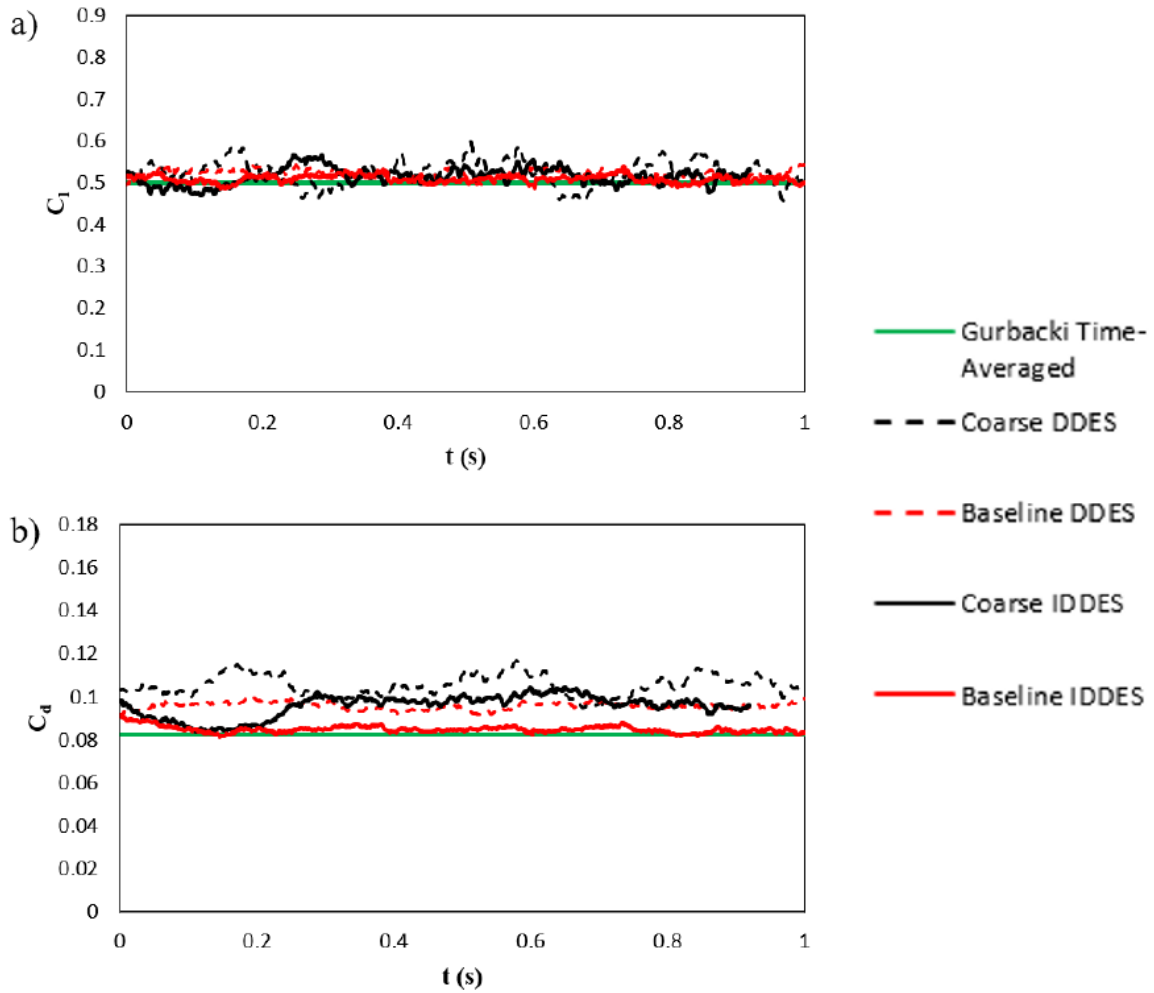


Fig. 37. Comparison of variation in a) coefficient of lift and b) coefficient of drag over time at  $\alpha = 5$ -deg. for various numerical methods. [50]

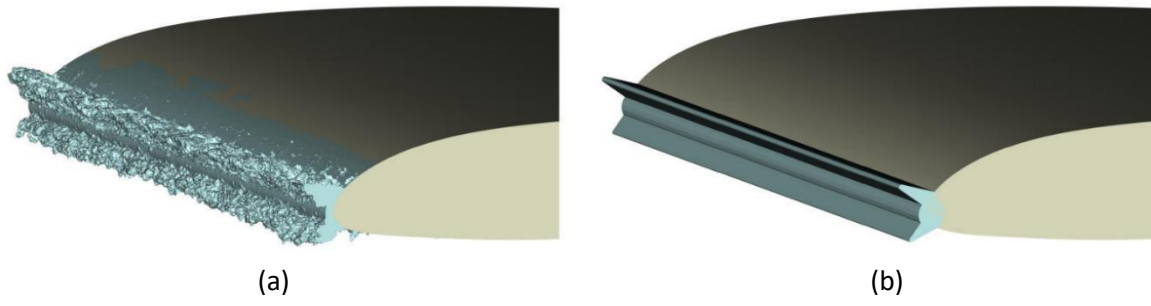


Fig. 38. Geometry of a) ED1978 and b) ED1978s on leading edge of extruded NACA0012 airfoil. [31]

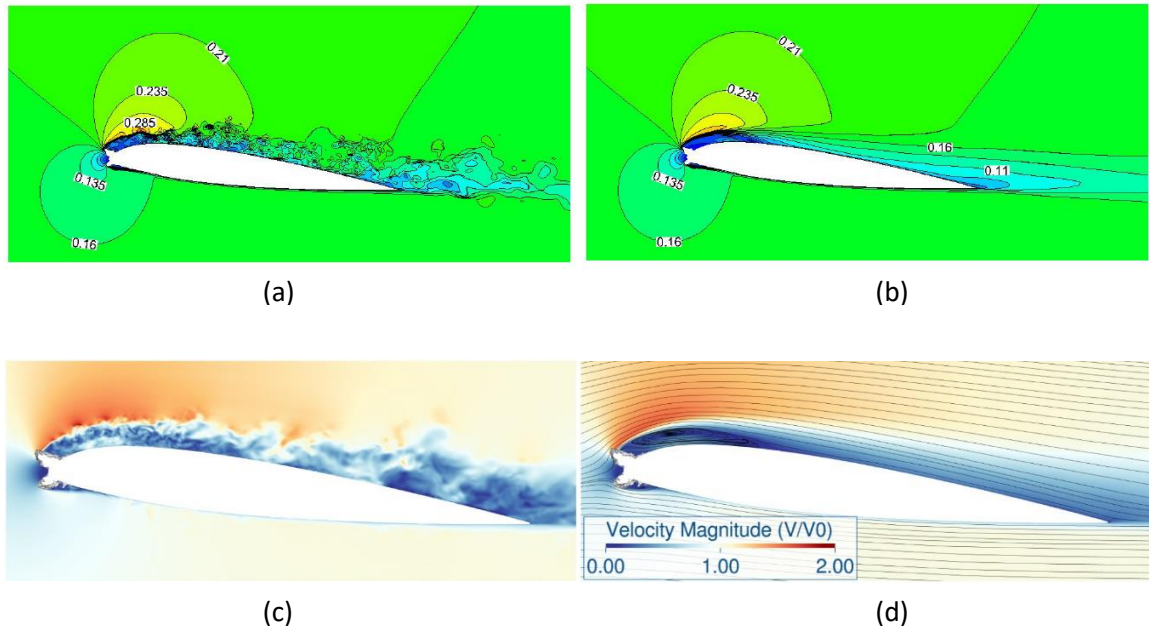


Fig. 39. a, c) Instantaneous and b, d) time-averaged Mach/velocity magnitude contour plots for extruded NACA23012 airfoil with a-b) an extruded ice shape and c-d) an ice shape with spanwise variation at  $\alpha = 6$ -deg. [32] [51]

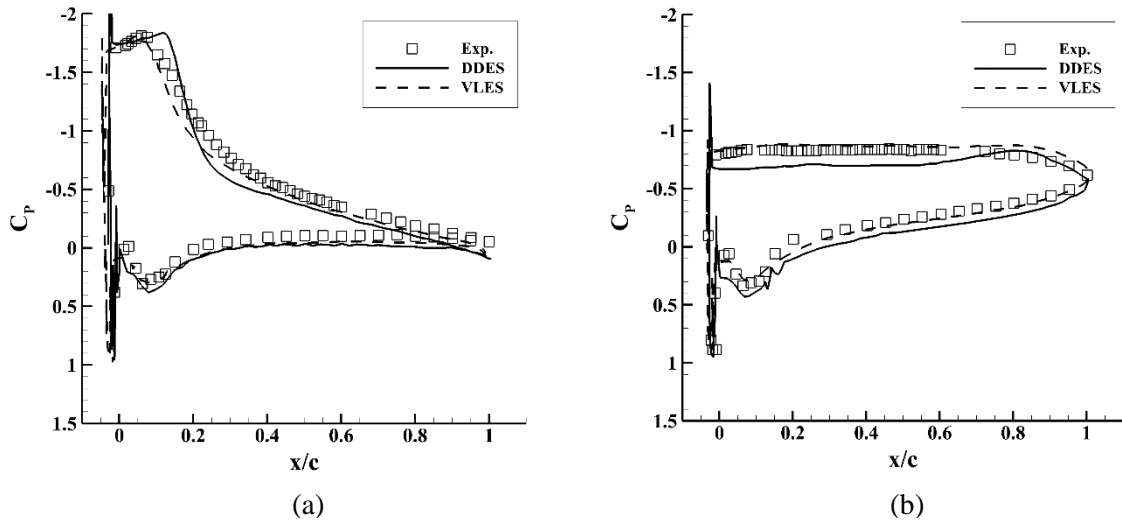


Fig. 40. Pressure distribution comparison for iced extruded NACA23012 airfoil at angles of attack of a) 6 deg. and b) 12 deg. [32], [51]

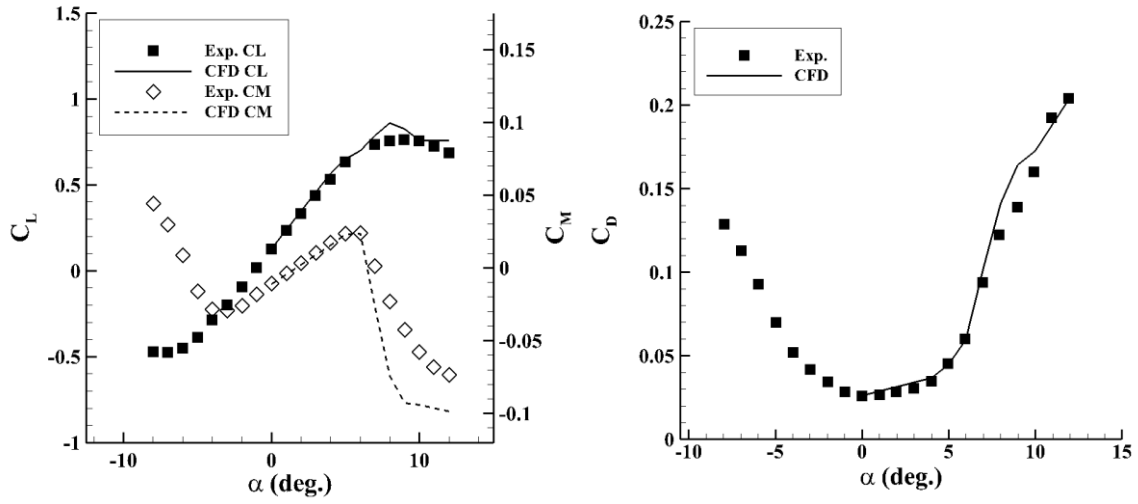
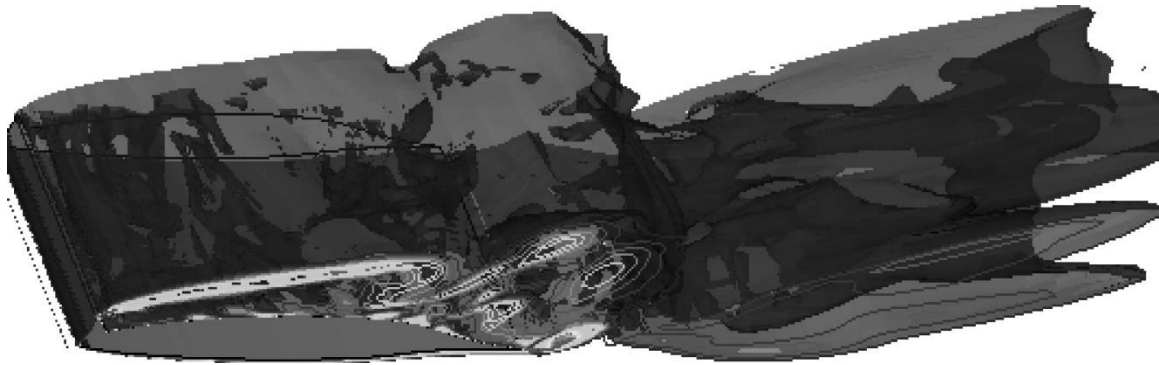
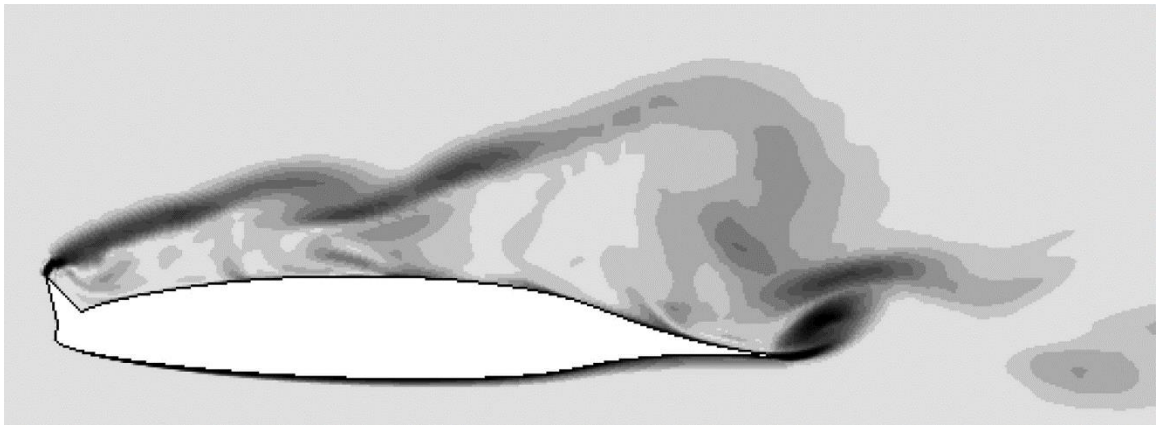


Fig. 41. Comparison of aerodynamic coefficients for iced extruded NACA23012 airfoil. [32]



(a)



(b)

Fig. 42. a) Orthogonal and b) cross-sectional view of instantaneous vorticity contours for iced extruded NLF0414 airfoil at  $\alpha = 3$ -deg. [53]

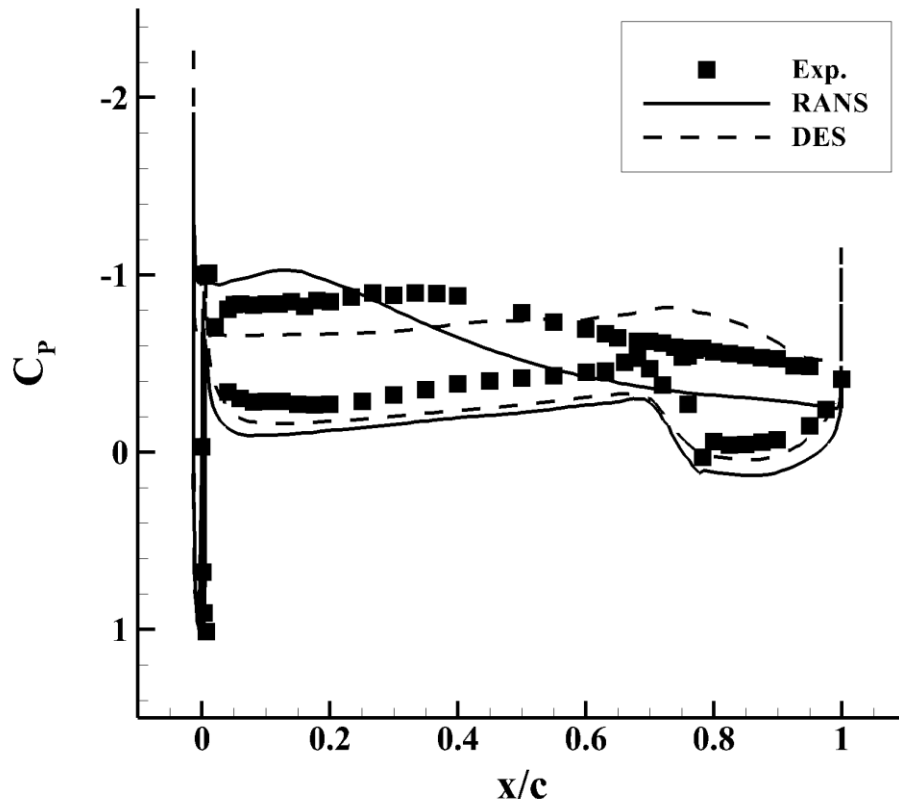


Fig. 43. Pressure distribution comparison for iced extruded NLF0414 airfoil at  $\alpha = 3$ -deg. [53]

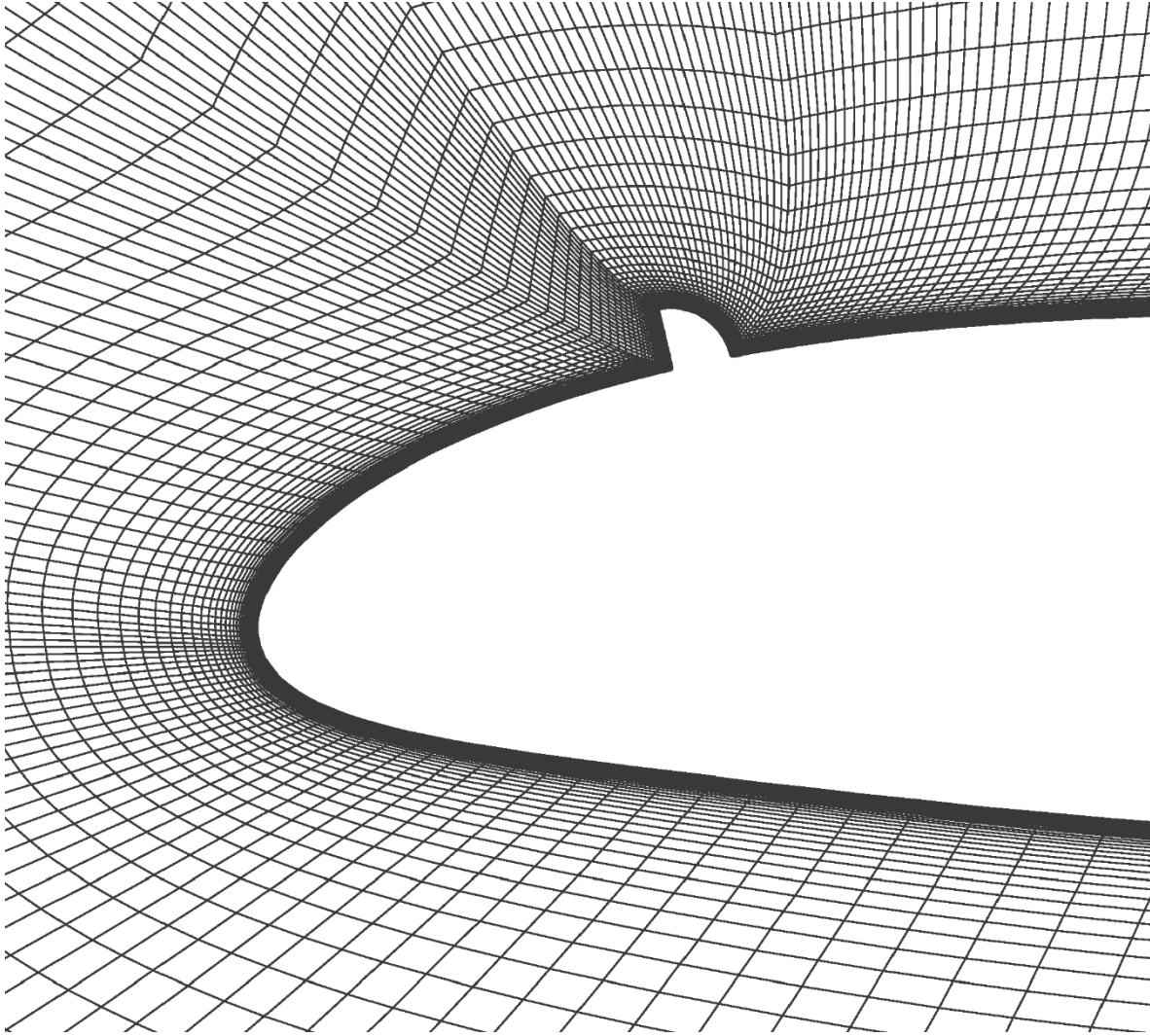


Fig. 44. Cross-sectional view of a NACA23012 with a quarter-round ice shape on the upper surface replicating a realistic spanwise ridge ice shape. [53]

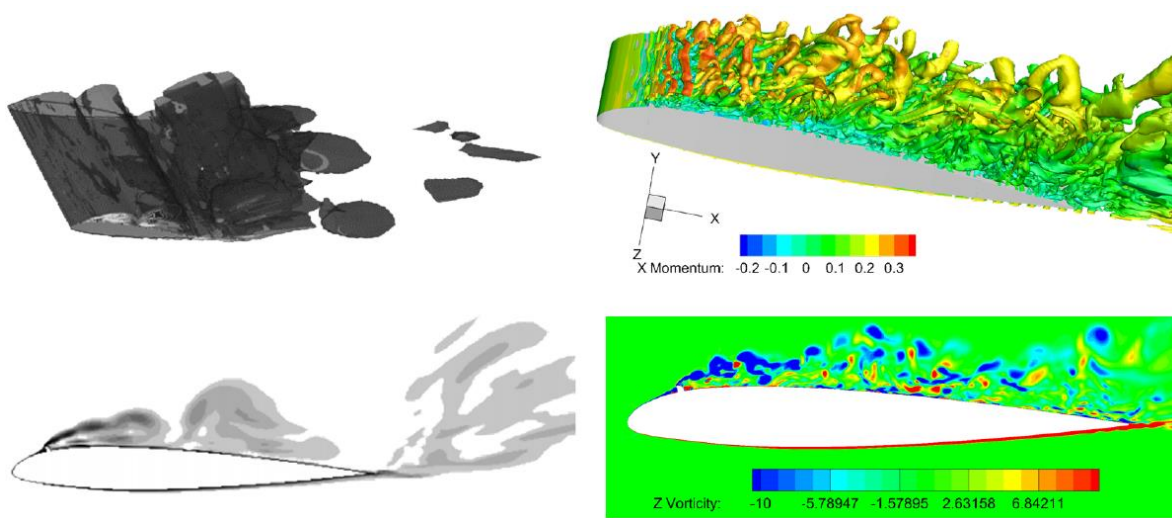


Fig. 45. Comparison of instantaneous vorticity contours for an iced extruded NACA23012 airfoil at  $\alpha = 5$ -deg. using DES (left) and IDDES (right). [55]

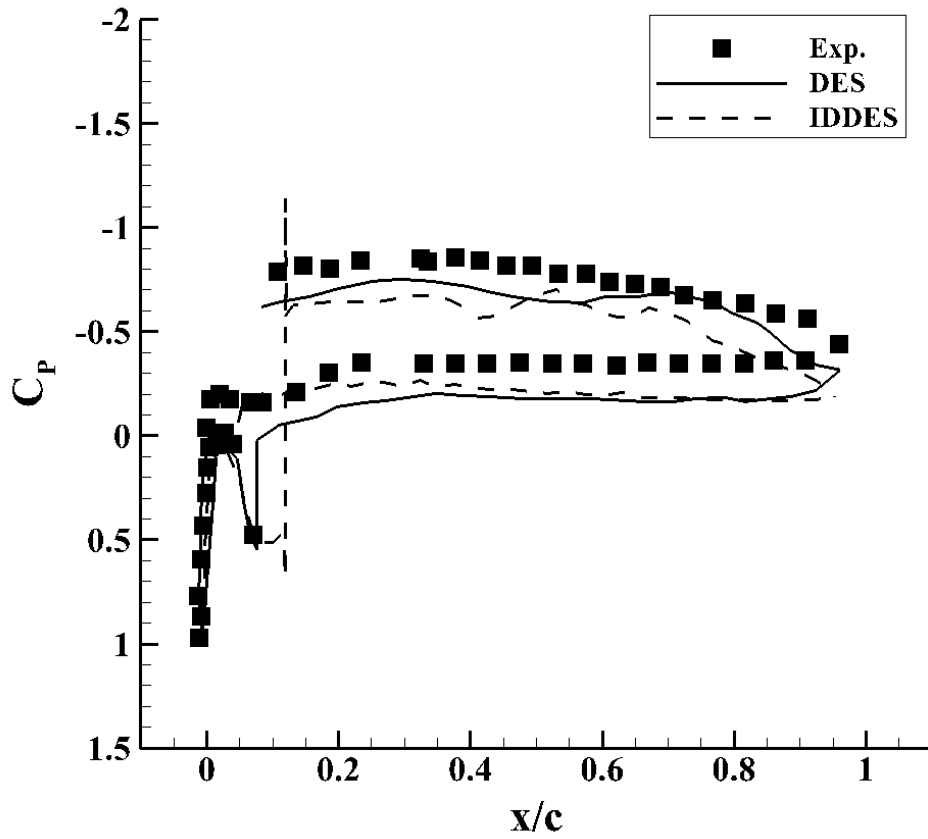


Fig. 46. Pressure distribution comparison of DES and IDDES for flow over an iced extruded NACA23012 airfoil at  $\alpha = 5$ -deg. [54], [55]

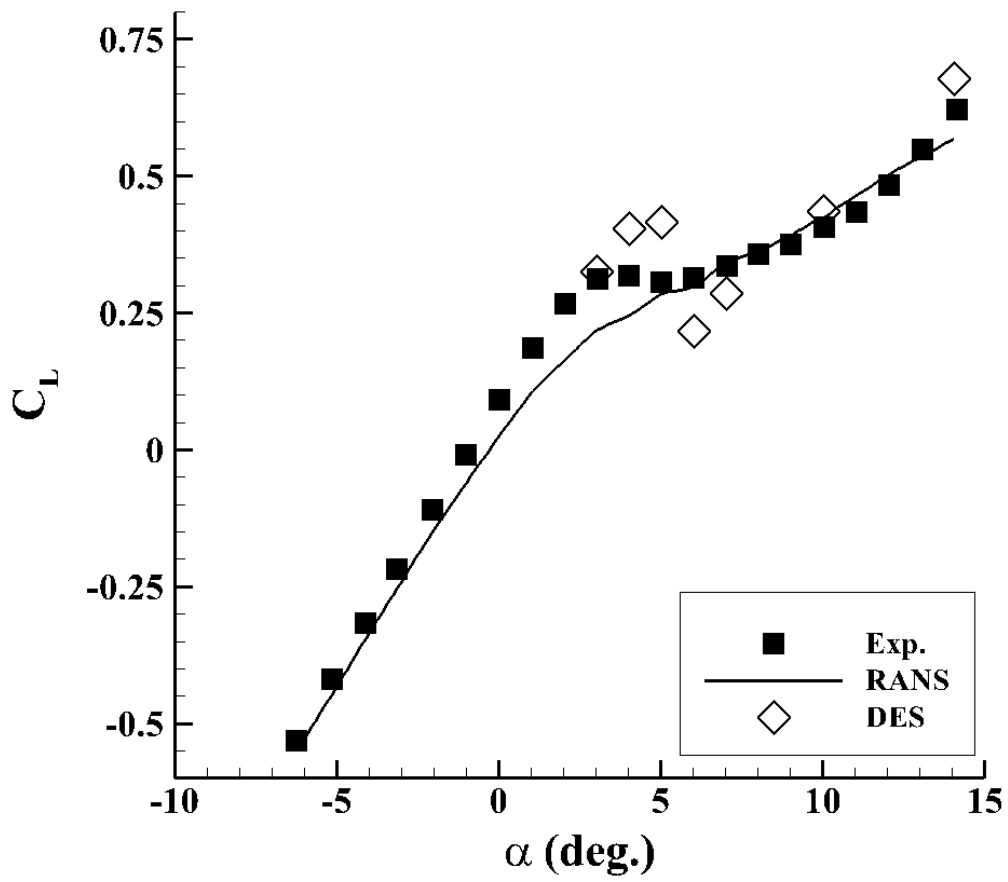


Fig. 47. Comparison of coefficient of lift for an iced extruded NACA23012 airfoil. [53]

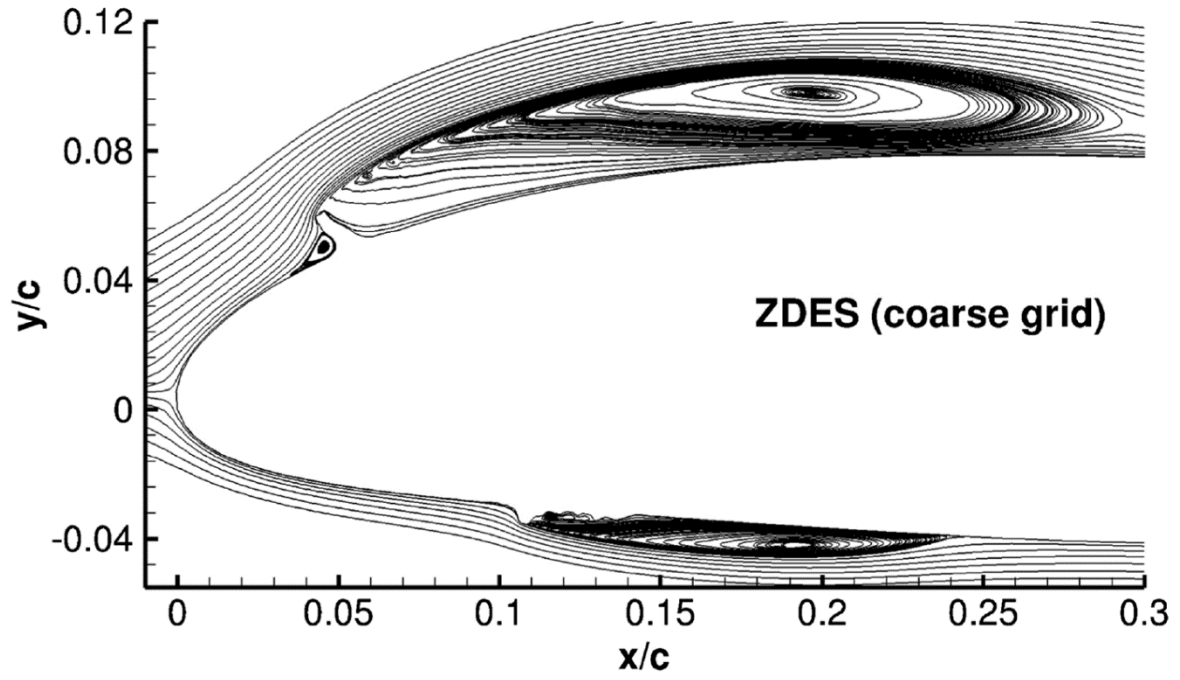


Fig. 48. Time-averaged velocity streamlines over an iced extruded NACA23012 airfoil. [41]

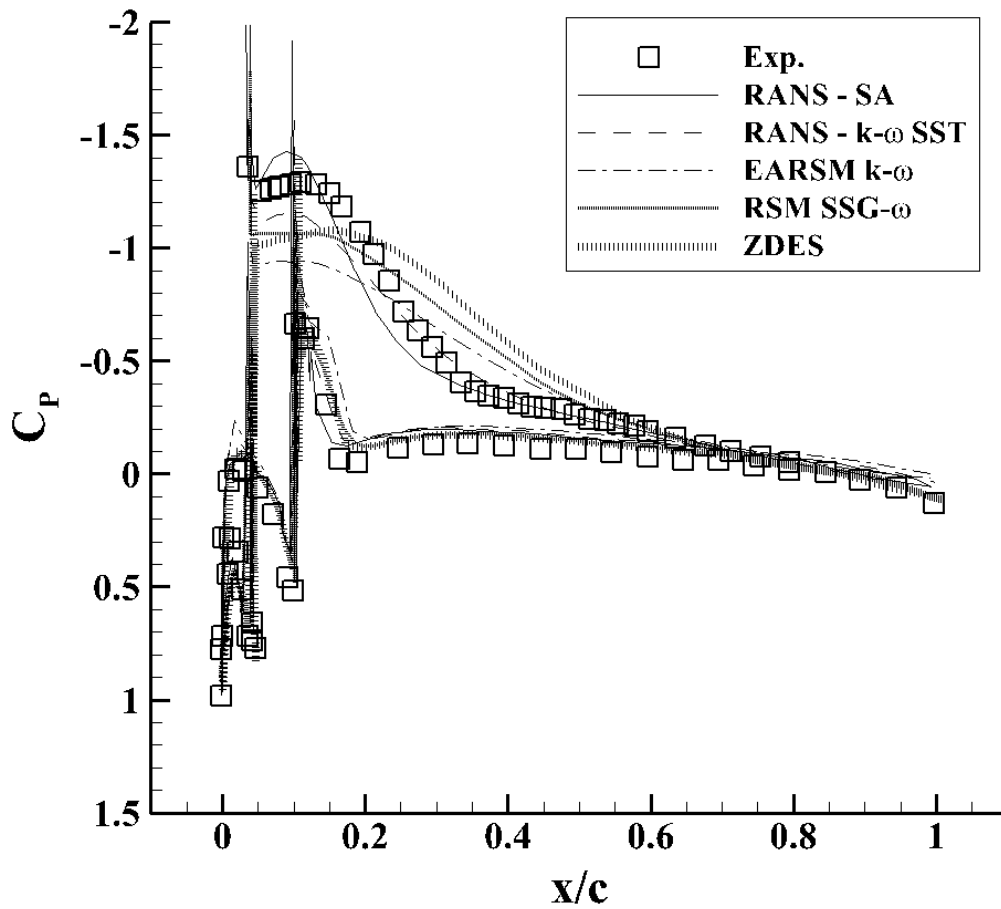


Fig. 49. Pressure distribution comparison (solid line representing CFD and markers representing experimental data) over an extruded NACA23012 airfoil with spanwise ridge ice at  $\alpha = 2$ -deg. for various numerical methods: a) RANS – SA, b) RANS –  $k-\omega$  SST, c) EARSM  $k-\omega$ , d) RSM SSG- $\omega$ , and e) ZDES. [58]

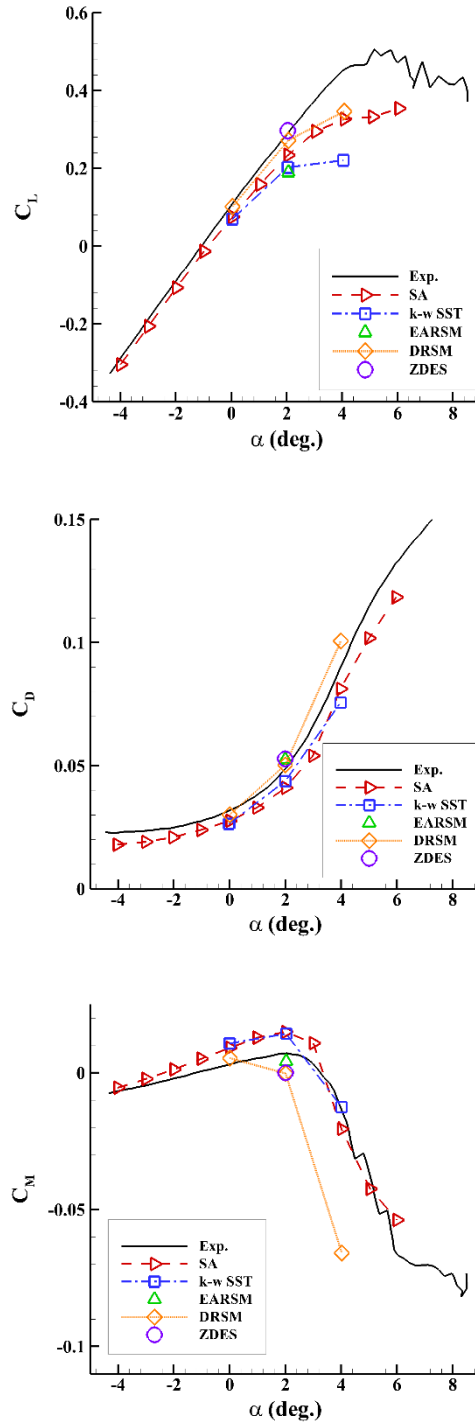
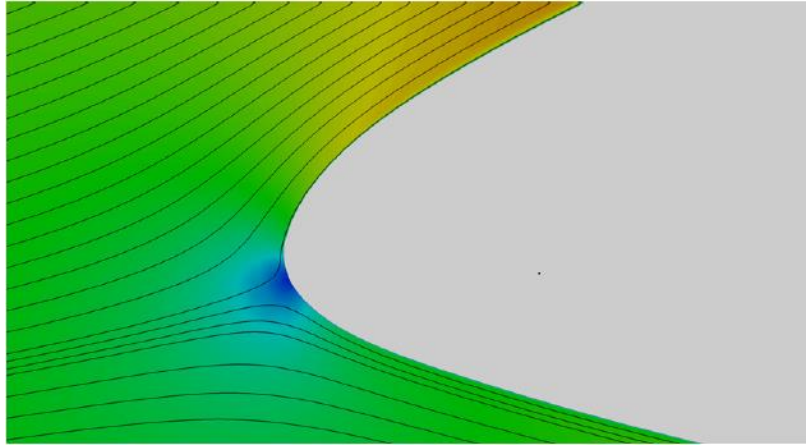
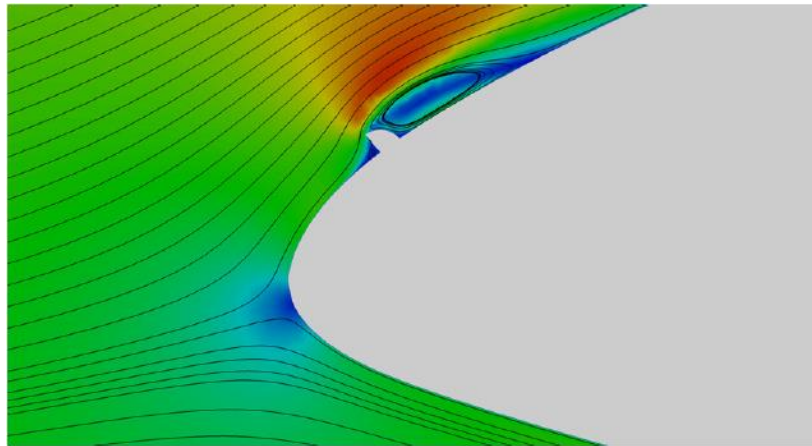


Fig. 50. Comparison of aerodynamic coefficients for an iced extruded NACA23012 airfoil using various numerical methods. [58]



(a)



(b)

Fig. 51. Velocity magnitude contour and streamline comparison of a clean and iced wing at  $\alpha \approx 7$  deg. [59]

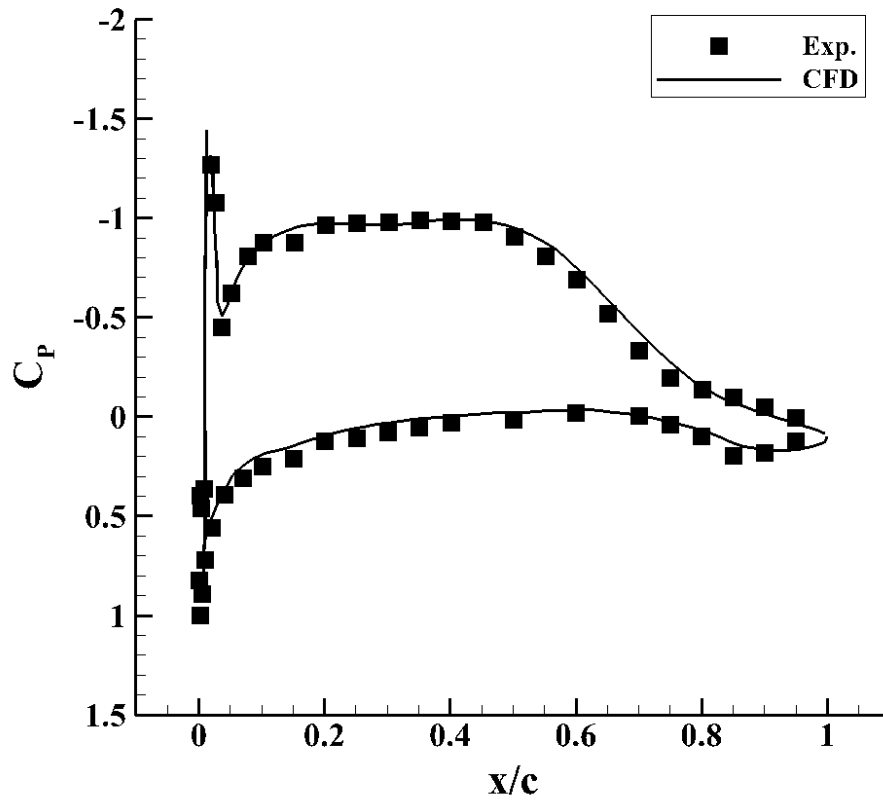


Fig. 52. Comparison of predicted pressure distribution to experimental data. [59]

## Chapter 2 References

- [1] T. Carroll and W. H. McAvoy, “The Formation of Ice Upon Airplanes in Flight,” Washington, D.C., 313, 1929.
- [2] W. M. Leary, “We Freeze to Please: A History of NASA’s Icing Research Tunnel and the Quest for Flight Safety,” Washington, D.C., 2002.
- [3] F. T. Lynch and A. Khodadoust, “Effects of ice accretions on aircraft aerodynamics,” *Prog. Aerosp. Sci.*, vol. 37, 2001.
- [4] M. B. Bragg, A. P. Broeren, and L. A. Blumenthal, “Iced-airfoil aerodynamics,” *Prog. Aerosp. Sci.*, vol. 41, 2005.
- [5] P. Lynch, “Richardson’s Forecast : What Went Wrong?,” in *Symposium on the 50th Anniversary of Operational Numerical Weather Prediction*, 2004.
- [6] F. R. Menter, “Turbulence Modeling for Engineering Flows,” 2011.
- [7] K. Fujii, “Progress and future prospects of CFD in aerospace - Wind tunnel and beyond,” *Prog. Aerosp. Sci.*, vol. 41, no. 6, pp. 455–470, 2005.
- [8] P. R. Spalart, “Strategies for turbulence modelling and simulations,” *Int. J. Heat Fluid Flow*, vol. 21, 2000.
- [9] P. R. Spalart, “Detached-Eddy Simulation,” *Annu. Rev. Fluid Mech.*, vol. 41, 2009.
- [10] J. M. Diebold, A. P. Broeren, and M. Bragg, “Aerodynamic Classification of Swept-Wing Ice Accretion,” in *5th AIAA Atmospheric and Space Environments Conference*, 2013.
- [11] D. N. Anderson and J. Shin, “Characterization of ice roughness from simulated icing encounters,” in *35th Aerospace Sciences Meeting & Exhibit*, 1997.
- [12] J. Shin, “Characteristics of Surface Roughness Associated with Leading-Edge Ice accretion,” *J. Aircr.*, vol. 33, no. 2, pp. 316–321, 1996.
- [13] M. Papadakis, H. W. Yeong, R. Chandrasekharan, M. Hinson, T. P. Ratvasky, and J. Giriunas, “Experimental Investigation of Simulated Ice Accretions on a Full-Scale T-tail,” in *39th Aerospace Sciences Meeting and Exhibit*, 2001, no. January.
- [14] M. Papadakis, H. Yeong, R. Chandrasekharan, M. Hinson, and T. P. Ratvasky, “Effects of Roughness on the Aerodynamic Performance of a Business Jet Tail,” in *40th AIAA Aerospace Sciences Meeting & Exhibit*, 2002.
- [15] S. Arvidson, “Methodologies for RANS-LES interfaces in turbulence-resolving simulations,” Chalmers University of Technology, 2017.
- [16] S. J. Lawson, M. Woodgate, R. Steijl, and G. N. Barakos, “High performance computing for challenging problems in computational fluid dynamics,” *Prog. Aerosp. Sci.*, vol. 52, pp. 19–29, 2012.
- [17] C. Fureby, “Towards the use of large eddy simulation in engineering,” *Prog. Aerosp. Sci.*, vol. 44, no. 6, pp. 381–396, 2008.
- [18] J. Fröhlich and D. von Terzi, “Hybrid LES/RANS methods for the simulation of turbulent

- flows,” *Prog. Aerosp. Sci.*, vol. 44, no. 5, pp. 349–377, 2008.
- [19] T. Saad, “Turbulence Modeling for Beginners.”
- [20] D. C. Wilcox, *Turbulence Modeling for CFD*, 2nd ed. La Canada, CA: DCW Industries, 1994.
- [21] P. R. Spalart, S. R. Allmaras, and J. Reno, “A One-Equation Turbulence Model for Aerodynamic Flows,” in *30th Aerospace Sciences Meeting & Exhibit*, 1992.
- [22] F. R. Menter, “Two-Equation Eddy-Viscosity Turbulence Models for Engineering Applications,” *AIAA J.*, vol. 32, no. 8, 1994.
- [23] T. Nishino, G. T. Roberts, and X. Zhang, “Unsteady RANS and detached-eddy simulations of flow around a circular cylinder in ground effect,” *J. Fluids Struct.*, vol. 24, pp. 18–33, 2008.
- [24] P. R. Deck, S. Deck, M. L. Shur, K. D. Squires, M. K. Strelets, and A. Travin, “A new version of detached-eddy simulation, resistant to ambiguous grid densities,” *Theor. Comput. Fluid Dyn.*, pp. 181–195, 2006.
- [25] M. L. Shur, P. R. Spalart, M. Kh, and A. K. Travin, “A hybrid RANS-LES approach with delayed-DES and wall-modelled LES capabilities,” *Int. J. Heat Fluid Flow*, vol. 29, no. 6, pp. 406–417, 2008.
- [26] S. Deck, F. Gand, V. Brunet, and S. B. Khelil, “High-fidelity simulations of unsteady civil aircraft aerodynamics: stakes and perspectives. Application of zonal detached eddy simulation,” *Philosophical Trans. R. Soc.*, 2014.
- [27] S. Bhushan and D. K. Walters, “A dynamic hybrid Reynolds-averaged Navier Stokes – Large eddy simulation modeling framework,” *Phys. Fluids*, vol. 24, 2012.
- [28] M. F. Alam, D. S. Thompson, and D. K. Walters, “Hybrid Reynolds-Averaged Navier–Stokes/Large-Eddy Simulation Models for Flow Around an Iced Wing,” *J. Aircr.*, vol. 52, 2015.
- [29] T. J. Baker, “Mesh generation: Art or science?,” *Prog. Aerosp. Sci.*, vol. 41, no. 1, pp. 29–63, 2005.
- [30] J. Shewchuk, “Lecture Notes on Delaunay Mesh Generation,” 1999.
- [31] A. F. P. Ribeiro, D. Singh, B. König, and E. Fares, “On the Stall Characteristics of Iced Wings,” in *AIAA SciTech Forum*, 2017.
- [32] B. König, E. Fares, and A. P. Broeren, “Lattice-Boltzmann Analysis of Three-Dimensional Ice Shapes on a NACA 23012 Airfoil,” in *SAE 2015 International Conference on Icing of Aircraft, Engines, and Structures*, 2015.
- [33] G. R. Jun, D. Oriden, M. G. Potapczuk, and J. C. Tsao, “Computational aerodynamic analysis of three-dimensional ice shapes on a NACA 23012 airfoil,” in *6th AIAA Atmospheric and Space Environments Conference*, 2014.
- [34] D. Thompson, P. Mogli, S. Chalasani, H. Addy, and Y. Choo, “A Computational Icing Effects Study for a Three-Dimensional Wing,” in *42nd Aerospace Sciences Meeting and Exhibit*, 2004.

- [35] D. Thompson and P. Mogili, “Detached-Eddy Simulations of Separated Flow Around Wings With Ice Accretions: Year One Report,” Cleveland, OH, 2004.
- [36] P. Mogili, D. S. Thompson, Y. Choo, and H. Addy, “RANS and DES Computations for a Wing with Ice Accretion,” in *43rd AIAA Aerospace Sciences Meeting and Exhibit*, 2005.
- [37] X. Chi, B. Williams, N. Crist, R. E. Kreeger, R. Hindman, and T. I.-P. Shih, “2-D and 3-D CFD Simulations of Clean and Iced Wings,” in *44th AIAA Aerospace Sciences Meeting and Exhibit*, 2006.
- [38] X. Chi, B. Williams, R. E. Kreeger, R. G. Hindman, and T. I.-P. Shih, “Simulations of Finite Wings with 2-D and 3-D Ice Shapes: Modern Lifting-Line Theory versus 3-D CFD,” in *45th AIAA Aerospace Sciences Meeting and Exhibit*, 2007.
- [39] M. Faridul Alam, D. Keith Walters, and D. S. Thompson, “Simulations of Separated Flow around an Airfoil with Ice Shape using Hybrid RANS/LES Models,” in *29th AIAA Applied Aerodynamics Conference*, 2011.
- [40] J. Li, Z. Gong, and H. Zhang, “Hybrid RANS/LES Computations for Unsteady Separated Flow around Airfoil with Ice Accretion,” in *The Asian Symposium on Computational Heat Transfer and Fluid Flow*, 2015.
- [41] Y. Zhang, W. G. Habashi, and R. A. Khurram, “Zonal Detached-Eddy Simulation of Turbulent Unsteady Flow over Iced Airfoils,” *J. Aircr.*, vol. 53, 2016.
- [42] M. Xiao, Y. Zhang, and H. Chen, “Numerical Study of an Iced Airfoil Based on Delayed Detached- Eddy Simulation with Low Dissipation Scheme,” in *9th AIAA Atmospheric and Space Environment Conference*, 2017.
- [43] C. M. Brown, R. F. Kunz, M. P. Kinzel, J. W. Lindau, J. L. Palacios, and K. S. Brentner, “RANS and LES simulation of airfoil ice accretion aerodynamics,” in *6th AIAA Atmospheric and Space Environments Conference*, 2014.
- [44] Lorenzo, E. Valero, and V. De-Pablo, “DES/DDES post-stall study with iced airfoil,” in *49th AIAA Aerospace Sciences Meeting*, 2011.
- [45] O. Kwon and L. N. Sankar, “Numerical study of the effects of icing on finite wing aerodynamics,” in *28th Aerospace Sciences Meeting*, 1990.
- [46] M. G. Potapczuk, M. B. Bragg, O. J. Kwon, L. N. Sankar, and O. Kwon, “Simulation of Iced Wing Aerodynamics,” in *68th AGARD Fluid Dynamics Panel Specialists Meeting*, 1991.
- [47] M. B. Bragg, A. Khodadoust, R. Soltanr, S. Wells, and M. Kerho, “Aerodynamic Measurements on a Finite Wing with Simulated Ice,” in *9th Applied Aerodynamics Conference*, 1991.
- [48] M. Khalid and F. Zhang, “The Aerodynamic Studies of Aircraft Wings with Leading Edge Deformations due to Accreted Ice,” in *40th AIAA Aerospace Sciences Meeting & Exhibit*, 2002.
- [49] O. J. Kwon and L. N. Sankar, “Numerical simulation of the flow about a swept wing with leading-edge ice accretions,” *Comput. Fluids*, vol. 26, pp. 183–192, 1997.
- [50] C. Butler, C. Qin, and E. Loth, “Improved Delayed Detached-Eddy Simulation on a Swept

- Hybrid Model in IRT,” in *8th AIAA Atmospheric and Space Environments Conference*, 2016.
- [51] E. S. Oztekin and J. T. Riley, “Ice accretion on a NACA 23012 airfoil,” in *2018 Atmospheric and Space Environments Conference, AIAA AVIATION Forum*, 2018.
- [52] S. Kumar and E. Loth, “Detached eddy simulations of an iced-airfoil,” in *39th Aerospace Sciences Meeting and Exhibit*, 2001.
- [53] J. Pan and E. Loth, “Detached Eddy Simulations for Iced Airfoils,” *J. Aircr.*, vol. 42, no. 6, 2005.
- [54] J. Pan and E. Loth, “Detached Eddy Simulations for Airfoil with Ice Shapes,” in *42nd Aerospace Sciences Meeting and Exhibit*, 2004.
- [55] S. Hu, C. Zhang, H. Liu, F. Wang, and Y. Li, “IDDES simulation of flow separation on an 3-D NACA23012 airfoil with spanwise ridge ice,” in *2018 Atmospheric and Space Environments Conference, AIAA AVIATION Forum*, 2018.
- [56] M. Duclercq, V. Brunet, and F. Moens, “Physical Analysis of the Separated Flow around an Iced Airfoil based on ZDES Simulations,” in *4th AIAA Atmospheric and Space Environments Conference*, 2012, pp. 2012–2798.
- [57] M. Costes, F. Moens, and V. Brunet, “Prediction of iced airfoil aerodynamic characteristics,” in *54th AIAA Aerospace Sciences Meeting*, 2016.
- [58] M. Costes and F. Moens, “Advanced Prediction of Iced Airfoil Aerodynamics,” in *AIAA SciTech Forum*, 2018.
- [59] M. Papadakis, P. Strong, J. Wong, and S. Wong, “Simulation of Residual and Intercycle Ice Shapes Using Step Ice and Roughness,” in *4th AIAA Atmospheric and Space Environments Conference*, 2012.

---

## Computations of Swept Wing Icing Aerodynamics

---

### 1 – Introduction

Aircraft ice accretion is a critical national safety issue, but one which is not well understood in terms of the three-dimensional aerodynamics for commercial aircraft wing geometries. One reason is that experimental data for ice shapes has not been previously available for modern geometry aircraft wings. To determine the ice shapes which can arise for such wings, experimental data was collected at the NASA Glenn Research Center Icing Research Tunnel's (IRT) for a swept-wing icing project [1]. These ice shapes were accreted to the leading edge of a hybrid model that maintained a full-scale leading edge with a truncated body of a 65% scaled Common Research Model (CRM65) [1]. The resulting ice accretions reasonably matched the expected geometric complexity based on previous ice accretion testing of swept wings. The results also indicated that significant flow separation occurred even for moderate angles of attack and that the aerodynamics are generally complex and highly three-dimensional [2].

Predicting such flows can be challenging since ice accretions can cause large regions of flow separation which are often highly complex and highly unsteady. Recent Computational Fluid Dynamic (CFD) studies done by Alam *et al.* [3], Zhang & Habashi [4], and Xiao *et al.* [5], have shown that these unsteady flow features and associated fluctuating aerodynamic loads can adversely affect flight aerodynamics and thus, aircraft operation and safety. This underlying problem requires manufacturers to pursue icing certification, which represents a large potential cost due to the combination of wind tunnel tests and flight tests that can be involved. Zeppetelli & Habashi [6] have shown that CFD offers a potential solution to this problem due its ability to identify a problem at the beginning or early phases of the design processes for an aircraft. With the advancement of simulation methodologies and development of proper resolution of the flow structures relevant to iced aerodynamics, CFD can save a large number of costs in the aircraft design and icing certification processes. For modern iced wings, very little CFD has been completed so it is not clear as to which flow conditions lead to highly unsteady flow. This requires advanced computational techniques in which conditions can be addressed with conventional turbulence modeling.

Unsteady advanced simulation techniques for high Reynolds number aerodynamic flows are generally based on the Detached Eddy Simulations (DES) method by Spalart *et al.* [7]. This methodology is a robust hybrid coupling of Reynolds–Averaged Navier-Stokes (RANS) and Large Eddy Simulation (LES) techniques. The DES approach was first successfully applied to iced airfoil

and wings by Pan & Loth [8] to capture wake effects. While hybrid RANS-LES (HRL) models have shown results that reasonably predicted high Reynolds number aerodynamic flows of iced airfoils with complex substantial flow separation, it is first necessary to apply RANS to the computational domain. The application of RANS allows researchers to understand the basic nature of various systems. The application of RANS for this complex geometry allows a better understanding of when its application is no longer feasible and it becomes necessary to apply more complex turbulence modeling techniques such as DES and etc.

Once again, despite their promise, the aforementioned computational techniques have not been investigated nor evaluated for three-dimensional ice shapes on modern commercial aircraft wings. Furthermore, there has not been a detailed comparison of a RANS technique against experimental data for such flows. This comparison can be useful to help determine “which tool is best for the job”. Thus, the present study is part of an initiative to understand iced wing aerodynamics by a consortium of organizations including NASA, the Federal Aviation Administration (FAA), the Office National d’Etudes et Recherches Aéropatiales (ONERA), Boeing, the University of Illinois, the University of Virginia, and the University of Washington. The goal of this study is to both explore the fidelity and robustness of RANS and develop a basic understanding of the flow physics for an 8.9% scaled version of the CRM65 wing with and without an ice shape at various angles of attack.

## **2 – Computational Domain & Methodology**

### **2.1 – Problem Description**

An 8.9% scale version of the semi-span swept CRM65 wing is studied in this paper. The CRM65 wing is based upon the Common Research Model (CRM) developed by Vassberg *et al.* [9],[10] in order to help fulfill the need to have a contemporary experimental database that would directly support the validation of specific applications of CFD and was comparable in design to modern day commercial airplanes. The designation CRM65, was derived from the necessity to reduce the potential adverse effects associated with the hybrid modeling of a full CRM wing and installation into NASA’s IRT. Thus, researchers scaled down the wing by 65% and developed a hybrid model based on the new dimensions. This scaled geometry remains comparable to modern day commercial aircraft similar to the Airbus A320 and Boeing 73-800 [1]. The final 8.9% scale was done in order to allow for full aerodynamic testing in the Wichita State University’s Walter H. Beech Wind Tunnel, as seen in Fig. 1.

For the present computations, a computational domain with a cross section selected to match the aforementioned WSU’s wind tunnel was used in this study. Unlike the physical wind tunnel, this study used the mean aerodynamic chord (MAC) of the wing as the reference chord to define the outflow boundary condition at a location of 30 chords downstream and an inflow boundary condition located at 10 chords upstream from the center of rotation. The corner chamfers of the wind tunnel, which can be seen in if Fig. 1, was not included in the computational domain. While the specific dimensions of the wing examined are outlined in Broeren *et al.*’s paper [11], the key features for this wing is that it has a 1.524 m span, 0.4234 m MAC, taper ratio of 0.23, and a leading-edge sweep angle of 37.2-deg. Unlike in the experimental tests, this study did not model the streamline shroud, but a 6.23 cm gap between the bottom of the wing geometry and the floor was modeled. The final computational domain measured 2.134 m high by 3.048 m wide by 19.68 m long and can be seen in Fig. 2. Previous CFD work presented by Broeren *et al.* modeled the

wing without an ice shape and only modelled the floor of the wind tunnel. The present study modeled all of the walls of the wind tunnel in order to utilize the uncorrected aerodynamic data collected during the experimental tests.

The experimental studies that are used for validating this study's numerical method were performed by Broeren *et al.* [11] and Camello *et al.* [2]. These studies collected data via force balance measurements, surface pressure taps, oil flow visualizations, mini tufts, and wake surveys at a Reynold's number of  $1.8 \times 10^6$  and a Mach number of 0.18. The overall flow properties were selected to match the experimental setup of Broeren *et al.* [11]. A velocity boundary condition was assigned to the inlet, while a pressure outlet boundary condition was assigned to the outlet. Finally, the angles of attack for this study were selected in order to not only determine stall mechanisms in the flow field, but also determine at which point RANS could theoretically no longer sufficiently predict the flow field due to possible unsteadiness and large amounts of separation.

The 8.9% scaled CRM65 wing was studied with and without an ice shape on the leading edge. The latter case allowed for validation of both the discretization method used in this paper and the RANS k- $\omega$  SST method to capture swept wing aerodynamics. Though examining the flow field characteristics of a clean swept wing does provide a variety of insights into different flow field characteristics, the intent of this study is to understand the flow field features caused by the presence of the ice shape along the leading edge of the upper surface. The ice shape examined by this paper was derived from ice accretions created in NASA's IRT, which can be seen in Fig. 3. As noted by the papers detailing the ice shape, the full-scale ice accretions on the hybrid models were captured via laser scans and then digitized for ease of manipulation. These data sets were then handled by Camello *et al.* [12] in order to develop water-tight CAD models that could then be scaled down to get the 3D-printed sub-scaled ice shapes for the 8.9% model. Thus, as seen in Fig. 3, the specific ice shape used was a model developed from simplifying the spanwise variation in the highly three-dimensional ice shapes captured by interpolating along the span via user-defined splines that replicated the major cross-sectional ice features in 2.54 cm increments.

## 2.2 – Numerical Methodologies

To numerically solve the Navier-Stokes equation, one approach, called Reynolds averaging, decomposes the solution variables into the mean and the fluctuating components. This leads to Reynolds-averaged Navier-Stokes (RANS) equations that have the same general form as the original Navier-Stokes equation, but the equations are represented with time-averaged variables or values. However, a Reynolds stress term is generated and must be modeled in order to close the equations. Two-equation eddy-viscosity turbulence models are widely used in many engineering applications because of their computational economy and reasonable accuracy. The standard k- $\epsilon$  model is the baseline model that solves two transport equations for the turbulence kinetical energy (k) and its dissipation rate ( $\epsilon$ ). It is worth noting that the standard k- $\epsilon$  model is valid for fully turbulent flow since it assumes the flow is fully turbulent while deriving the equations. As the strengths and weaknesses of this standard k- $\epsilon$  model have become known, modifications have been introduced to improve its performance. Wilcox [13] developed the standard k- $\omega$  model to improve the model performance for low-Reynolds number effects, compressibility, and shear flow spreading. The Wilcox k- $\omega$  model chooses to model the sublayer of the boundary layer, and the model solves the second equation in the term of the specific dissipation ratio ( $\omega$ ), which is the ratio of  $\epsilon$  to k. Compared to previous two-equation models, the Wilcox k- $\omega$  model has better numerical

stability and better agreement with Direct Numerical Simulation (DNS) predictions. In equilibrium adverse pressure gradient flow and in compressible flow, the performance of the k- $\omega$  model in the logarithmic region of a boundary layer is superior to that of the k- $\epsilon$  model. However, the weakness of the standard k- $\omega$  model is obviously shown in the freestream sensitivity, and this seems to be a fair compromise, compared to the standard k- $\epsilon$  model. Therefore, Menter [14] proposed a new two-equation model that combine both the k- $\omega$  model and the k- $\epsilon$  model. To achieve the desired features in the different regions, a blending function is utilized and makes sure the standard k- $\omega$  model is activated in the near-wall region and the modified k- $\epsilon$  model is switched back in the free-shear region. Furthermore, to improve the performance in the adverse pressure gradient flow as well as the accuracy of prediction of the location of flow separation, Menter [14] modified the turbulent viscosity formulation to account for the transport effects of the principal turbulent shear stress. The resulting model called the Shear-Stress Transport (SST) k- $\omega$  model.

In the present study, the RANS equations with the SST k- $\omega$  model is chosen, and the simulations were implemented by employed ANSYS Fluent, a commercially available CFD code. In this model, k and  $\omega$  are solved in two transport equations:

$$\frac{\partial(\rho k)}{\partial t} + \frac{\partial(\rho k u_i)}{\partial x_i} = \frac{\partial}{\partial x_j} \left[ (\mu + \sigma_k \mu_t) \frac{\partial k}{\partial x_j} \right] + G_k - Y_k$$

(1)

$$\frac{\partial(\rho \omega)}{\partial t} + \frac{\partial(\rho \omega u_i)}{\partial x_i} = \frac{\partial}{\partial x_j} \left[ (\mu + \sigma_\omega \mu_t) \frac{\partial \omega}{\partial x_j} \right] + G_\omega - Y_\omega + D_\omega$$

(2)

where  $\rho$  is density,  $u$  refers to the fluid mean velocity, while the turbulent kinetic energy generation terms ( $G_k$ ,  $G_\omega$ ), the destruction terms ( $Y_k$ ,  $Y_\omega$ ), and the cross-diffusion term ( $D_\omega$ ) are described in Ref. [14] and the ANSYS Fluent Theory Guide. Each constant in this model is a blend of two constants by using a blending equation, and the blending function was designed to be unity in the sublayer and logarithmic region of the boundary layer and to gradually switch to zero in the wake region. Other definitions and value of the constants can be found in the reference as well.

### 2.3 – Meshing Technique

All mesh generation in the present study was performed with Pointwise using its anisotropic tetrahedral extrusion method (T-Rex) [15] to create unstructured boundary layer meshes. The meshing process begins with first discretizing the surface of the wing, which can be seen in Fig. 4. When discretizing the wing surface, it becomes imperative to ensure that the leading edge and trailing edge of the wing is well defined in order to properly capture the flow physics. When comparing the meshing requirement between the geometry with and without ice, the ice shape introduces complex curvatures to the surface that must be well defined. Without properly discretizing the geometry of the ice shape by using a highly refined mesh, the resulting mesh can inappropriately smooth out a lot of the ice shape's features. Camello *et al.* [2] found that spanwise variation does a play an important role in the resulting fluid flow over the wing. Any change in the modeling of the ice shape can then have a direct impact on the ability of the simulation to predict the flow physics captured in the experimental tests. Thus, as can be seen in Fig. 4, the number of

nodes for the geometry of the ice shape along the leading-edge portion of the wing was drastically increased.

As for the rest of the domain, for the un-iced geometry's baseline mesh, the boundary layer grid for the configurations was grown to a maximum layer count of 50 layers using a growth rate of 15% and a boundary decay of 0.95. In order to ensure a  $y^+$  equal to 1, an initial step,  $\Delta s$ , of  $6.452 \mu\text{m}$  was imposed on the extrusion. Similar to the clean geometry, the boundary layer for the iced geometry was grown with the same characteristics. From Fig. 4, the most notable difference between the two meshes is the extent of the boundary layer growth into the far field. The reason behind this difference is due to the T-rex methodology, which grows layers until the final layer either reaches a stopping criterion or the local cells are isotropic. With the same initial step size and growth rate, a geometry's surface that is discretized by smaller cell sizes will thus reach isotropy sooner. Fig. 5 provides another view of this artifact via cross-sectional views of both geometries alongside close-ups of the leading edge. Averaging over every angle of attack, the domain for the un-iced wing is composed of  $24.4 \cdot 10^6$  nodes and  $52.3 \cdot 10^6$  cells, while the domain for the iced-wing is composed of  $28.1 \cdot 10^6$  nodes and  $70.2 \cdot 10^6$  cells. A brief grid convergence study was performed for the iced wing at an angle of attack of 8-deg. For the refined mesh, the number of nodes along the upper surface of the wing was doubled in order to ensure finer discretization of both the wing surface and the T-rex methodology away from the wall. In combination with refining the surface, the far field was also refined only in the region directly near the wing. This refinement was done by reducing the connector spacings defining the wall boundary conditions from 5.08 cm to 2.54 cm. The refined mesh is composed of  $36.0 \cdot 10^6$  nodes and  $101.0 \cdot 10^6$  cells.

### 3 – Results

This section will focus on presenting results produced by simulating the 8.9% scaled CRM65 wing with and without a leading-edge ice shape. Both sets of results will present data in the form of pressure distribution and aerodynamic coefficients (i.e. lift, drag, and moment) at angles of attack of 4, 6, and 8 deg. For the geometry with an ice shape, additional computational data will be provided via a comparison of experimentally gathered oil flow visualization data and computationally calculated wall shear stress.

#### 3.1 – Flow Field Analysis

Oil flow visualization and mini-tufts were used experimentally in order to examine the flow near the surface of the wing. Both of these experimental sets are compared to the wall shear stress calculated by the numerical methodology. Poll *et al.* [16] provide an in-depth analysis on the separation characteristics of a swept wing. Fig 6. is a rendition of the figure provided in their text and caters more towards the specific geometry analyzed in this study. For a swept wing during flow separation, a leading-edge vortex tends to form and run from the root of the wing to the tip. This leading-edge vortex is composed of a separation line, a vortex core, and a reattachment line. The separation line is just aft of the leading edge of the wing while the reattachment line is further down the chord with a location dependent upon the strength of the vortex. Between these two lines, the flow tends to move from the reattachment line towards the separation line. Treating the separation and reattachment lines as asymptotes, the flow between the two lines tend to exhibit a pattern similar to a cubic function. As seen in Fig. 6, this cubic-like flow stream has an inflection

point that can be correlated to the vortex core. As the angle of attack increases, the starting location of the separation tends to move closer and closer to the root of the wing and the separation tends to grow in length in the chordwise direction.

Fig. 7 presents a comparison between the experimentally gathered flow visualization data and the computationally calculated wall shear stress using RANS for the 6-deg. iced wing case. Both the mini tufts and the oil flow visualization show that there are regions of separation just aft of the leading edge. For the mini tufts, attached flow is reflected by the tufts pointing towards the leading edge. In the regions of separation, the tufts point in the spanwise direction or towards the leading edge. For the oil flow visualization and wall shear stress images, white lines were added along the reattachment lines that were consistent with Poll *et al.*'s definition [16]. As seen in the oil flow visualization, there are regions of separation just aft of the leading edge that grow in size towards the wing tip.

Computationally, RANS is able to predict the overall pattern of flow separation seen in the oil flow visualization. However, it does not accurately predict the extent of the separation in the chordwise direction. From the experimental data, between the spanwise locations of  $y/b = 0.11$  and  $0.28$ , the separation has progressed from just aft of the leading edge to further downstream along the chord. However, RANS' prediction of the same separation characteristics does not occur until closer to  $y/b = 0.28$ . Beyond  $y/b = 0.28$ , the experimental data shows some spanwise variation in the width of the separation region with a number of breaks in the separation patterning. Unlike the experimental data, the wall shear stress data produced by RANS shows some variation in the width of the separation region and does not exhibit as many breaks in the flow patterning. Further examining these breaks shows that the flow has very little influence on the oil the surface of the wing which reflects a weak flow velocity in this region. This inference is further proved by the relatively small magnitude of the vectors defining the wall shear stress computed by RANS. Thus, these breaks in the separation pattern can be associated with complete separation of the flow in these regions.

For the 8-deg. case, only mini tufts data was collected experimentally. As shown in Fig. 8, starting near the Yehudi break, majority of the tufts are pointing either towards the wing tip or the leading edge. This suggests the presence of stall along majority of the upper surface of the wing. The computed wall shear stress shows that RANS is able to accurately predict this large region of stall. The wall shear stress shows the flow begins to separate around a spanwise location of  $y/b = 0.11$  and grows in the chordwise direction until the wing is completely stalled near the Yehudi break. Comparing the baseline mesh to the refined mesh, there is very little difference between the two. Both exhibit similar wall shear patterns along the upper surface of the wing. Overall, while there are some small discrepancies between the experimental data and computational data at 6-deg., RANS is able to well predict the flow field captured by the oil flow visualization for the iced swept wing at the angles of attack studied.

### 3.2 – Aerodynamic Coefficients

Experimentally, pressure taps were placed in 10 rows along the surface of the wing [11]. These rows were either oriented parallel to the streamwise direction or oriented normal to the leading edge of the wing. This paper focuses only on the streamwise oriented pressure taps' data. Their locations were at  $y/b = 0.11, 0.28, 0.44, 0.6, 0.81,$  and  $0.90$ . Figures 9 through 14 provides the coefficient of pressure contours along the upper surface of the wing geometries that were derived

from the RANS methodology. The figures also present a comparison of the pressure distribution along the wing without and with ice accretion at angles of attack of 4, 6, and 8 deg. The first pair of comparisons to consider is provided by Fig. 9 and 10 for the un-iced and iced geometries at an angle of attack of 4 deg. For both figures, the pressure contour shows very little variation in the pressure along the span of the wing. However, near the wing tip the pressure contour does show a lower pressure region that could be contributed to the onset of stall in this region. Unfortunately, the experimental data does not provide any information via pressure taps as to if this pressure variation is realistic or an artifact of the simulation. In terms of the pressure distribution, RANS k-w SST is able to accurately capture the data for these cases when compared to the experimental data. While the un-iced wing's pressure distribution reflects little variation in pressure along the span, the iced wing presents a different story. Starting around  $y/b = 0.28$ , both the experimental and predicted pressure distribution curves show a pressure plateau near the leading edge of the wing. Diebold *et al.* [17] have attributed this plateau to the presence of a leading-edge vortex being formed aft of the ice horn. The strength of the leading-edge vortex and associated flow separation increases as  $y/b$  increases.

Figures 11 and 12 show the pressure contour and pressure distribution for the un-iced and iced wing at an angle of attack of 6 deg. Similar to the 4 deg., at 6 deg., the un-iced wing shows very little variation in the pressure contour along the span, while the iced wing does exhibit some variance. The pressure distribution curves show that RANS is able to accurately capture the coefficient of pressure at all of the spanwise location for the un-iced wing and only three of the six spanwise locations for the iced wing ( $y/b = 0.11, 0.28, \text{ and } 0.90$ ). Compared to 4-deg., the plateaus present are more pronounced and extend further along the upper surface in the chordwise direction. This characteristic alludes to a stronger leading-edge vortex and larger region of flow separation. At  $y/b = 0.44, 0.60 \text{ and } 0.81$ , RANS fails to capture the exact trend of the pressure plateaus captured by the experimental data. This discrepancy reinforces the difference observed between the separation pattern captured by the oil flow visualization and the wall shear stress.

Figures 13 and 14 show the pressure contour and pressure distribution for the un-iced and iced wing at an angle of attack of 8 deg. In contrast to both the 4-deg. and 6-deg. cases, the un-iced wing at 8-deg. exhibits some spanwise variation in the pressure contour near the wing tip. This difference shows that while the flow is still attached along the upper surface, the wing is beginning to exhibit some stall characteristics in the wing tip region. This potential onset of stall is reflected by a relatively lower suction peak in the pressure distribution of both the experimental and RANS data at a spanwise location of  $y/b = 0.90$ .

In regards to accuracy, RANS is able to capture the overall pressure distribution of the un-iced wing at 8-deg. For the iced wing, while RANS is able to capture the general trend of the pressure distribution, there are some discrepancies. At  $y/b = 0.28$ , the numerical methodology overpredicts the pressure in the region where the experimental data exhibits a pressure plateau. At  $y/b = 0.44, 0.60, \text{ and } 0.81$ , the general trend of the pressure distribution is captured, but the pressure is once again overpredicted in the region in which the experiment captures separation and the pressure is underpredicted along the rest of the chord. At  $y/b = 0.90$ , RANS accurately determines the pressure plateau, but continues to underpredicts the pressure along the rest of the chord for each spanwise locations.

The aerodynamic coefficients are plotted in Figures 15 and 16. Fig. 15a shows that RANS was able to accurately capture the coefficient of lift and moment for the wing without out ice at 2, 4, 6 and 8 deg. As seen in Fig. 15b, RANS overpredicts the drag at 8 deg. Fig. 16a shows that at the

angles of attack simulated, RANS proves to be quite capable of predicting the coefficient of lift for the complex geometry of the iced swept wing. The largest error comes at an angle of attack of 8-deg where RANS underpredicts the coefficient of lift, moment and drag. This discrepancy can be associated with the difference between the experimental and computational pressure distributions. The underprediction of the coefficient of moment can be more specifically related back to the location of the moment arm and the pressure distributions along the wing. The moment arm is located at  $(x, y, z) = (17.483, 0, 0)$  and extends in the y-direction. Once again, starting at  $y/b = 0.44$ , RANS underpredicts the pressure distribution along majority of the chord. This underprediction results in a lower integrated force being applied along the wing and thus creates a lower coefficient of moment than the experimental data. Overall, RANS proved to be capable of predicting the aerodynamics of an 8.9% scaled CRM65 wing with and without ice up to stall.

## 4 – Conclusion

Ice accretion on the leading edge of commercial wing geometries is a dangerous phenomenon that is not well understood due to the lack of experimental data for such geometries. Recent work done has attempted to alleviate this issue and provide the community with more information. As seen in the experimental data, the flow around the 8.9% scaled CRM65 is highly complex and three-dimensional. CFD is able to provide insight into what flow field characteristics are influencing the aerodynamic performance parameters. The objective of this study is to assess the ability of RANS  $k-\omega$  SST to predict the flow physics and aerodynamic performance parameters for a swept wing with and without an ice shape. The wing was modelled and simulated in a domain similar to the experimental tests conducted at the Wichita State University's Walter H. Beech Wind Tunnel.

Simulated flow field data showed that starting at 4-deg., a spanwise running vortex forms just aft of the leading-edge of a swept wing. This vortex grows in strength as the angle of attack increases. RANS proved via wall shear stress data to be quite capable in accurately predicting the existence and strength of this vortex at 6 and 8-deg. The prediction capability of RANS to capture the wing stall is also reflected in the pressure distribution plots and the time-averaged aerodynamic coefficients. The prediction of the aerodynamic performance parameters for the un-iced and iced geometries were well resolved by the RANS solution. However, the coefficient of moment at 8-deg., was underpredicted for the iced geometry and could be linked to the underprediction of the pressure distribution near the trailing edge of the wing. Future work will consist of pursuing 4 main points: 1) understanding the influence of the spanwise running flow and its impact on iced swept wing aerodynamics, 2) exploring why the coefficient of moment was not correctly predicted by RANS near stall, 3) improving the accuracy of calculating the pressure distribution along the swept wing and 4) comparing the simulated flow physics and aerodynamic parameters between the simplified and high fidelity version of the ice shape studied in this paper.

## Chapter 3 Figures



Fig. 1. 8.9% scaled CRM65 wing installed in Wichita State University's Walter H. Beech Wind Tunnel. [11]

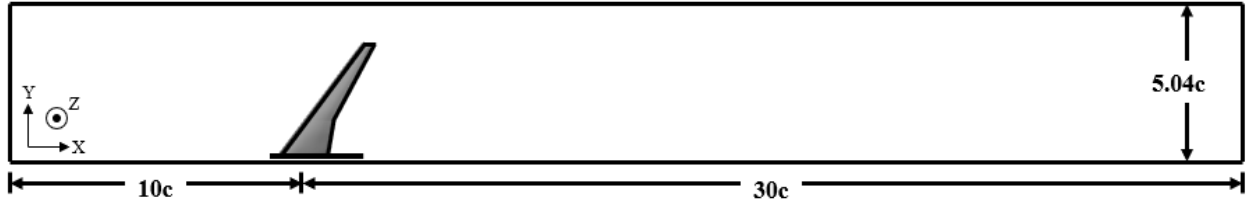
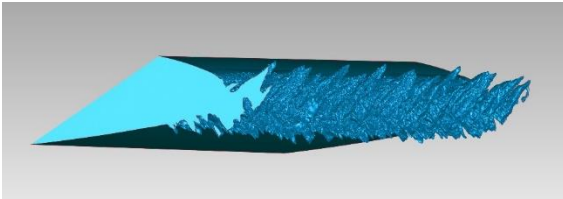


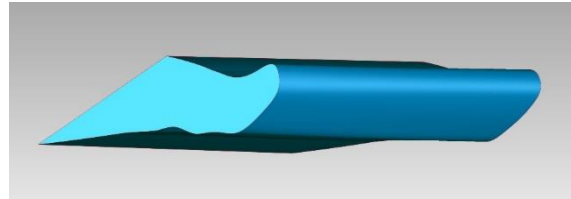
Fig. 2. Schematic of the computational domain used for the simulations, where “c” is defined by the MAC = 0.423 m.



(a)

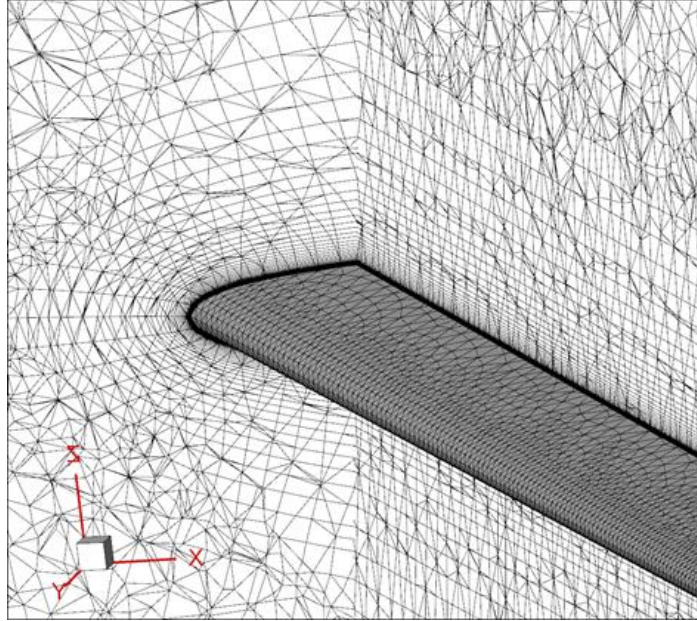


(c)

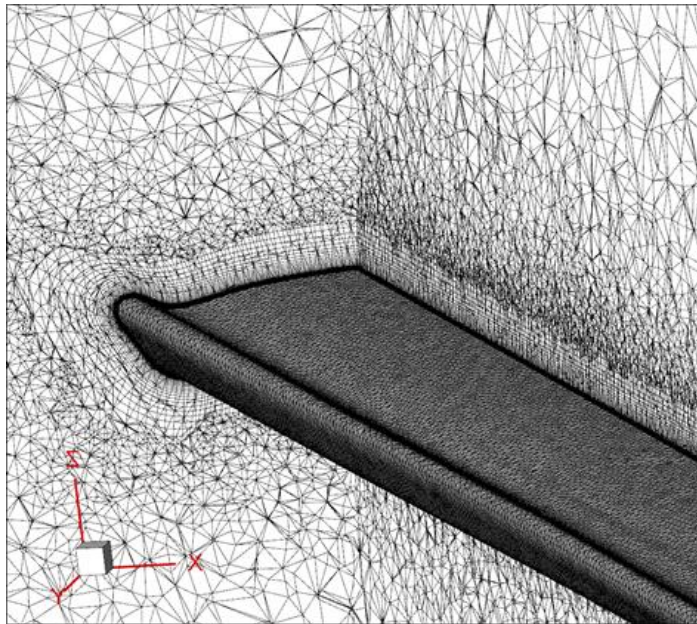


(d)

Figure 3. a) Photograph of ice accretion on the Outboard model with b) resulting laser scan, c) representative computer model, and d) simplified model as defined by Camello et al. [12]



(a)



(b)

Fig. 4. Orthogonal cross-sectional view of the mesh generated for both the a) non-iced wing and b) iced wing.

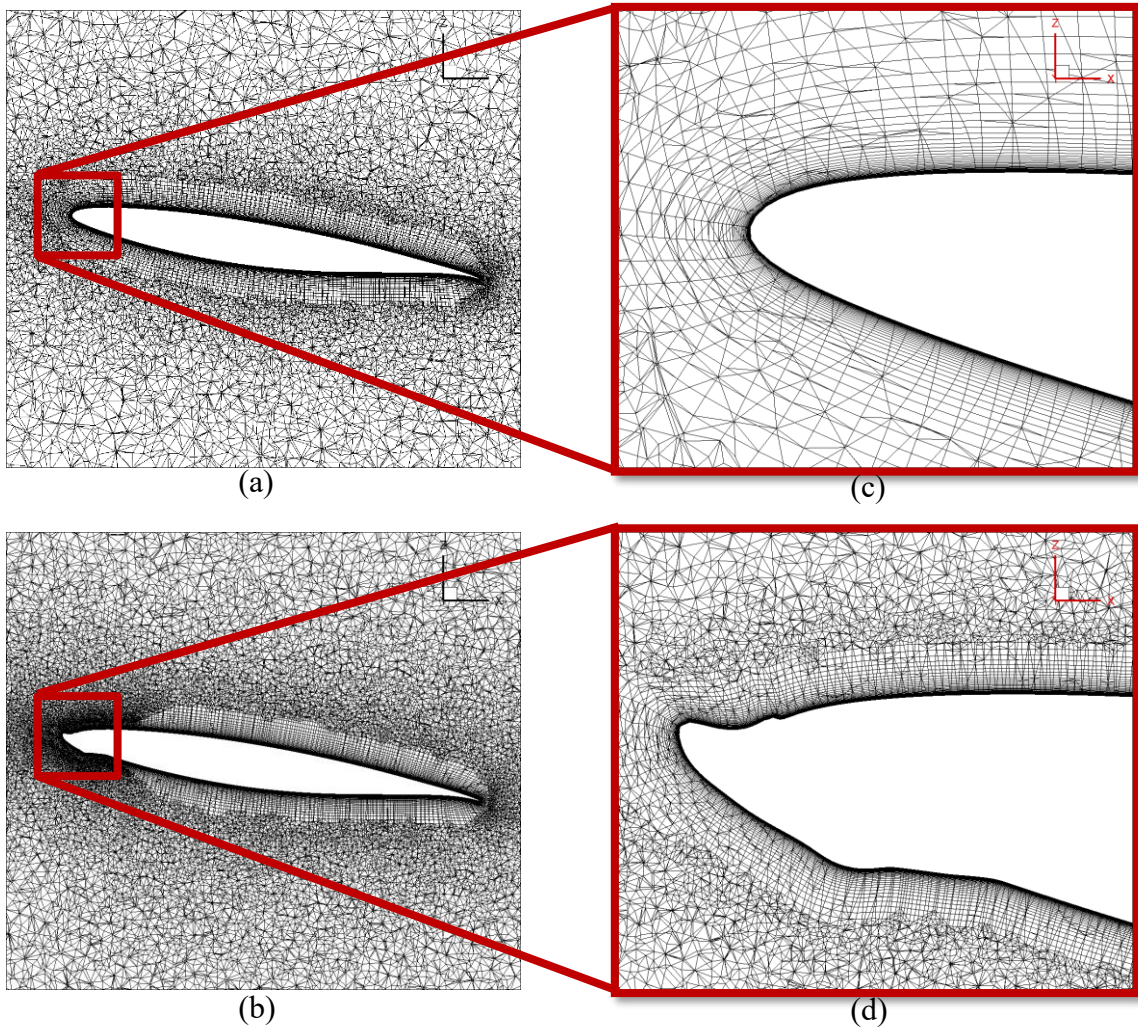


Fig. 5. a-b) Cross-sectional view of the mesh generated for both the non-iced and iced wings at a  $y/b = 0.28$  and c-d) close up of the leading edge of the geometries.

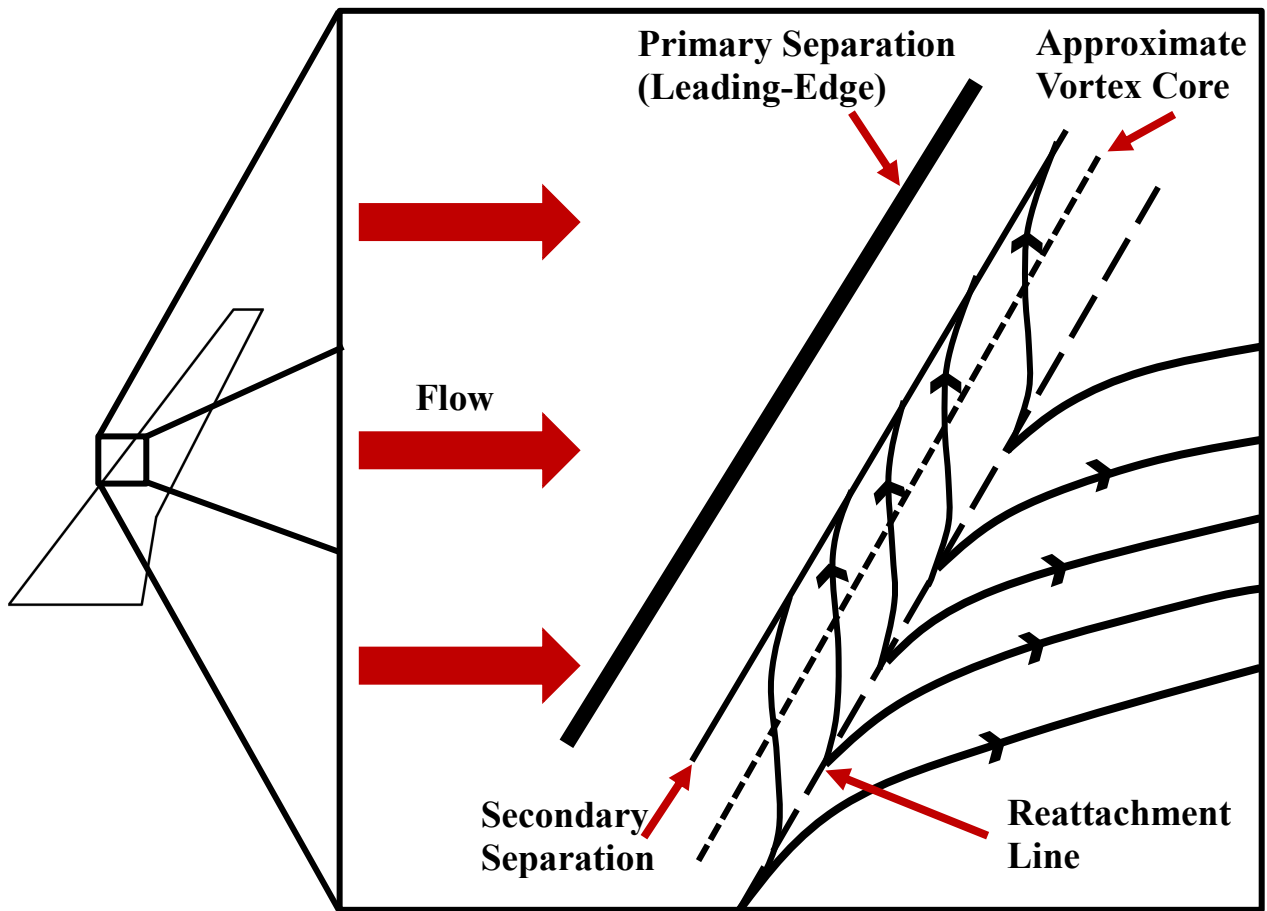


Fig. 6. Schematic of leading-edge vortex with separation and reattachment lines.

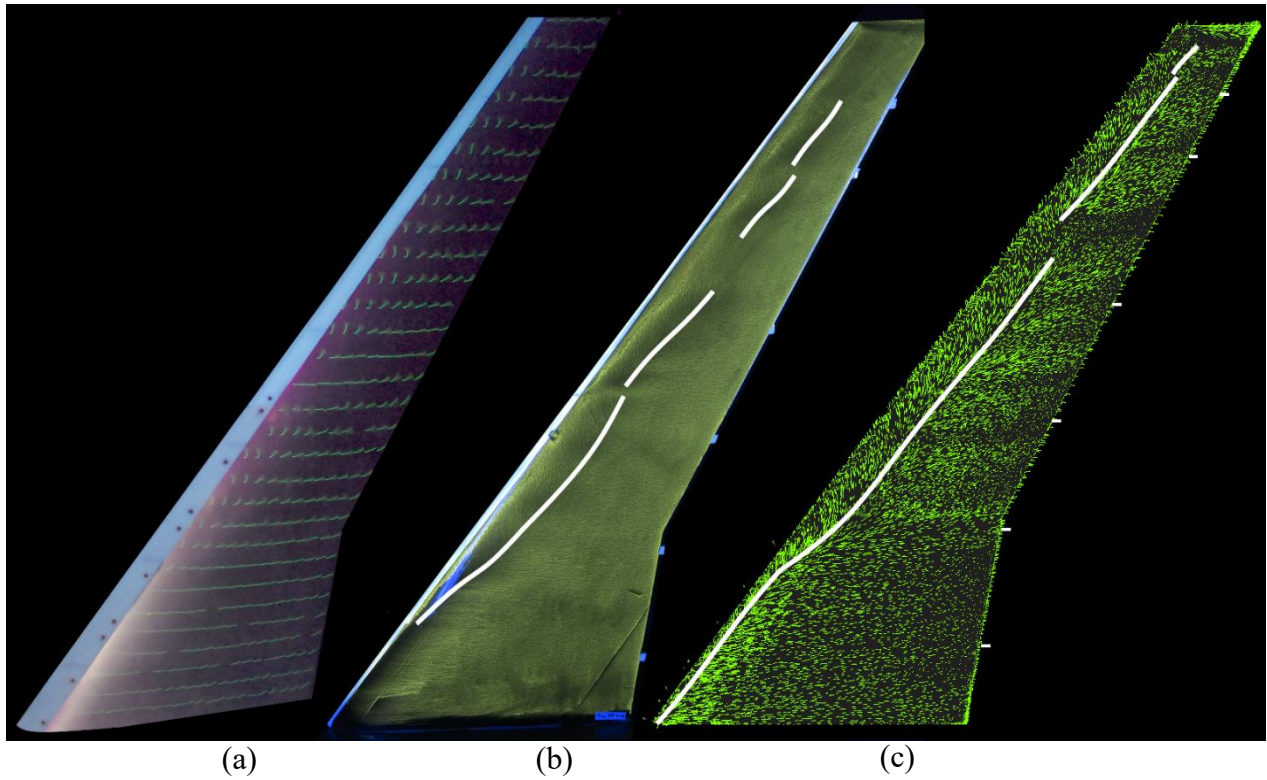
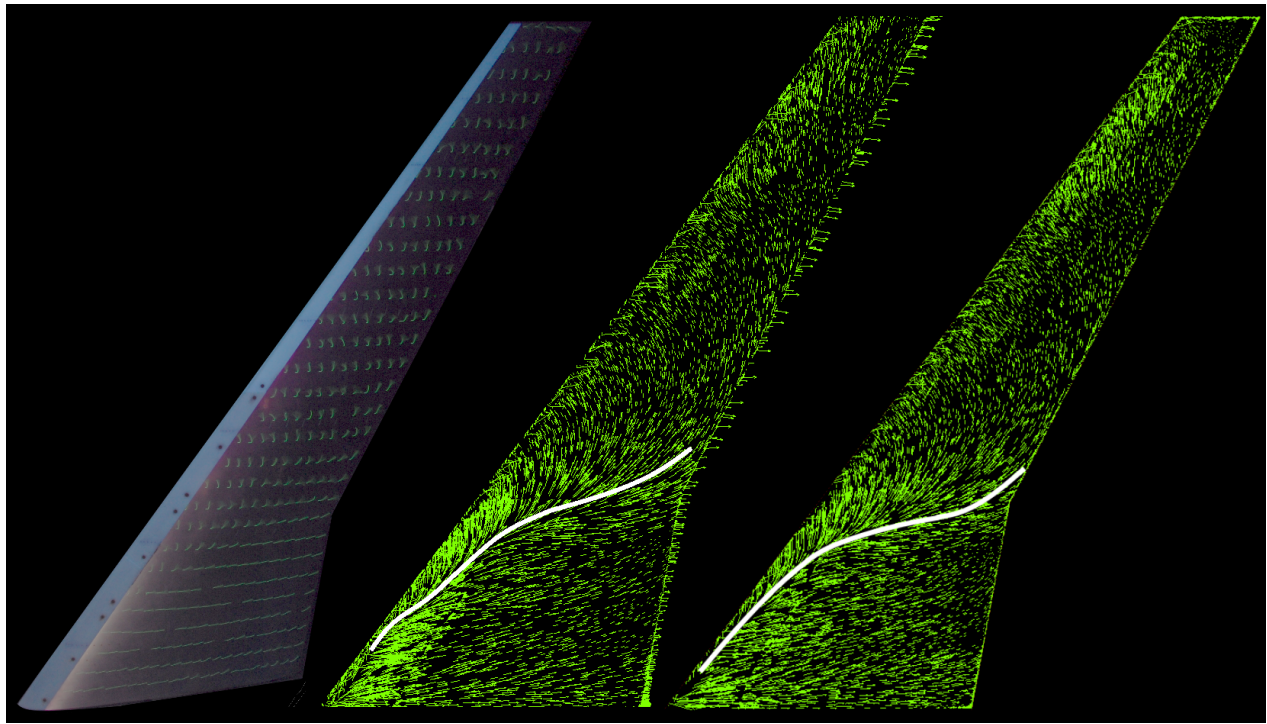


Fig. 7. Comparison of experimental a) mini tufts and b) oil flow visualization to computationally calculated wall shear stress via c) RANS at 6-deg.



(a)

(b)

(c)

Fig. 8. Comparison of a) experimental mini-tufts to computationally calculated wall shear stress via RANS using b) baseline mesh and c) refined mesh at 8 deg.

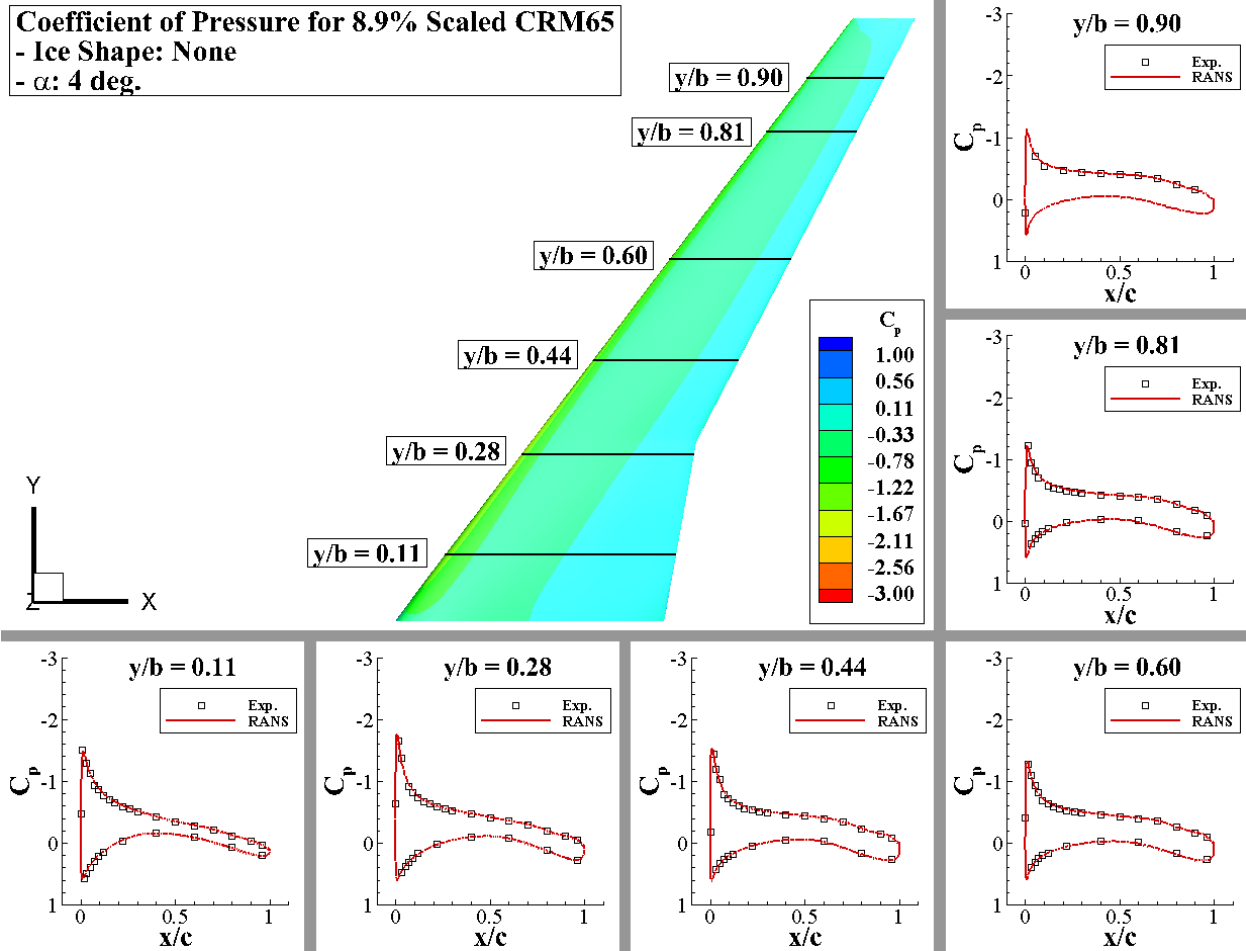


Fig. 9. Calculated coefficient of pressure contour for non-iced wing at 4-deg. with coefficient of pressure distribution comparisons at various spanwise locations.

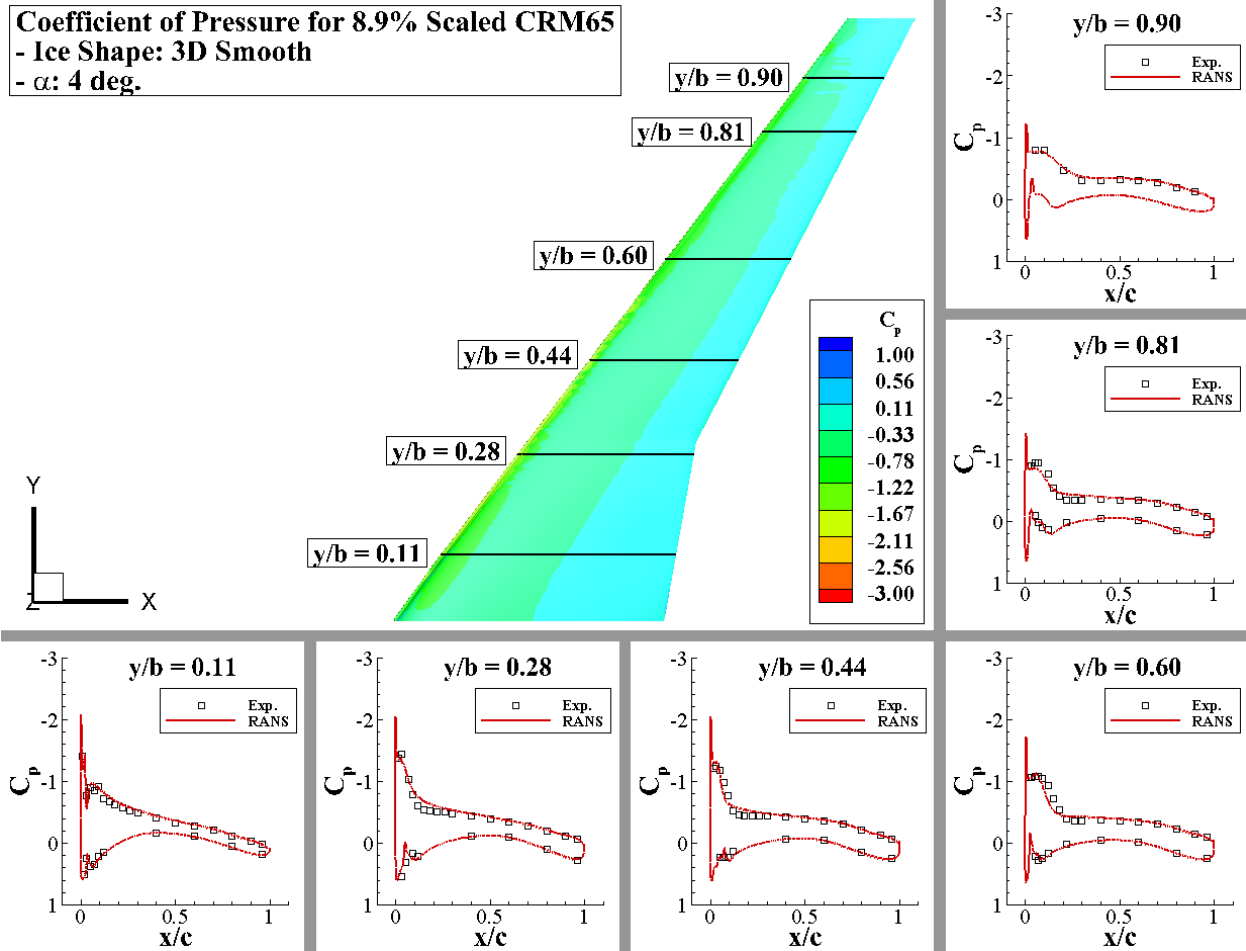


Fig. 10. Calculated coefficient of pressure contour for iced wing at 4-deg. with coefficient of pressure distribution comparisons at various spanwise locations.

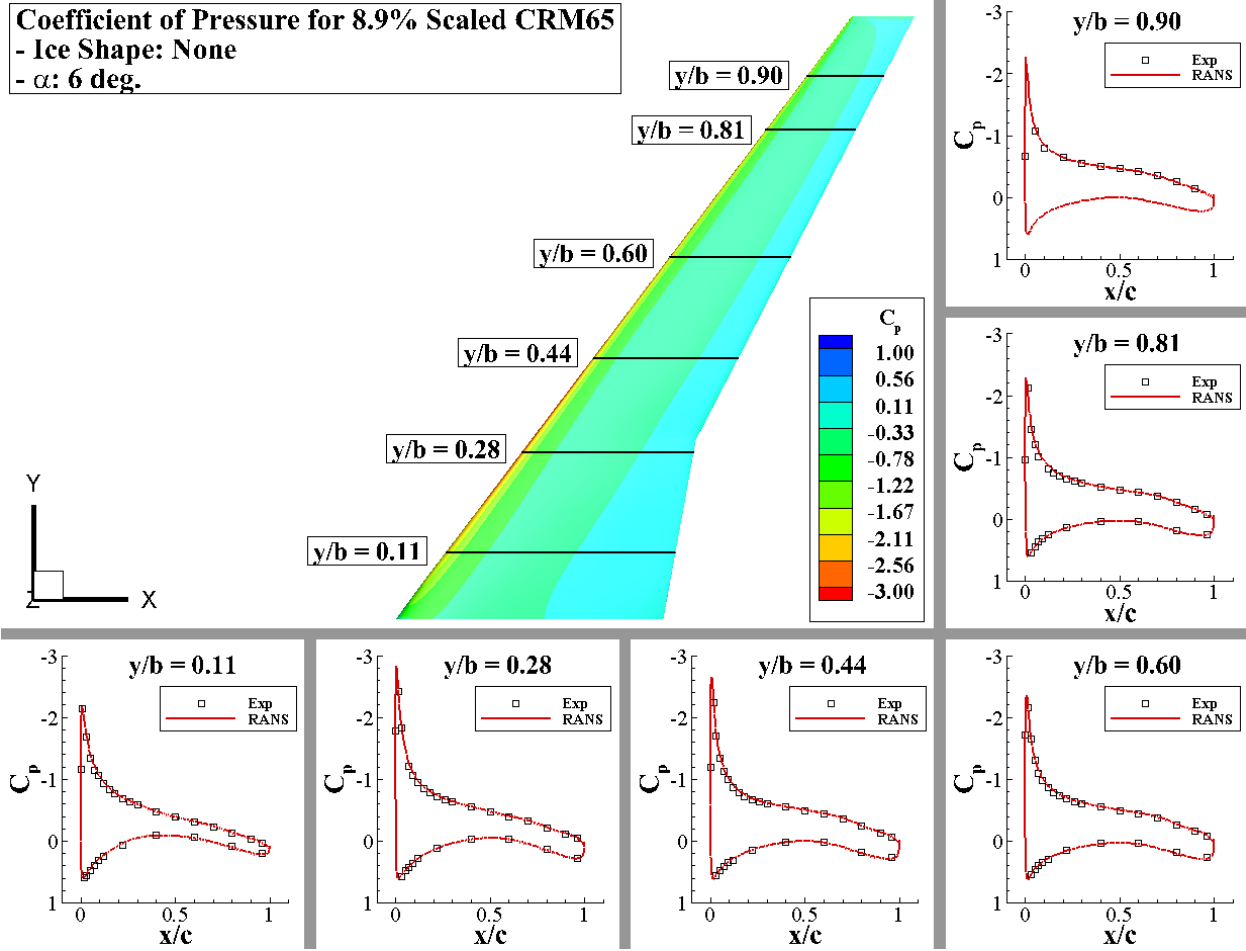


Fig. 11. Calculated coefficient of pressure contour for non-iced wing at 6-deg. with coefficient of pressure distribution comparisons at various spanwise locations.

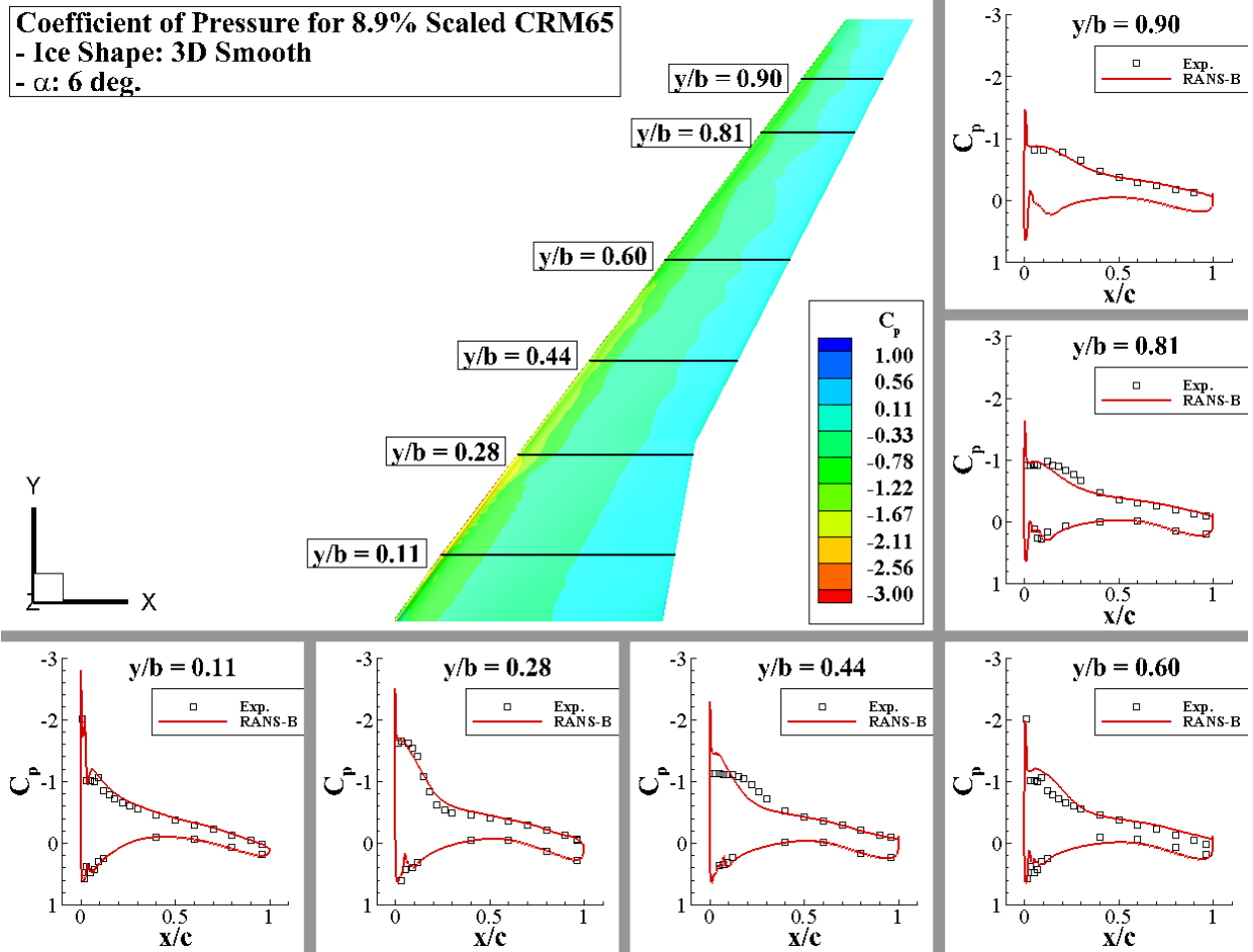


Fig. 12. Calculated coefficient of pressure contour for iced wing at 6-deg. with coefficient of pressure distribution comparisons at various spanwise locations. (B – Baseline)

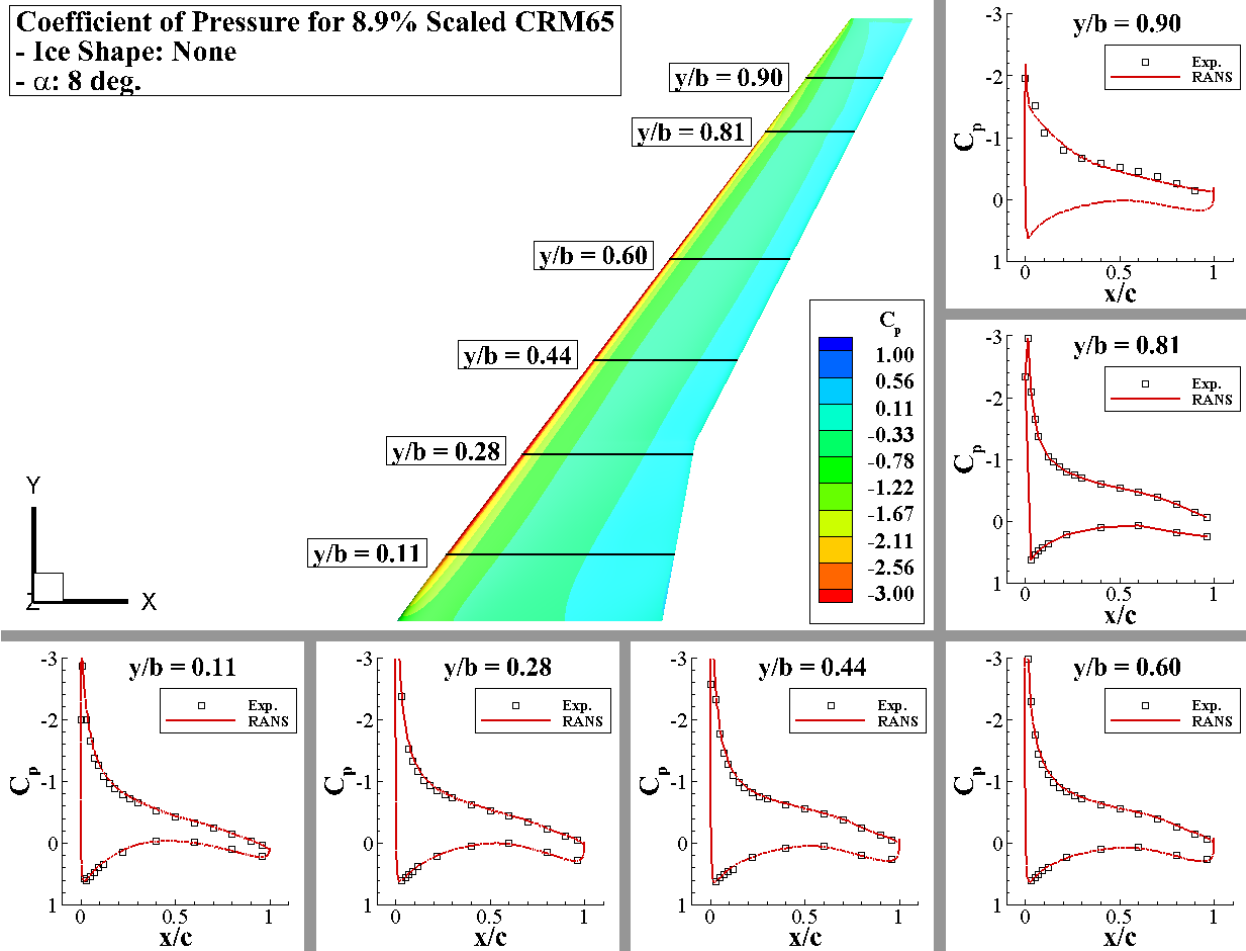


Fig. 13. Calculated coefficient of pressure contour for non-iced wing at 8-deg. with coefficient of pressure distribution comparisons at various spanwise locations.

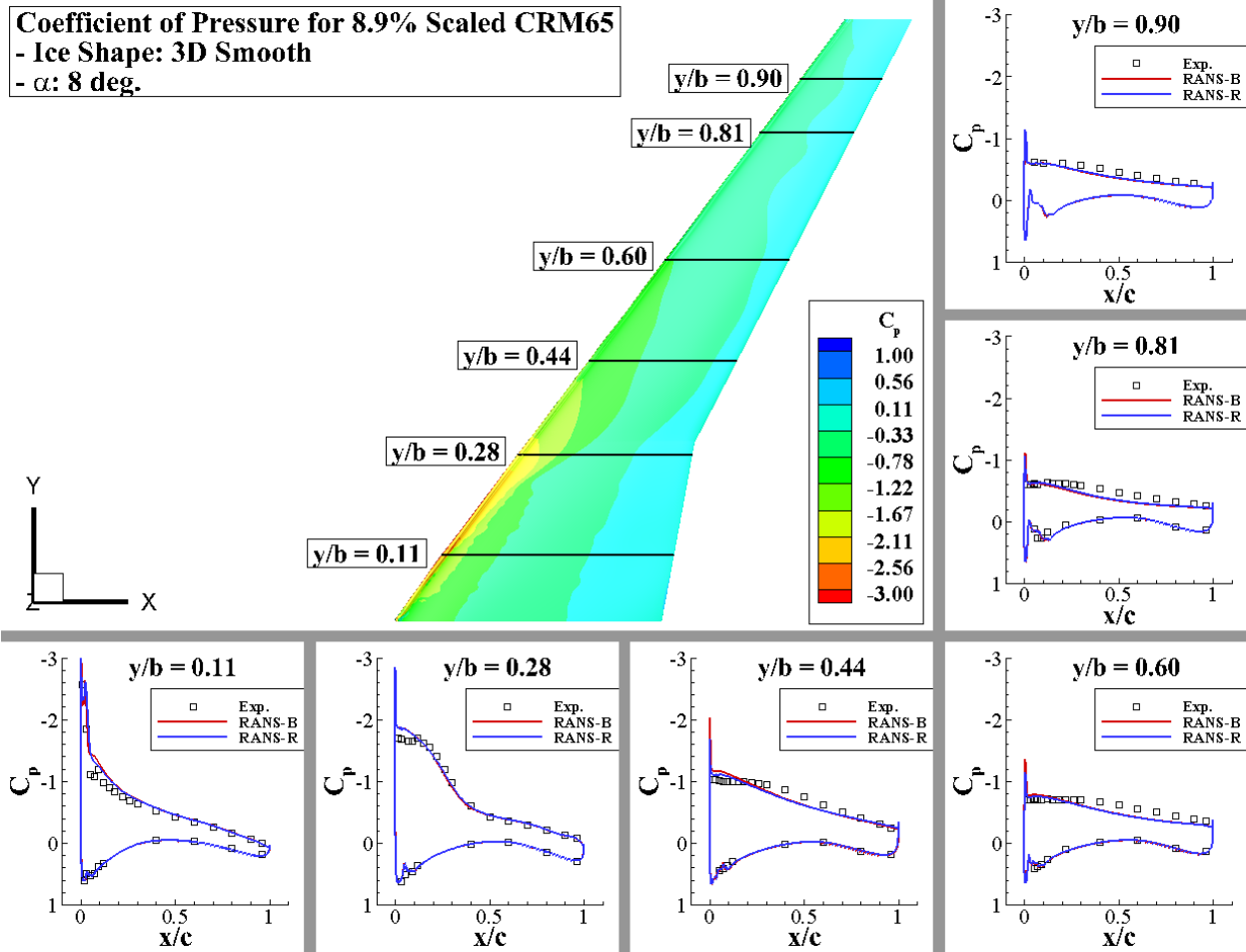


Fig. 14. Calculated coefficient of pressure contour for iced wing at 8 deg. with coefficient of pressure distribution comparisons at various spanwise locations. (B – Baseline; R – Refined)

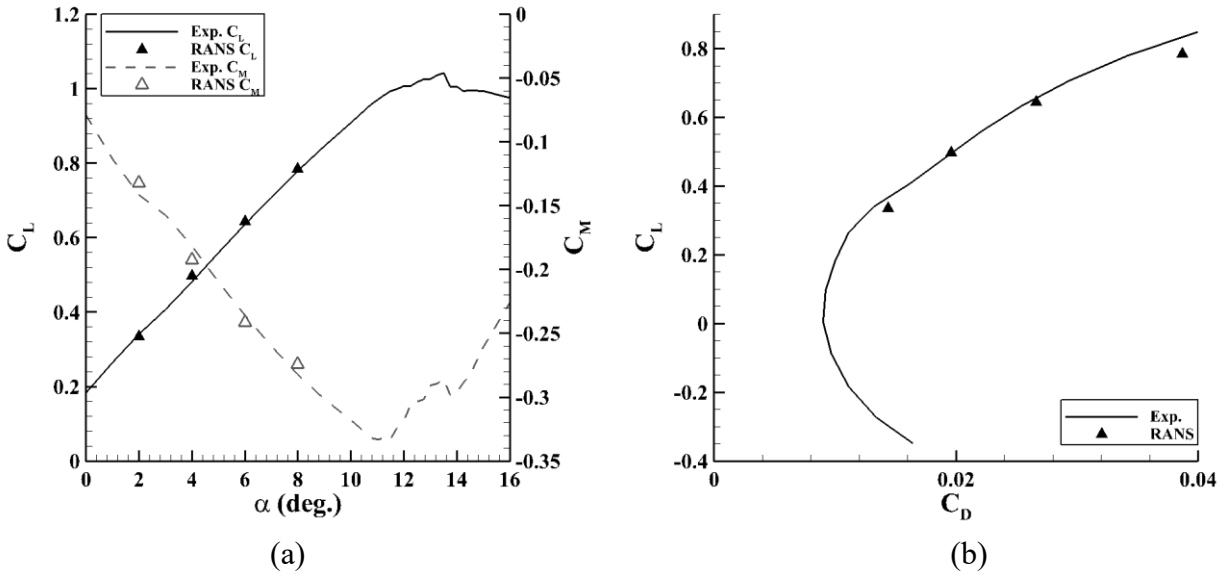


Fig. 15. Comparison of experimental and computed a)  $C_L$  and  $C_M$  vs. angle of attach and b)  $C_L$  vs.  $C_D$  for non-iced wing.

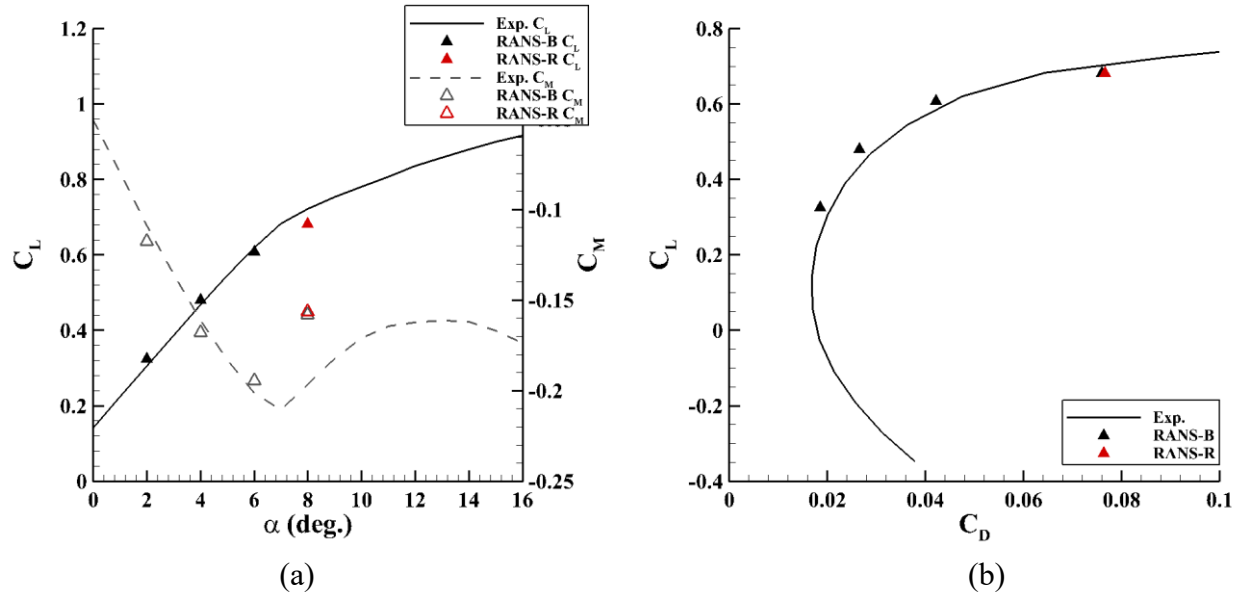


Fig. 16. Comparison of experimental and computed a)  $C_L$  and  $C_M$  vs. angle of attack and b)  $C_L$  vs.  $C_D$  for iced wing. (B – Baseline; R – Refined)

## Chapter 3 References

- [1] A. P. Broeren, M. G. Potapczuk, S. Lee, A. M. Malone, B. P. Paul, and B. Woodard, “Ice-Accretion Test Results for Three Large-Scale Swept-Wing Models in the NASA Icing Research Tunnel,” in *8th AIAA Atmospheric and Space Environments Conference*, 2016, pp. 1–30.
- [2] S. C. Camello, M. B. Bragg, and C. W. Lum, “Effect of Ice Shape Fidelity on Swept-Wing Aerodynamic Performance,” in *9th AIAA Atmospheric and Space Environment Conference*, 2017.
- [3] M. F. Alam, D. S. Thompson, and D. K. Walters, “Hybrid Reynolds-Averaged Navier–Stokes/Large-Eddy Simulation Models for Flow Around an Iced Wing,” *J. Aircr.*, vol. 52, 2015.
- [4] Y. Zhang, W. G. Habashi, and R. A. Khurram, “Zonal Detached-Eddy Simulation of Turbulent Unsteady Flow over Iced Airfoils,” *J. Aircr.*, vol. 53, 2016.
- [5] M. Xiao, Y. Zhang, and H. Chen, “Numerical Study of an Iced Airfoil Based on Delayed Detached- Eddy Simulation with Low Dissipation Scheme,” in *9th AIAA Atmospheric and Space Environment Conference*, 2017.
- [6] D. Zeppetelli and W. G. Habashi, “In-Flight Icing Risk Management Through Computational Fluid Dynamics-Icing Analysis,” *J. Aircr.*, vol. 49, no. 2, pp. 611–621, 2012.
- [7] C. Liu, Z. Liu, and L. Sakell, “Comments on the feasibility of LES for wings, and on a hybrid RANS/LES approach,” in *Advances in DNS/LES*, 1997.
- [8] J. Pan and E. Loth, “Detached Eddy Simulations for Iced Airfoils,” *J. Aircr.*, vol. 42, no. 6, 2005.
- [9] J. Vassberg, M. Dehaan, M. Rivers, and R. Wahls, “Development of a Common Research Model for Applied CFD Validation Studies,” *26th AIAA Appl. Aerodyn. Conf.*, no. August, 2008.
- [10] J. C. Vassberg, M. A. DeHaan, M. S. Rivers, and R. A. Wahls, “Retrospective on the Common Research Model for Computational Fluid Dynamics Validation Studies,” *J. Aircr.*, vol. 55, no. 4, pp. 1325–1337, 2018.
- [11] A. P. Broeren, B. Woodard, J. M. Diebold, and F. Moens, “Low-Reynolds Number Aerodynamics of an 8.9% Scale Semispan Swept Wing for Assessment of Icing Effects,” in *9th AIAA Atmospheric and Space Environments Conference*, 2017.
- [12] S. C. Camello, S. Lee, C. W. Lum, and M. B. Bragg, “Generation of Fullspan Leading-Edge 3D Ice Shapes for,” in *8th AIAA Atmospheric and Space Environments Conference*, 2016.
- [13] D. C. Wilcox, *Turbulence Modeling for CFD*, 2nd ed. La Canada, CA: DCW Industries, 1994.
- [14] F. R. Menter, “Two-Equation Eddy-Viscosity Turbulence Models for Engineering Applications,” *AIAA J.*, vol. 32, no. 8, 1994.
- [15] J. P. Steinbrenner, “Construction of Prism and Hex Layers from Anisotropic Tetrahedra,”

in *22nd AIAA Computational Fluid Dynamics Conference*, 2015.

- [16] D. Poll, "Spiral Vortex Flow Over a Swept-Back Wing," *Aeronaut. J.*, vol. 90, no. 85, pp. 185–199, 1986.
- [17] J. M. Diebold, A. P. Broeren, and M. Bragg, "Aerodynamic Classification of Swept-Wing Ice Accretion," in *5th AIAA Atmospheric and Space Environments Conference*, 2013.

---

## Conclusions

---

The objective of this research was to first provide a comprehensive review and commentary on experimentally-validated CFD studies of the aerodynamic impact of icing on lifting surfaces. The review only focused on computational studies published in the last three decades, and only on those which include aspects of experimental validation. The review summarized the findings in order to help guide engineers who seek to understand the capabilities and characteristics of the numerical methods, and help guide researchers who seek to develop computational methods to support new understanding of three-dimensional icing on airfoil and wing geometries guidance. The review found that both the rationale for turbulence model selection and meshing techniques for each ice shape is very similar. The main differences between each ice shape is the expected flow field behavior. Based on the flow field behavior, certain parameters of the numerical methodology could change accordingly. In terms of turbulence modeling, at low angles of attack, researchers found RANS to be sufficient as long as the boundary layer was sufficiently discretized by a mesh. As the angle of attack increases, the point at which a user should implement either an HRL method or LES becomes more dependent upon how aggressive the ice shape is at causing flow separation and negatively effecting the aerodynamic performance parameters. The implementation of HRL methods or LES requires a proper discretization of the mesh in order for both methods to accurately resolve the turbulent structures present in the flow field.

This review also brought to light the gaps in knowledge present in current computational iced aerodynamic knowledge. While CFD is able to provide crucial information regarding the flow physics around an iced wing that would take considerable amount of resources and effort to do the equivalent experimentally, a large portion of studies not outlined in this paper, have examined the effects of ice accretion two dimensionally. Studies presented in the review showed that icing is not a two-dimensional phenomenon and cannot be evaluated as such. The review calls for future studies to not rely on two-dimensional information to infer the impact of ice on lifting surfaces, and analyze the effect of ice in a three-dimensional domain. Future work for the community includes: understanding the full impact of implementing various numerical methods through a parametric study, selecting more realistic lifting surfaces that impact modern day aircraft, and standardizing which computational data is relevant and important in understanding the impact of ice accretion.

In order to address some of the areas of future work, the second objective of this research was to utilize RANS  $k-\omega$  SST in order to understand how well the numerical method is able to predict the flow physics and aerodynamic performance parameters for a modern aircraft wing

geometry with and without and ice shape on the leading edge. The work done showed that RANS proved to be quite capable in accurately predicting the existence and strength of leading-edge vortices along the upper surface of the wing at angles of attack of 4, 6 and 8-deg. The prediction capability of RANS to capture the wing stall was reflected in the pressure distribution plots and the aerodynamic coefficients. The prediction of the aerodynamic performance parameters for both geometries was well resolved by the RANS solution, except the coefficient of moment at 8-deg. Overall, at angles of attacks leading up to stall, RANS was able to well predict both the flow field and aerodynamic characteristics of the swept wing with and without ice, while at stall, the flow proved to be complex and was not properly predicted. Future work for this research will consist of pursuing 4 main points: 1) understanding the influence of the spanwise running flow and its impact on iced swept wing aerodynamics, 2) exploring why the coefficient of drag and moment were not correctly predicted by RANS, 3) improving the accuracy of calculating the pressure distribution along the swept wing and 4) comparing the simulated flow physics and aerodynamic parameters between the simplified and high fidelity version of horn ice shapes on swept wings using RANS and a hybrid RANS-LES model.